

**A Precast Pier System for Accelerated Bridge  
Construction in Seismic Zones**

by

Corey Marshall

A thesis

submitted in partial fulfillment

of the requirements for the degree of

Master of Science in the Department of Civil and Environmental Engineering

Idaho State University

Spring 2020

To the Graduate Faculty:

The members of the committee appointed to examine the thesis of COREY MARSHALL find it satisfactory and recommend that it be accepted.

---

Mustafa Mashal

Major Advisor

---

Arya Ebrahimpour

Committee Member

---

Andrew Chrysler

Graduate Faculty Representative

## **Acknowledgment**

I would like to thank my supervisor, Dr. Mustafa Mashal, who has helped and encouraged me throughout the project. Without his support and confidence, I would not have been able to complete this research. I would also like to thank Dr. Arya Ebrahimpour, who is my co-supervisor for this research project. Dr. Ebrahimpour provided vital information throughout the research project. I am also grateful for Dr. Andrew Chrysler who served as a Graduate Faculty Representative.

I would like to thank the students who assisted in the investigation and construction of the large-scale test specimens. Some students who helped immensely are Jared Cantrell, Katie Hogarth, Ali Shokrgozar, Mahesh Acharya, and Mahesh Mahat.

I would also like to acknowledge the Idaho Transportation Department for funding this research project. Without their funding, this research would not have been possible.

Finally, I am thankful for the continuous support of my friends, family, and wife who have continually supported and encouraged me every step of the way.

## Table of Contents

List of Figures .....	viii
List of Tables .....	xii
List of Abbreviations .....	xiii
Abstract .....	xiv
Chapter 1: Introduction .....	1
1.1 Introduction.....	1
1.2 Background.....	2
1.3 Precast Concrete Bridges in the United States.....	3
1.4 Research Motivation .....	5
1.5 Scope and Objectives.....	7
1.6 Thesis Structure .....	8
1.7 Summary.....	9
Chapter 2: Literature Review.....	10
2.1 Introduction.....	10
2.2 Research.....	11
2.3 Conclusions.....	26
Chapter 3: Cast-In-Place Cantilever Pier System .....	27
3.1 Introduction.....	27
3.2 Prototype Structure .....	27
3.3 Testing Arrangement .....	29
3.4 Loading Protocol.....	30
3.5 Instrumentation and Test Arrangement .....	33

3.6 Material Properties.....	35
3.7 Design of Cast-In-Place Specimen .....	35
3.8 Column and Footing Capacities.....	36
3.9 Construction.....	39
3.10 Experimental Testing.....	42
3.11 Test Results.....	46
3.12 Conclusions.....	55
Chapter 4: Precast Cantilever Pier System .....	57
4.1 Introduction.....	57
4.2 Connection Overview .....	57
4.3 Material Properties.....	59
4.4 Design of Precast Specimen .....	60
4.5 Construction.....	69
4.6 Experimental Testing.....	72
4.7 Test Results.....	77
4.8 Conclusions.....	84
Chapter 5: Comparison of Cast-In-Place and Precast Cantilever Pier Systems .....	86
5.1 Introduction.....	86
5.2 Loading Protocol.....	86
5.3 Hysteresis Test Results .....	90
5.4 Test Results for Curvature Distribution.....	96
5.5 Dissipated Energy Test Results .....	98
5.6 Area-Based Hysteretic Damping Test Results.....	100

5.7 Residual Drift.....	101
5.8 Conclusions.....	102
Chapter 6: Design, Detailing Considerations, and Repair Methodologies for the Precast Pier System.....	103
6.1 Introduction.....	103
6.2 Design and Detailing Considerations .....	103
6.2.1 Selecting Size of the HSS Member .....	103
6.2.2 Embedment Length of the HSS Member .....	105
6.2.3 Unbonded length.....	108
6.2.4 Development of Interaction Diagrams .....	109
6.3 Construction Technology and Assembly .....	111
6.4 Limitations of the Precast Column .....	114
6.5 Proposed Repair Methodologies .....	115
6.6 Conclusions.....	120
Chapter 7: Conclusions and Recommendations .....	121
7.1 Introduction.....	121
7.2 Conclusions from Research .....	122
7.3 Future Research Suggestions .....	124
Appendix A: Construction Drawings.....	128
A.1 Cast-in-place Column Drawings.....	128
A.2 Precast Column Drawings.....	130
Appendix B: Design Calculations of the Specimens .....	133
B.1 Cast-In-Place Column Calculations .....	133

B.2 Precast Column Calculations .....	134
Appendix C: Interaction Diagrams and Tables for the Precast Column.....	135
C.1 HSS Pipe Connection $f'_c = 4$ ksi .....	135
C.1.1 HSS thickness = 0.174 in.....	135
C.1.2 HSS thickness = 0.233 in.....	135
C.1.3 HSS thickness = 0.291 in.....	136
C.1.4 HSS thickness = 0.349 in.....	136
C.1.5 HSS thickness = 0.465 in.....	137
C.1.6 HSS thickness = 0.581 in.....	137
C.2 HSS Pipe Connection $f'_c = 8$ ksi .....	138
C.2.1 HSS thickness = 0.174 in.....	138
C.2.2 HSS thickness = 0.233 in.....	138
C.2.3 HSS thickness = 0.291 in.....	139
C.2.4 HSS thickness = 0.349 in.....	139
C.2.5 HSS thickness = 0.465 in.....	140
C.2.6 HSS thickness = 0.581 in.....	140
C.4 Cast-in-place Moment Capacities with $f'_c = 4$ ksi .....	141
Appendix D: Grout Product Data Sheet.....	142

## List of Figures

Figure 1.1: Walnut Lane Memorial Bridge (courtesy: Zollman et al. 1992).....	3
Figure 1.2: Pipe connection assembly .....	6
Figure 1.3: Thesis Structure.....	8
Figure 2.1: Thin-walled columns with varying thicknesses .....	11
Figure 2.2: Reinforcement and cross-sectional details for grouted couplers.....	13
Figure 2.3: Details for bent cap pocket connections.....	15
Figure 2.4: Precast column for testing mechanical bar splices.....	16
Figure 2.5: Hollow precast concrete columns.....	17
Figure 2.6: Grouted splice sleeve connection located in the plastic hinge of the column.....	19
Figure 2.7: Column to footing connection alternatives .....	21
Figure 2.8: CIP and precast bent column details .....	21
Figure 2.9: Low-damage seismic design .....	23
Figure 2.10: Precast bent with member socket and grouted duct connections.....	24
Figure 2.11: Pipe-Pin connection detail.....	25
Figure 3.1: Detail views of a typical bridge in Idaho. ....	28
Figure 3.2: Scaling of a typical column. ....	28
Figure 3.3: Testing arrangement. ....	30
Figure 3.4: ACI Testing protocol.....	31
Figure 3.5: Loading protocol. ....	32
Figure 3.6: Column instrumentation. ....	33
Figure 3.7: Typical test setup with load cells. ....	34
Figure 3.8: Comparison of Sap-2000 and Response-2000. ....	37

Figure 3.9: Cast-in-place footing reinforcing rebar layout. ....	38
Figure 3.10: Cast-in-place test specimen. ....	39
Figure 3.11: Cast-in-place column construction images.....	41
Figure 3.12: Loading protocol for the cast-in-place column. ....	43
Figure 3.13: Images from cast-in-place testing procedure.....	45
Figure 3.14: Force vs. Displacement plot for the cast-in-place column. ....	47
Figure 3.15: Force vs. Drift plot for the cast-in-place column. ....	48
Figure 3.16: Backbone curve for the cast-in-place column. ....	49
Figure 3.17: Cast-in-place curvature distribution. ....	51
Figure 3.18: Dissipated energy plot for the cast-in-place column. ....	52
Figure 3.19: Corrected area-based hysteretic damping for the cast-in-place column.....	55
Figure 4.1: Pipe connection assembly. ....	58
Figure 4.2: Plastic Stress Distribution. ....	62
Figure 4.3: Embedment length with embedded ring.....	63
Figure 4.4: Precast column detail.....	66
Figure 4.5: Precast column to footing assembly.....	68
Figure 4.6: Precast column construction images. ....	71
Figure 4.7: Location of strain gauges on the HSS member. ....	72
Figure 4.8: Pipe failure during the testing procedure. ....	73
Figure 4.9: Loading protocol for the precast column. ....	74
Figure 4.10: Images from the precast testing procedure.....	76
Figure 4.11: Force vs. Displacement plot for the precast column. ....	78
Figure 4.12: Force vs. Drift plot for the precast column. ....	79

Figure 4.13: Backbone curve for the precast column. ....	80
Figure 4.14: Precast curvature distribution. ....	81
Figure 4.15: Dissipated energy plot for the precast column. ....	82
Figure 4.16: Area-based hysteretic damping for the precast column. ....	83
Figure 5.1: Loading protocol for the cast-in-place column. ....	87
Figure 5.2: Loading protocol for the precast column. ....	87
Figure 5.3: Images from the cast-in-place testing procedure. ....	88
Figure 5.4: Images from the precast testing procedure. ....	89
Figure 5.5: Force vs. Displacement plot for the cast-in-place column. ....	92
Figure 5.6: Force vs. Displacement plot for the precast column. ....	92
Figure 5.7: Force vs. Drift plot for the cast-in-place column. ....	93
Figure 5.8: Force vs. Drift plot for the precast column. ....	93
Figure 5.9: Backbone curve for the cast-in-place and precast columns. ....	94
Figure 5.10: Cast-in-place curvature distribution. ....	97
Figure 5.11: Precast curvature distribution. ....	97
Figure 5.12: Cumulative dissipated energy for both columns. ....	99
Figure 5.13: Dissipated energy for each cycle for both columns. ....	99
Figure 5.14: Corrected area-based hysteretic damping for both columns. ....	100
Figure 5.15: Residual drift for the cast-in-place and precast columns. ....	101
Figure 6.1: Embedment length determination flow chart .....	107
Figure 6.2: Embedment length comparison for HSS round (in.) .....	107
Figure 6.3: Embedment length comparison for pipe (in.) .....	108
Figure 6.4: HSS member moment capacity interaction diagram. ....	110

Figure 6.5: Precast column construction images. ....	113
Figure 6.6: Repair methods.....	116
Figure 6.7: Finite element model for repair methods .....	116
Figure 6.8: Moment vs. drift for repair methods .....	117
Figure 6.9: Pedestal rotation for repair methods.....	118
Figure 6.10: Repair methods with highest results.....	118
Figure 6.11: Proposed repair method for the precast column connection. ....	119
Figure A.1: Cast-in-place footing details.....	128
Figure A.2: Cast-in-place column Details. ....	129
Figure A.3: Precast footing details.....	130
Figure A.4: Precast column details. ....	131
Figure A.5: Connection details for the precast column. ....	132

## List of Tables

Table 3.1: Actual $f'_c$ values (ksi). .....	35
Table 3.2: Summary of the cast-in-place loading protocol. ....	44
Table 3.3: Damage observation from testing of the cast-in-place column. ....	49
Table 3.4: Summary of the performance points from testing of the cast-in-place column. ....	49
Table 3.5: Equivalent viscous damping coefficients for hysteretic damping component .....	54
Table 4.1: Actual $f'_c$ values for the precast column (ksi). .....	59
Table 4.2: Summary of performance values from testing of the precast column. ....	75
Table 4.3: Damage observation from testing of the precast column. ....	80
Table 4.4: Summary of the performance points from testing of the precast column.....	80
Table 5.1: Damage observation from testing of the cast-in-place column. ....	95
Table 5.2: Summary of the performance points from testing of the cast-in-place column. ....	95
Table 5.3: Damage observation from testing of the precast column. ....	95
Table 5.4: Summary of the performance points from testing of the precast column.....	95
Table 5.5: Summary of performance factors for the cast-in-place and precast columns.....	102
Table 6.1: Common corrosion rates from WSDOT Bridge Design Manual .....	104

## List of Abbreviations

ABC	Accelerated Bridge Construction
CFST	Concrete Filled Steel Tubes
HSS	Hollow Structural Section
PBES	Prefabricated Bridge Elements and Systems
PVC	Polyvinyl Chloride
SLAB	Structural LAB
SIBC	Slide-in Bridge Construction
WSDOT	Washington State Department of Transportation

## A Precast Pier System for Accelerated Bridge Construction in Seismic Zones

Thesis Abstract--Idaho State University (2020)

Accelerated Bridge Construction (ABC) in seismic regions is currently a research focal point. ABC is bridge construction that uses innovative planning, design, materials, and construction methods in a safe and cost-effective manner to reduce the onsite construction time that occurs when building new bridges or replacing and rehabilitating existing bridges. The research at Idaho State University included large scale testing of an experimental cantilever precast column and a cast-in-place column. The precast column design incorporated a hollow structural steel member into the column to footing connection. The test specimen is tested to failure following the ACI guide for testing reinforced concrete structural elements under slowly applied simulated seismic loads. The testing procedure is accomplished using a uniaxial quasi-static loading protocol. Results revealed that the experimental column achieved a higher drift ratio, resisted greater force, and dissipated more energy compared to a traditional cast-in-place column.

Key Words: Accelerated Bridge Construction

## **Chapter 1: Introduction**

### **1.1 Introduction**

For the past several years, Accelerated Bridge Construction (ABC) has amazed individuals around the world. The federal highway administration has defined ABC as bridge construction that uses innovative planning, design, materials, and construction methods in a safe and cost-effective manner to reduce the onsite construction time that occurs when building new bridges or replacing and rehabilitating existing bridges (U.S. Department of Transportation/Federal Highway Administration 2019). In 1991 approximately 50% of bridges are constructed from prestressed concrete (Collins and Mitchell 1991). Two of the most common ABC methods used are Prefabricated Bridge Elements and Systems (PBES) and Slide-In Bridge Construction (SIBC).

“PBES are structural components of a bridge that are built offsite, or adjacent to the alignment and includes features that reduce the onsite construction time and mobility impact time that occurs during conventional construction methods (U.S. Department of Transportation/Federal Highway Administration 2019).” Precast concrete products are PBES. Due to a large number of bridges being built from precast concrete, there are numerous construction projects that are considered ABC projects.

SIBC involves constructing a new bridge, from PBES, on temporary supports parallel to an existing bridge. After the bridge is constructed, the road is closed, and the existing bridge is either demolished or slid out of the way. After the old bridge has been removed, the new bridge is slid into place and paved typically within days.

While ABC offers great advantages, however applications of ABC in seismic regions have been limited due to concerns about the seismic performance of the connection between precast

elements. Past earthquakes have shown vulnerability of the connection between precast elements due to limited ductility and strength.

## **1.2 Background**

In 2017 ASCE published an infrastructure report card for the nation. The report states that there are 614,387 bridges in the United States. Approximately 4 in 10 of the bridges are 50 years old or older. 56,007 of the nation's bridges are considered structurally deficient in the year 2016, with approximately 188 million trips across a structurally deficient bridge each day. A structurally deficient bridge requires a significant amount of maintenance, rehabilitation, or needs to be replaced. Overall, the number of structurally deficient bridges is decreasing, but at the same time the average age of the bridges in the nation is rising, 43 years old, and approaching the end of their designed service life. The ASCE 2017 infrastructure report card states that "The most recent estimate puts the nation's backlog of bridge rehabilitation needs at \$123 billion" (ASCE 2017).

ASCE also published an infrastructure report for the state of Idaho in 2018. When the report was published, there are 4,492 bridges in Idaho. Out of the total number of bridges, 393 are considered structurally deficient, 45 of which are located on the state highway system, and 280 on local highway systems. 837 of the bridges located along the state highway system had reached or exceeded their designed 50-year life span. According to the ASCE report, the number of bridges on the state highway system that are at or exceeding their designed 50-year life span will increase to 911 in 2021 (ASCE 2018).

To improve the next infrastructure report card, the bridges in the United States need to be either repaired or replaced quickly and efficiently. One of the ways the bridges can be replaced quickly and efficiently is by incorporating ABC methods. Fortunately, the state and highway officials are

making a difference, but more techniques need to be developed to hasten the process. In addition, bridges located in seismic zones have to be designed using ABC connections that will offer adequate performance during an earthquake.

### **1.3 Precast Concrete Bridges in the United States**

The Walnut Lane Memorial Bridge, shown in Figure 1.1, is in Philadelphia, Pennsylvania. It was the first ABC project in the United States. The design and construction of this bridge led to the prestressed industry in the United States. The bridge consisted of thirteen post-tensioned beams that spanned 160 ft and had a depth of 79 in. The dimensions of the beams were designed similarly to the AASHTO girders that are used today. Because the Walnut Lane Memorial Bridge design was the first precast bridge in the United States a full-size test beam was required to prove the capacity of the bridge. In October 1949, the full-size test beam was loaded to failure and witnessed by approximately 300 engineers. The beam performed as Gustave Mangel designed (Zollman et al. 1992). Since the testing and construction of the Walnut Lane Memorial Bridge, thousands of research projects have been conducted to further develop the range of possibilities that can be achieved with the use of ABC methods.



Figure 1.1: Walnut Lane Memorial Bridge (courtesy: Zollman et al. 1992).

There are several advantages to using the ABC methods, which are evident in most ABC projects. One of the advantages is limiting the duration of the disruptions to traffic during construction because of the increased construction speed. Another advantage is improved public perception. The public's perception is improved because they see the construction progressing faster than usual. Faster project delivery is also an advantage to ABC. Due to the speed of the construction, the negative economic impact on local businesses is reduced which is counted as another advantage. The use of precast concrete is an advantage because formwork can be reused which reduces costs. Other noteworthy advantages include the following: better quality control of the materials being used, lower machinery and equipment costs, higher durability of the bridge elements, a reduced weight of the bridge structure, increased level of safety, and less environmental impacts to the surrounding area (U.S. Department of Transportation/Federal Highway Administration 2019).

The disadvantages associated with using ABC and precast concrete will now be discussed. One of the disadvantages is the difficulty of maintaining tight tolerances. As projects develop with precast concrete, occasionally the precast elements do not fit or align as intended. If the concrete members are not aligning, then a new concrete element will need to be constructed and precious time and money are wasted. Misalignment issues become more common with longer/taller precast elements. Another disadvantage is encountered when the concrete elements have bars extruding from the concrete. In a case where bars are extruding from the concrete, the bars need to be protected from being damaged during transportation and installation. Another disadvantage is the cost of each concrete member. The process involved with precast concrete elements requires a specific skillset to prepare, pour, transport, and install the member, which is not the same as the traditional skillsets required for cast-in-place concrete. One more disadvantage

related to the overall cost occurs during the transportation of the precast elements. Concrete is heavy and as a result, the cost associated with the transportation process is high.

When considering the seismic performance of an ABC structure, other challenges arise. Some of the challenges are: inelastic deformations develop during cyclic behavior, large concentrated forces develop where key elements join together, and a rapid loss of strength may be evident due to localized buckling (Marsh 2018).

Precast connections are classified in two different ways, emulative and non-emulative. An emulative connection mimics the seismic performance of a traditional cast-in-place connection while a non-emulative connection improves the performance of the connection. The connections that are emulative may incorporate bar couplers, grouted ducts, pocket connections, and member socket connections while the non-emulative connections are segmental post-tensioned rocking piers and hybrid or dissipative controlled rocking connections (Mashal et al. 2016). Emulative connections are usually more desirable than a non-emulative connection because of the confidence with regards to the durability and seismic performance of cast-in-place connections (Marsh et al. 2011).

#### **1.4 Research Motivation**

The motivation to conduct this research project stems from the list of disadvantages associated with ABC discussed previously. Many of the current ABC methods that require couplers or grouted ducts have difficulties connecting the concrete elements due to alignment issues. As a result of the alignment issues a new connection needs to be proposed, built, and tested to reduce and hopefully eliminate the issue. The proposed connection incorporates hollow structural sections (HSS) made from steel located within the plastic hinge of the column and is referred to as, a pipe connection. HSS is installed at the end of the precast column. Approximately half of

the HSS is extruding out of the precast column and have centering fins welded to the outside edge of the pipe. The centering fins are not important structurally, but rather are only for inserting the column into the footing. The precast column is inserted into a void protruding into the footing created by a second HSS member. Once the precast column is inserted into the footing, high strength grout is used to fill the remaining voids in the pipe connection via grout vents. Other significant components include the elastomeric bearing pad and unbonded length. Figure 1.2 depicts the pipe connection assembly.

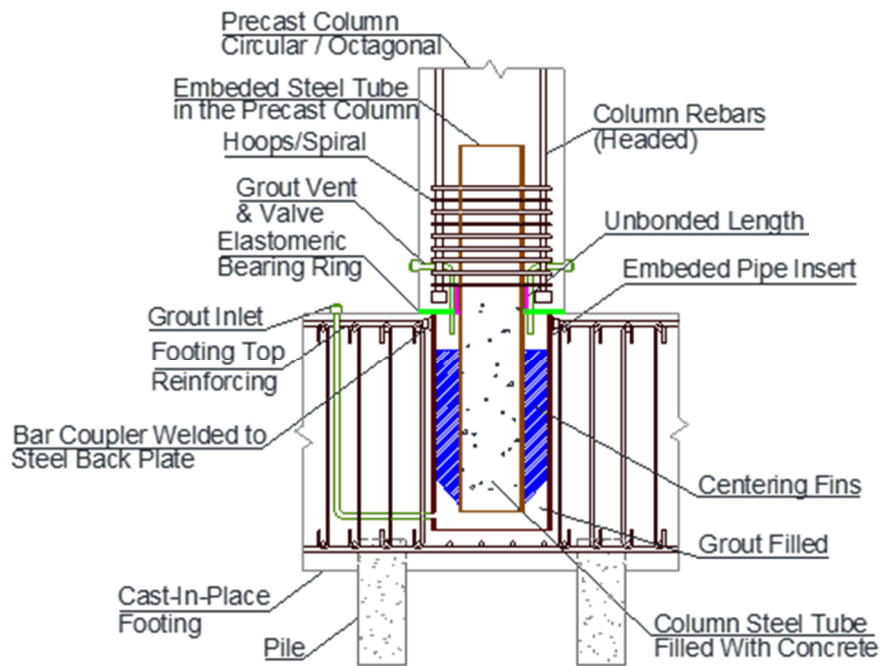


Figure 1.2: Pipe connection assembly

One of the anticipated advantages of using the pipe connection is the ease of installment. Installation is easier with the self-centering fins. The fins allow larger initial tolerances while the column is being lowered into the footing. The fins also ensure the precast column is located at the center of the hole it is being inserted to. The Washington State Department of Transportation (WSDOT) has performed similar research with Concrete Filled Steel Tubes (WSDOT 2019) and incorporating a steel annular ring, respectively. However, the research in this thesis uses CFST

only in the plastic hinge zones and other parts of the pier are normal precast reinforced concrete sections. The proposed concept in Figure 1.2 for a precast pipe connection will need to be tested to demonstrate that it can match the capacity and ductility of a traditional cast-in-place column.

### **1.5 Scope and Objectives**

The scope of this research is testing of large scale precast and cast-in-place specimens to demonstrate the adequacy of the proposed pipe connection during an earthquake. The precast connection is compared against a cast-in-place solution using the results and observation from experimental testing.

The objectives of this research are as follows:

- 1) Review current ABC technologies and connections for seismic regions
- 2) Testing of a benchmark cast-in-place specimen under quasi-static cyclic loading
- 3) Outline the design procedure and detailing considerations for the proposed pipe connection
- 4) Experimentally validate the pipe connection via large-scale testing of a cantilever test specimen with similar dimensions and capacity to the cast-in-place benchmark
- 5) Compare the seismic performance of the pipe connection against the traditional cast-in-place column
- 6) Provide recommendations regarding repair considerations for the proposed pipe connection.

To accomplish objective 1, a literature review will be written. To achieve objectives 2-5, two large scale cantilever test specimens will be designed, constructed, and tested. One of the columns will be cast-in-place and the second will be precast. Objective 6 will then be addressed based on experimental results and observations.

**1.6 Thesis Structure**

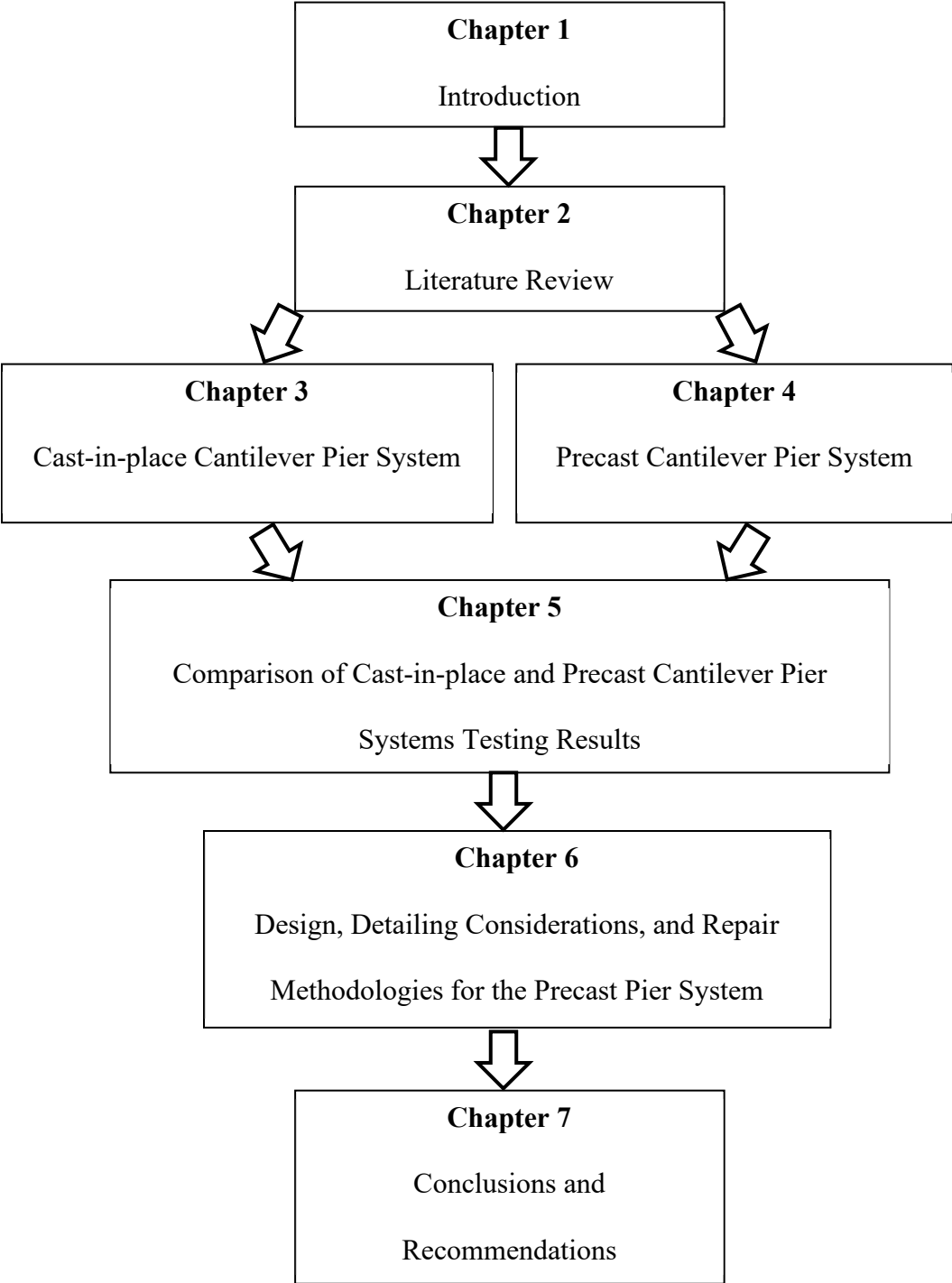


Figure 1.3: Thesis Structure

## **1.7 Summary**

The Walnut Lane Memorial Bridge in Pennsylvania was a significant landmark in the precast industry. The use of ABC techniques can save time, money, and lives. Despite the use of ABC, the bridge infrastructure in the United States is still in poor condition. More ABC methods need to be developed and implemented to improve the nation's infrastructure report card. The research proposed can have a positive impact on the construction of future ABC bridges especially those located in seismic regions.

## **Chapter 2: Literature Review**

### **2.1 Introduction**

Several research projects have been devoted to the expansion of ABC methodologies. Some of the institutions that have contributed to ABC research include the University of Nevada-Reno, Texas A&M, the University of Canterbury in New Zealand, Idaho State University, and Washington State University. This chapter will briefly discuss a variety of related literature which includes thin-walled steel columns, high-strength precast concrete, pocket connections, socket connections, grouted ducts, grouted splice sleeves, mechanical bar splices, hollow precast reinforced concrete, precast shell column, dissipative controlled rocking, and pipe-pin connections.

## 2.2 Research

Al-Kaseasbeh and Mamaghani (2019) investigated the hysteretic behavior of circular thin-walled steel columns. The control test column had a continuous wall thickness while the five experimental columns had gradient wall thicknesses with volumes and outside diameters equaling that of the control specimen. The columns are analyzed with a constant axial load and a bidirectional cyclic horizontal loading protocol. The analysis of the members is completed using a finite-element model that allows the material and geometric properties to vary along the length of the pipe, as shown in Figure 2.1. The gradient columns displayed a significant increase in ultimate strength, ductility, and post-buckling behavior compared to the controlled column with a uniform thickness.

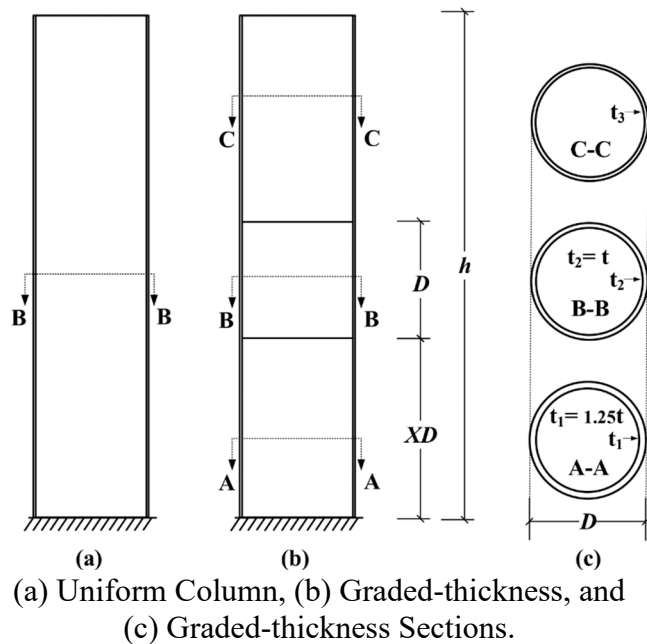
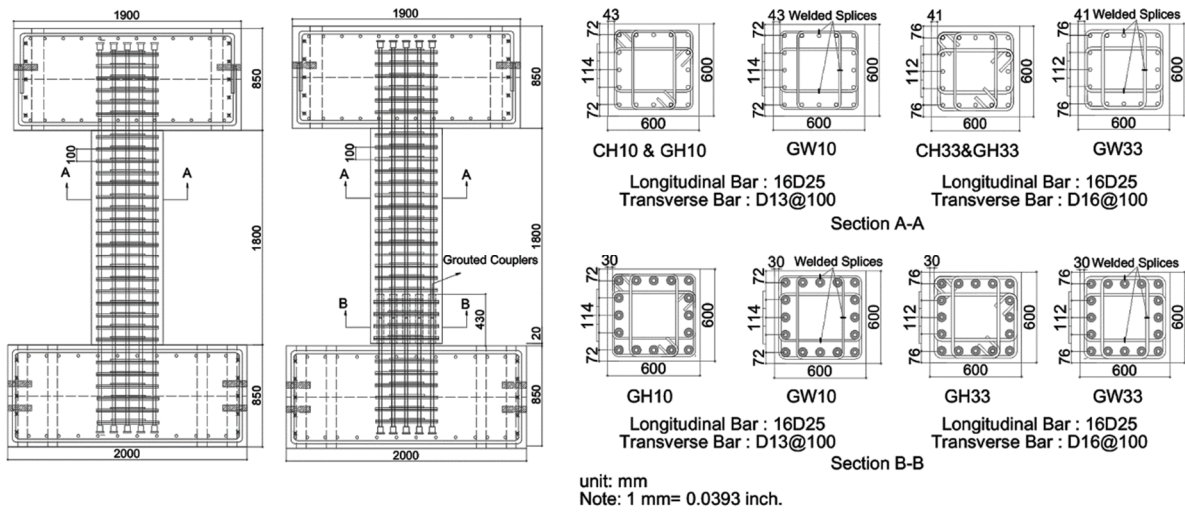


Figure 2.1: Thin-walled columns with varying thicknesses (courtesy of Al-Kaseasbeh and Mamaghani 2019).

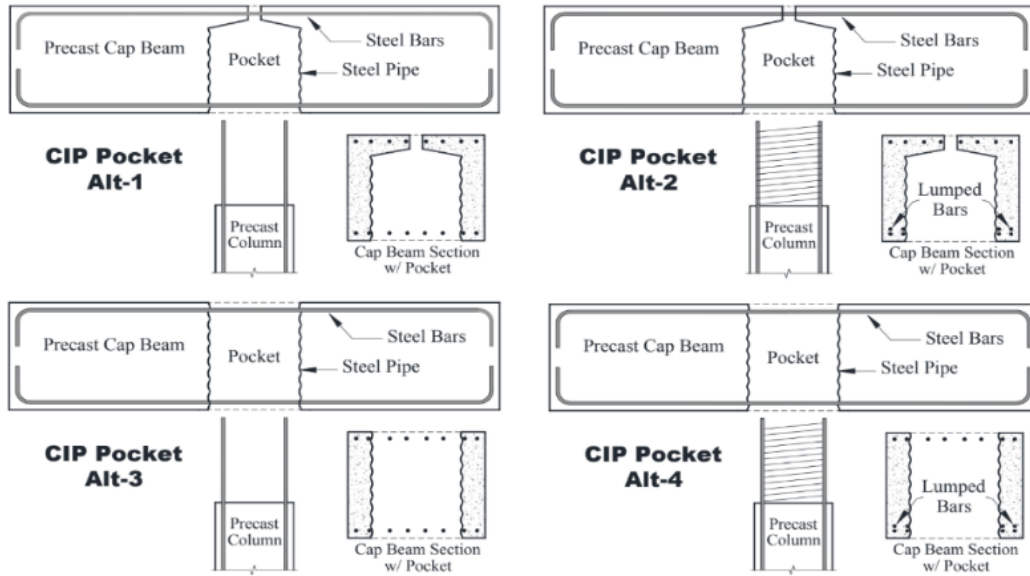
Ou et al. (2015) performed six cyclic tests on large-scale columns. These large-scale tests are part of Taiwan's new reinforced concrete research effort to develop standards for high strength reinforced concrete structures to incorporate into high-rise building construction projects. The purpose of the research is to investigate the seismic performance of high strength concrete in precast reinforced columns. Each of the six columns is constructed from high-strength concrete, high strength longitudinal bars, and transverse reinforcing bars. Two different construction methodologies are incorporated into the design of the columns. The two methodologies are grouted coupler splices for the longitudinal reinforcement in the plastic hinge zones and butt-welded splices for the transverse reinforcement, shown in Figure 2.2. The effect of using grouted coupler splices and butt-welded splices in the plastic hinge zone is compared to a cast-in-place column using conventional construction methods. After analyzing the results, it appears that the performance of the precast grouted coupler splices is equivalent to the conventional cast-in-place column. The results also showed the precast columns with butt-welded splices had a lower ultimate drift capacity compared to the conventional hooked transverse reinforcement. The reduction in ultimate drift capacity is a result of the longitudinal reinforcement buckling sooner than the traditional transverse hook methodology.



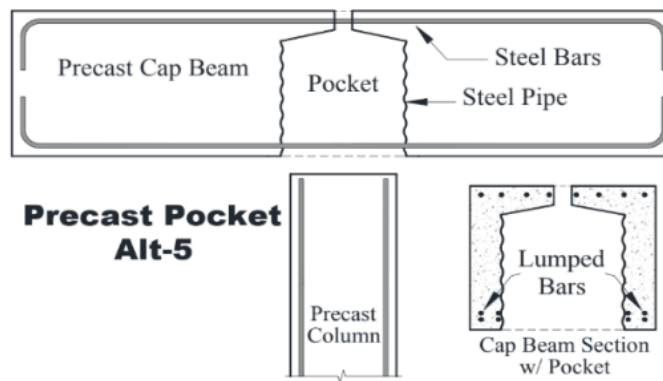
(a) column without grouted couplers; (b) columns with grouted couplers; and  
(c) cross section designs.

Figure 2.2: Reinforcement and cross-sectional details for grouted couplers  
(courtesy of Ou et al. 2015).

Tazarv and Saiidi (2015a) investigated the use of pocket connections in high seismic regions. Although the AASHTO Scan 11-02 had studies regarding the seismic performance of these pocket connections, additional research is required to develop practical and reliable pocket connections. As a result of the research project, pocket connections are found to be a useful way to join precast columns and pier caps together. Through their literature review research, it was discovered that if the bent cap is properly designed the effects of pockets, with regards to the seismic performance of the cap, are negligible and the connection simulated a cast-in-place column connection. Based on the lessons learned from the research, five details for precast pocket connections are shown in Figure 2.3. Some of the previous precast cap beam models that were constructed with a pocket connection yielded. The failure of the pocket connections is a result of inadequate design. The use of precast pocket Alt-5 connections, shown in Figure 2.3, reduced the onsite construction time by 75%. The other pocket connections reduced the onsite construction time by 42%.



(a) Cast-in-Place Pocket Connections



(b) Precast Pocket Connection

Figure 2.3: Details for bent cap pocket connections (courtesy of Tazarv and Saiedi 2015a).

Tazarv and Saiidi (2015b) also investigated mechanical bar splices located in the plastic hinge. One of the precast columns is shown in Figure 2.4. Through their research revealed that the performance of a coupler is dependent upon the loading rate and the manufacturer of the coupler. It is also concluded that careful placement of large couplers in the column is crucial to obtaining the ultimate capacity of the coupler. In most cases, the seismic performance of smaller couplers is determined to be adequate. Finally, it is estimated that incorporating the mechanical bar splices at both ends of a precast column can reduce the construction time by nearly 60%.



Figure 2.4: Precast column for testing mechanical bar splices (courtesy of Tazarv and Saiidi 2015b).

Kim et al. (2016) developed two types of cast-in-place concrete-filled hollow precast concrete columns to reduce the weight of large precast concrete columns and to increase the structural integrity of the cap beam to column joints. The two proposed types of hollow precast concrete columns are shown in Figure 2.5. Cyclic loading tests are performed on the two columns and a conventional reinforced concrete column to measure the seismic resistance of the columns. The results from the test procedure showed that the stiffness and the maximum strength of the experimental test columns are comparable to the controlled conventional reinforced column. However, the displacement ductility of the experimental columns is lower. The energy dissipated from the experimental columns is slightly lower than the controlled reinforced column. The experiment also concluded that the hollow core sections reduced the weight of the precast elements by 62 and 51%.

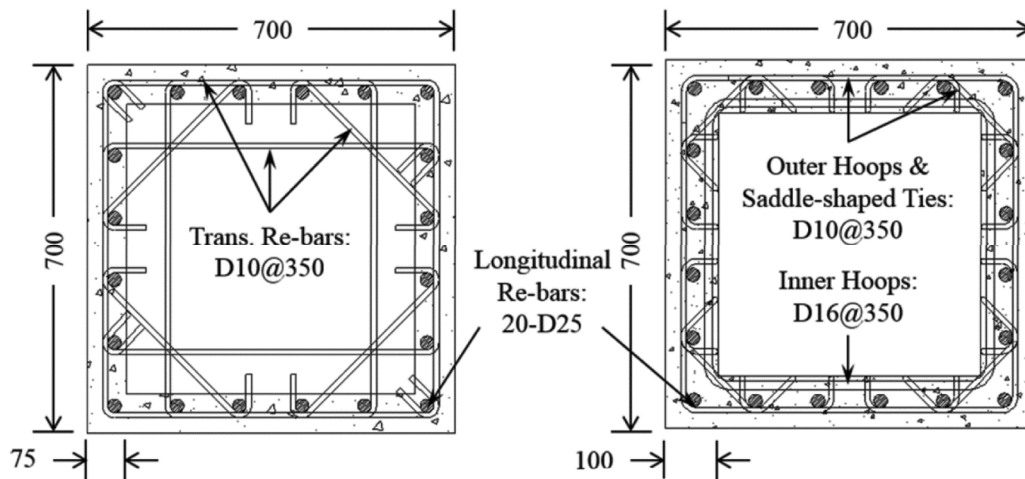
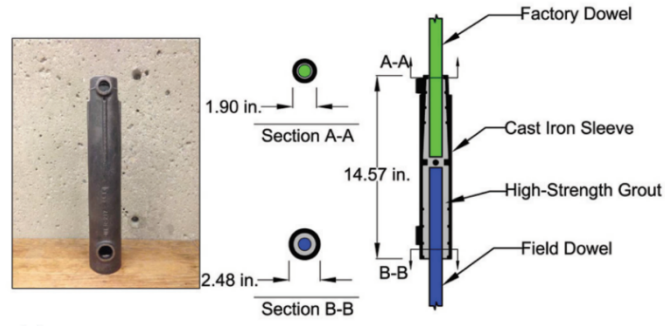
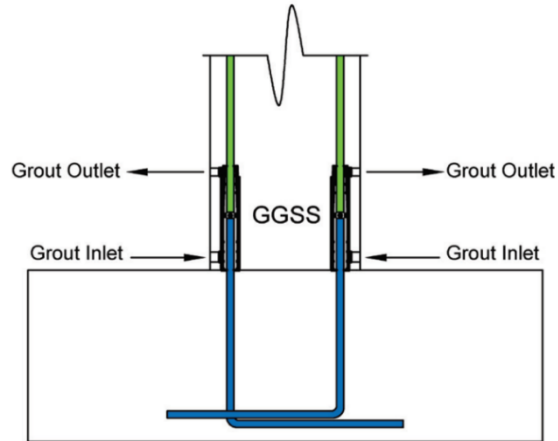


Figure 2.5: Hollow precast concrete columns (courtesy of Kim et al. 2016).

Ameli et al. (2016) performed tests on seismic column-to-footing connections using grouted splice sleeves. The location of the connection is located in either the column or footing, depending on the test specimen. The grouted splice sleeves are selected to be tested because they have good construction tolerances and offer a bond-related load transfer mechanism. Figure 2.6 shows a typical grouted connection located in the plastic hinge of the column. To test the connections, three half-scale precast cantilever column test specimens and one cast-in-place cantilever control test specimen are constructed to be tested under quasi-static cyclic loads. The results from the test demonstrated that the columns with grouted splice sleeves located in the plastic hinge of the column had a lower displacement ductility capacity compared to the conventional cast-in-place column. The results improved for the columns with grouted splice sleeves located in the footing. To expand the test results, the reinforcing bars inside of the footing are intentionally de-bonded a length equal to eight times the diameter of the reinforcing bars. Displacement ductility is any performance of the connection past the yielding point without a significant decrease in the structure, or column, lateral capacity.



(a)



(b)

Figure 2.6: Grouted splice sleeve connection located in the plastic hinge of the column (courtesy of Ameli et al. 2016).

Galvis and Correal (2017) investigated the characterization of the seismic behavior of a column foundation connection for Accelerated Bridge Construction. This research indicated that grouted duct connections have the potential to be improved. Several challenges arise during the design and construction of grouted ducts, such as construction tolerances and large diameter bars. An alternative to the grouted duct connections is a pocket connection. The pocket connection investigated is created from a corrugated steel tube and non-shrinkage grout that bonds all of the longitudinal reinforcing bars together. The benefits of using a pocket connection are large construction tolerances. A disadvantage to using a pocket connection is a large amount of connecting materials and the foundation's reinforcement details are complex. Another alternative to grouted ducts is a socket connection. A socket connection allows the column to be installed without any additional connecting members between the column and footing. To improve the bond strength of the column and footing, the pre-cast column has a roughened surface where it is in contact with the footing. A benefit of using the proposed socket connection is there are not any reinforcing bars extruding out of the base which makes transporting and handling the precast elements easier. A disadvantage of using the socket connection is the same as the pocket connection discussed prior (e.g. placing of footing rebars). A drawing of both the pocket and socket connections are shown in Figure 2.7.

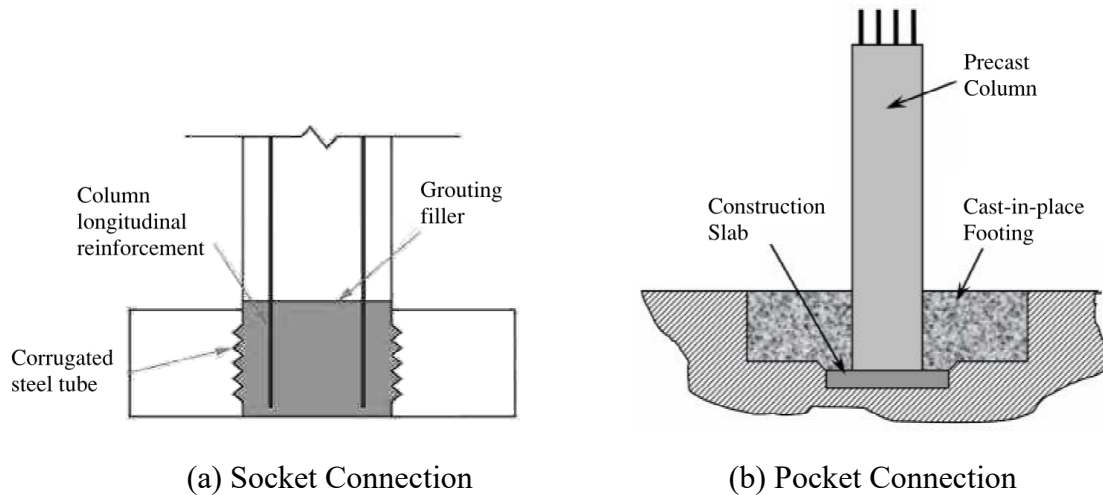


Figure 2.7: Column to footing connection alternatives (courtesy of Galvis and Correal 2017).

Mehraein and Saïidi (2016) examined the seismic performance of bridge column-pile-shaft pin connections. The experimental test specimens for this project are two bent assemblies. The cap beam is precast, which is connected to columns via a pocket connection. One of the columns in each of the bents is cast-in-place, while the other is constructed using a precast shell. The reinforcement for each of the columns is shown in Figure 2.8. The shake table testing results confirmed that the proposed precast shell design satisfies the safety and performance requirements outlined in the code.

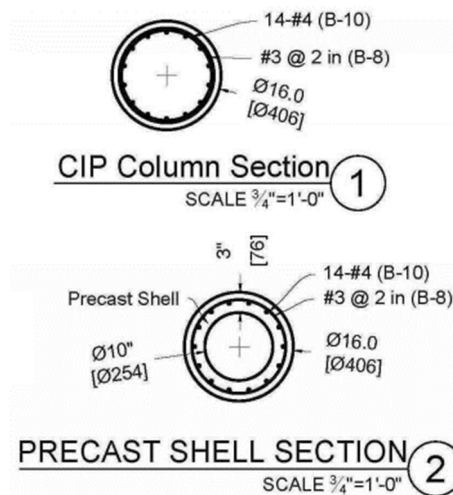


Figure 2.8: CIP and precast bent column details (courtesy of Mehraein and Saïidi 2016).

Mashal and Palermo (2019a) performed experimental work investigating a low-damage seismic design for Accelerated Bridge Construction. The project intends to minimize the amount of damage imposed on precast bridge elements during an earthquake. The experiment utilized dissipative controlled rocking connections between the precast column and the footing or cap beam as shown in Figure 2.9. The use of the dissipative controlled rocking connections keeps the traditional plastic hinges located at the column to footing and column to cap beam interfaces from forming. The connection utilizes an unbonded post-tensioned tendon located inside of the precast column to encourage the column to centering itself to its original position after a seismic event. The dissipaters located on the exterior of the column are used to dissipate the seismic kinetic energy. A steel jacket armor is used to increase the confinement of the concrete and reduce any damage that may occur during a seismic event. After several cycles of quasi-static testing of the connection, there was no damage or measurable post-seismic displacement. As a result of the experiment, the design was used in the Wigram-Magdala Link Bridge located in Christchurch, New Zealand. The bridge continues to stand today after enduring through a 7.8 magnitude earthquake in 2016, just months after it was built. The epicenter of the earthquake was close to the bridge, nonetheless, the bridge is expected to perform well during future seismic events.



Figure 2.9: Low-damage seismic design (courtesy of Mashal and Palermo 2019a).

Mashal and Palermo (2019b) also performed experimental work investigating the use of two different types of connections in a single precast column. The two connections are a member socket connection at the base connecting the columns to the footings and a grouted duct connection at the top connecting the columns to the cap beam. A half-scale test specimen is constructed with the intent to simulate a cast-in-place connection. Quasi-static cyclic loading is used during testing. The results from the experiment showed similar amounts of energy being dissipated in the plastic hinges of the columns. Several large cracks developed where the member socket connections are located and only a few large cracks at the grouted duct locations. The member socket connections exhibited a larger amount of strength deterioration than the grouted duct connections which is a result of the starter bars intentionally being de-bonded a length of 100 mm during the construction. The results indicate that including an unbonded length of the starter bars at the connection can reduce the amount of spalling and strength degradation in the plastic hinges. Figure 2.10 depicts an accurate representation of the tested column.

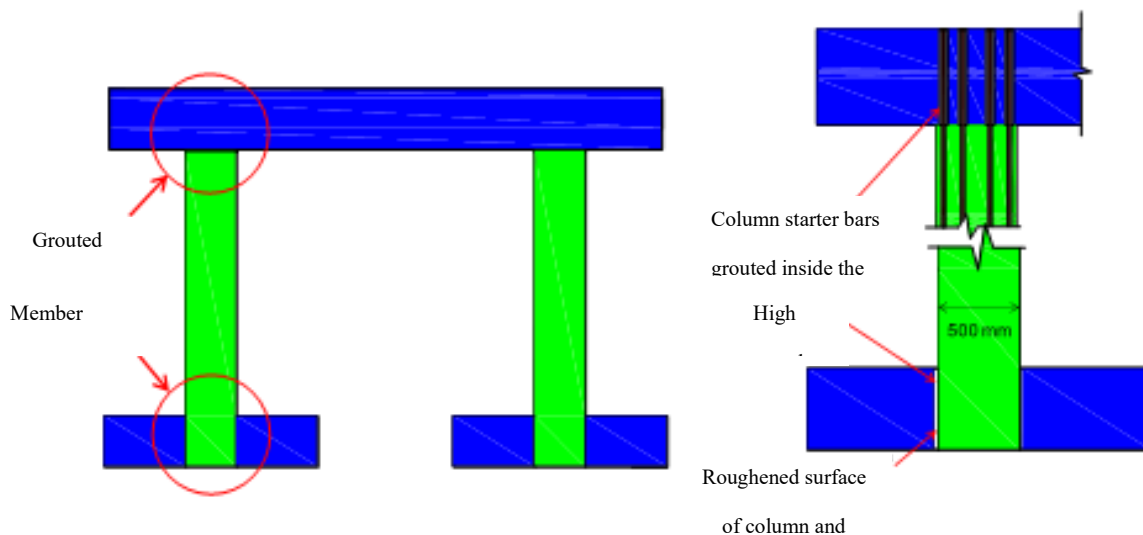


Figure 2.10: Precast bent with member socket and grouted duct connections (courtesy of Mashal and Palermo 2019b).

Zaghi and Saiidi (2010) experimented with the use of a pipe-pin connection. A pipe-pin connection is essentially a concrete-filled steel tube embedded at the end of a column. More details of the connection are shown in Figure 2.11. The observations and conclusions from this research are numerous. An observation is the column can rotate significantly without altering the performance of the connection. The mode failure that is assumed when designing the test specimens is a shear failure, however, if the pipe thickness is large the connection can fail in shear or a result of bearing failure of the concrete surrounding the pipe. One of the conclusions from the experiment is that the bearing strength of concrete against the pipe is two to six times the axial compressive strength of the concrete. After the experiment had concluded, the pipe-pin connection is disassembled, and the pipes are straight, intact, and damage-free; while the steel exterior can receive small dents located where the pipe came in contact with it. The finite element analysis used to model the pipe-pin connections returned results that are within 5% of the actual experimental data.

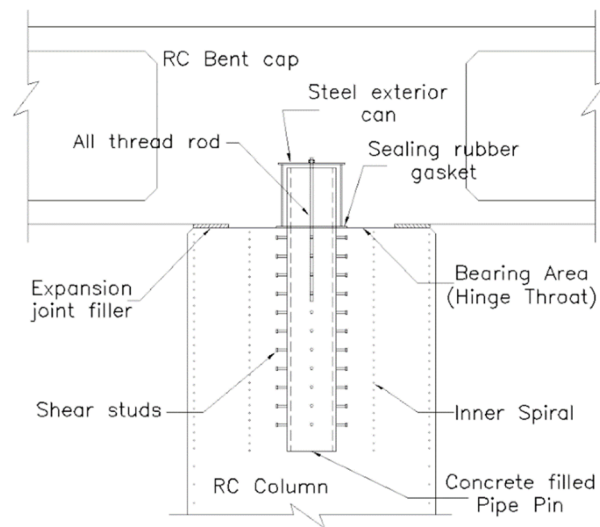


Figure 2.11: Pipe-Pin connection detail (courtesy of Zaghi and Saiidi 2010).

### **2.3 Conclusions**

A significant amount of research has been conducted to improve and expand the ABC scope and knowledge in seismic regions. The connections discussed include thin-walled steel columns, high strength precast concrete, pocket connections, socket connections, grouted ducts, grouted splice sleeves, mechanical bar splices, hollow precast reinforced concrete, precast shell column, dampers, and pipe-pin connections. Research for ABC in seismic regions continues to be performed to improve and/or simplify the construction of bridges. The following research aims to improve and simplify connections that are similar such as the grouted duct, pocket, socket, and pipe-pin connections.

## **Chapter 3: Cast-In-Place Cantilever Pier System**

### **3.1 Introduction**

This chapter presents the design, construction, and testing of a cast-in-place cantilever column. The purpose of a cast-in-place cantilever column is to set a benchmark to compare the experimental precast cantilever column. The design discussed in this chapter follows the 2017 AASHTO LRFD Design Specifications (AASHTO 2017). The cast-in-place test specimen provides a benchmark to compare to the precast cantilever column, which is discussed in chapter 4. This chapter also presents a prototype structure and the testing arrangement for both the cast-in-place and precast columns.

### **3.2 Prototype Structure**

Details of a typical bridge located in Idaho, US-95 over US-20/26, are shown in Figure 3.1 and are used to determine reasonable dimensions for the prototype structure. The prototype structure can be assumed to be built in South-East Idaho which is the most seismically active region in the state. To obtain the height and diameter of the prototype structure, the typical bridge details are scaled by a factor of approximately 0.25. The 0.25 scale is used to accommodate for the height restraints within the Idaho State University Structural LAB (SLAB). Applying the ~0.25 scale to the typical drawings reduces the height from 40 ft-10 in. to 10 ft-2.5 in. and the diameter from 6 ft-0.75 in. to 1 ft-6.2 in., as shown in Figure 3.2.

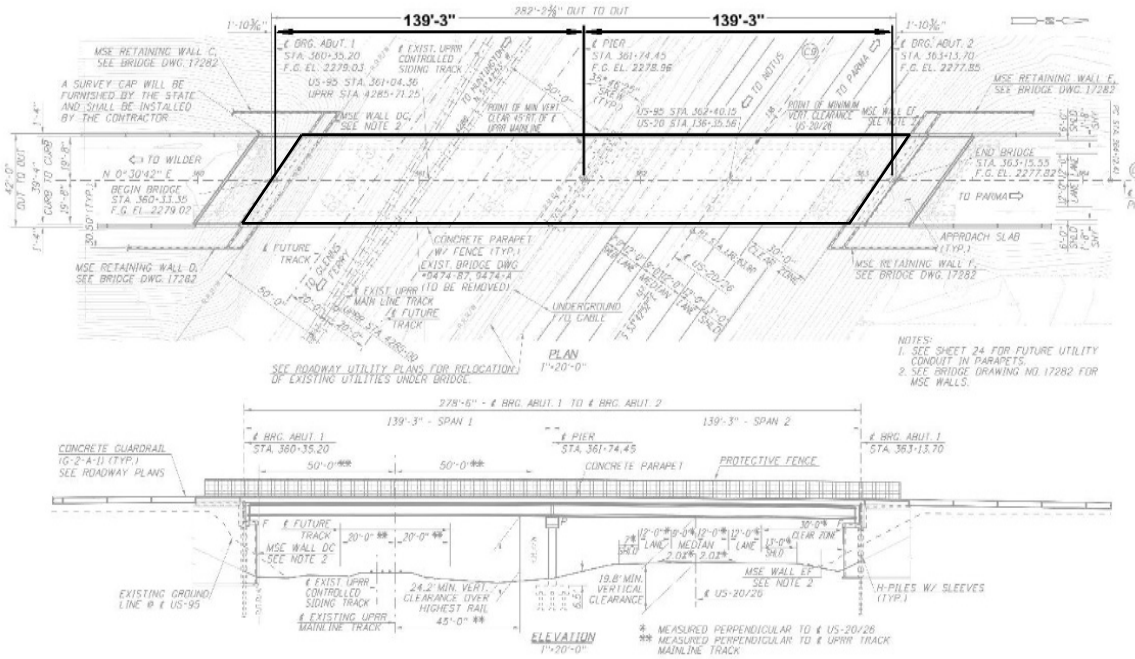
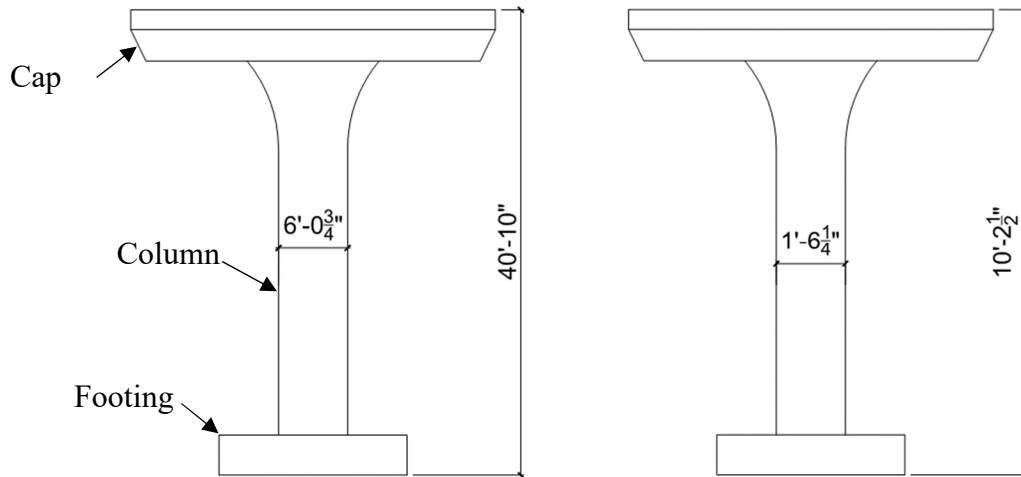


Figure 3.1: Detail views of a typical bridge in Idaho.



(a) full scale typical column

(b) 0.25 scale typical column

Figure 3.2: Scaling of a typical column.

After the typical drawings are appropriately scaled, the dimensions of the prototype column and footing are determined. The prototype structure will have an overall height of 10 ft-4 in. The footing size is 4 ft.x4 ft.x3 ft. (LxWxH). The logic behind the proposed dimensions is a result of

the SLAB's strong floor sleeve spacing and to ensure the footing will not fail before the column. The column is octagonal, having a diameter of 18 in., and a height of 7 ft-4 in. measured from the top of the footing up. Using a footing height of 3 ft, the distance from the top of the footing to the center of the actuator is 6.5 ft.

### 3.3 Testing Arrangement

The 0.25 (1/4<sup>th</sup>) scale cantilever columns are tested via a uniaxial lateral load. Using a uniaxial load to test the column represents a seismic event pushing and pulling the piers in the transverse direction. In this type of loading, the abutments are assumed to resist the loads in the longitudinal direction of the bridge. A 50-kip axial load is applied to the column throughout the entire testing procedure. The axial load is expected to vary slightly and is kept as close to a constant value as possible (deviation of less than approximately 5%). The deviation of the axial load is inconsequential to the testing results. This axial force corresponds to about 5% of the ultimate axial capacity of the column (axial ratio in % =  $\frac{50 \text{ kips}}{A_g f'_c} = 5\%$ ) where  $A_g$  is the gross cross-sectional area of the column and  $f'_c$  is the compressive strength of the concrete. The footing is assumed to be rigidly fixed to the ground (e.g. no soil-structure interaction). The appropriate loads are shown in Figure 3.3.

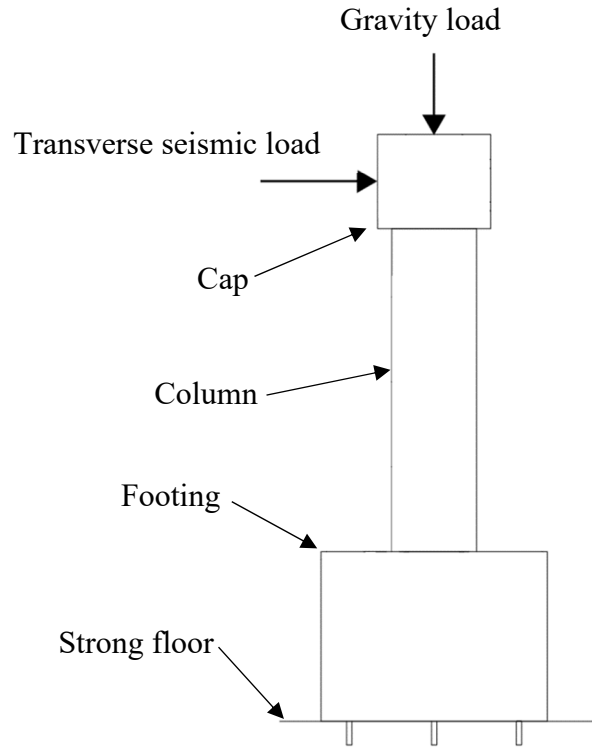


Figure 3.3: Testing arrangement.

### 3.4 Loading Protocol

The loading protocol established for the experiment is obtained from the American Concrete Institute (ACI) (ACI Committee 374 2013) which is a quasi-static cyclic loading protocol. The loading protocol begins at 0.5 of the yield displacement then proceeds to 1, 2, 3, 4 times of the yield displacement until failure, as shown in Figure 3.4.

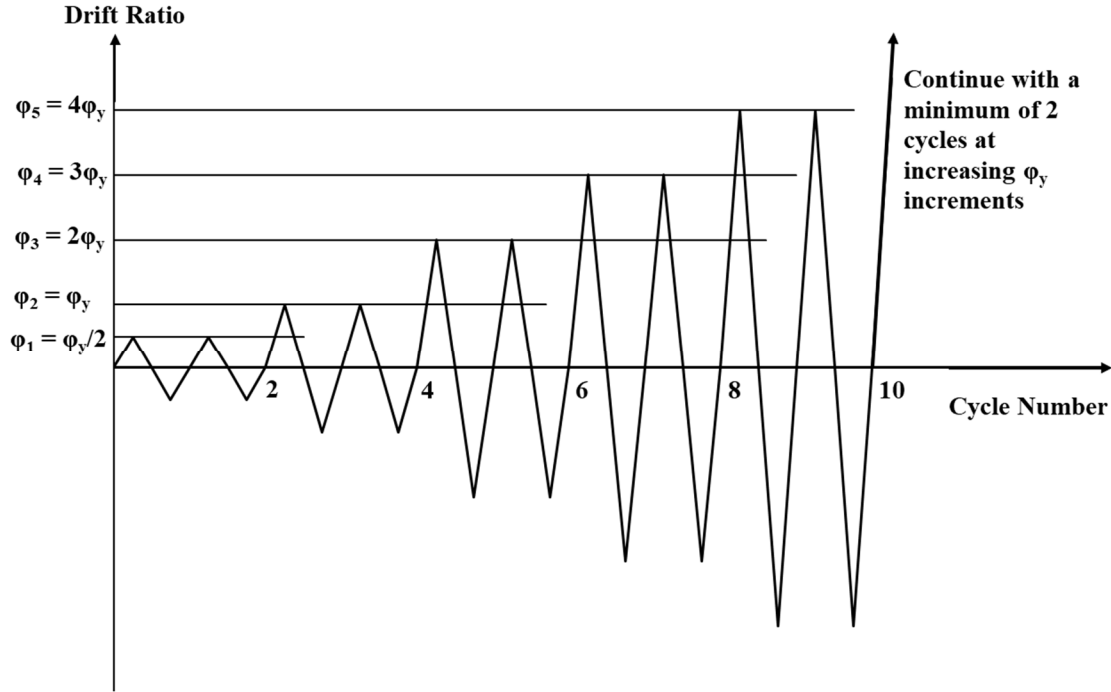


Figure 3.4: ACI Testing protocol.

The testing procedure is stopped when the column lateral capacity is reduced to 50% of the ultimate lateral force. The yield displacement is calculated using the following equation from Priestley et al. (2007):

$$\Delta_y = \frac{\phi_y(H + L_{SP})^2}{3} \quad (1)$$

Where  $\phi_y$  is the yield curvature, H is the height of the column (inches), and  $L_{SP}$  is the strain penetration length. The yield curvature is calculated using the equation shown below.

$$\phi_y = \frac{2.25(1.1F_y)}{E_s D} \quad (2)$$

Where  $F_y$  is the yield strength of the steel (ksi),  $E_s$  is the modulus of elasticity of the longitudinal rebars (ksi), and D is the column diameter (inches). The strain penetration is calculated using the following equation:

$$L_{sp} = 0.15(1.1F_y)d_{bl} \quad (3)$$

Where  $d_{bl}$  is the diameter of the longitudinal rebars (inches). Using the appropriate values, the yield displacement equation becomes:

$$\Delta_y = \frac{0.000284 * (78 + 7.425)^2}{3} = 0.692 \text{ in.}$$

Figure 3.5 shows a graphical representation of the loading protocol used during the testing procedure. The loading rate of the lateral actuator is 1 mm / sec with appropriate pauses to allow adequate time to observe and record any changes in the column during testing.

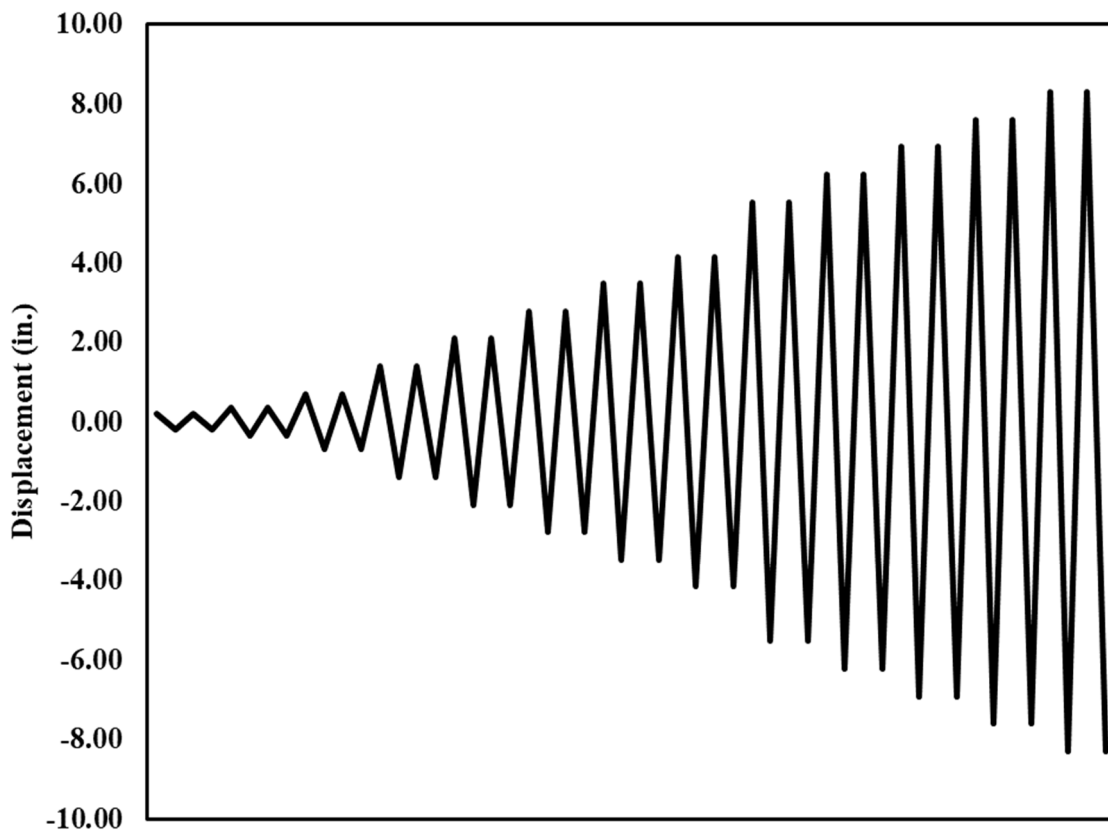


Figure 3.5: Loading protocol.

### 3.5 Instrumentation and Test Arrangement

A Campbell Scientific data acquisition system is used to collect important data points from the instruments such as load cells, strain gauges, and linear potentiometers. to analyze data after the testing procedure. A total of 39 instruments are used and are discussed in the following paragraphs and summarized in Figure 3.6. The testing arrangement is shown in Figure 3.7.

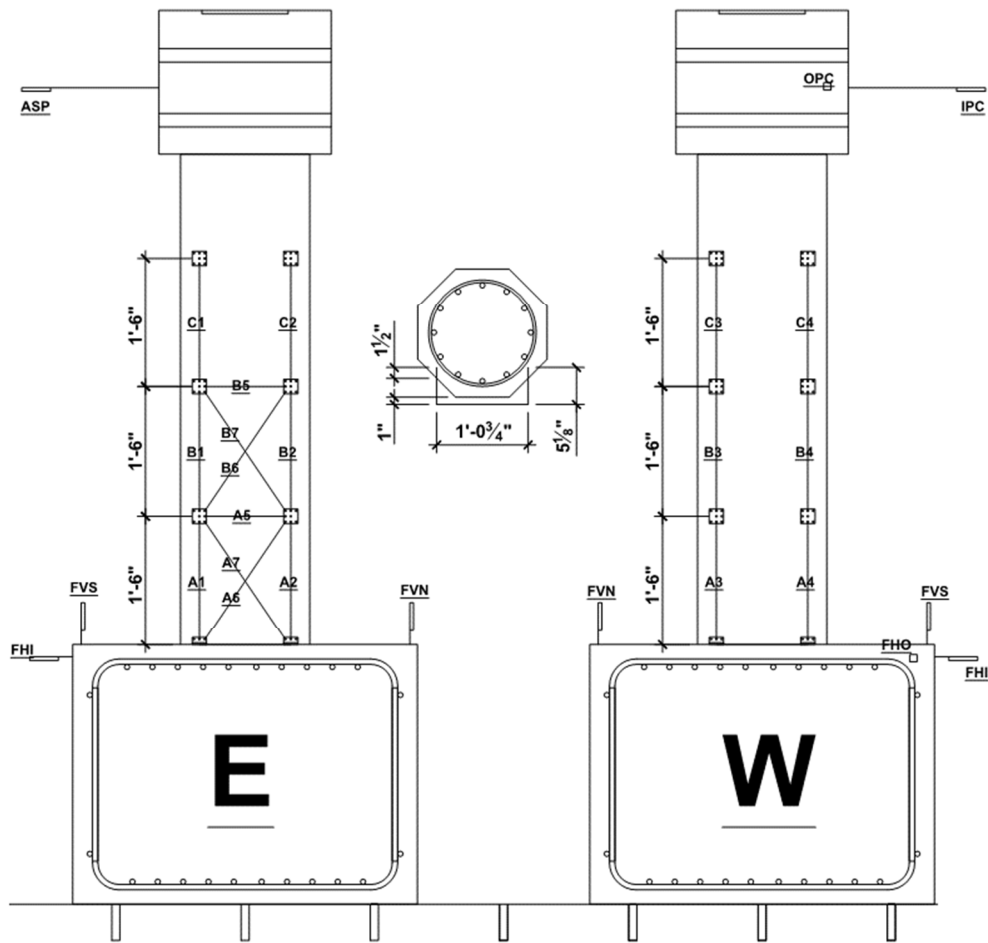


Figure 3.6: Column instrumentation.

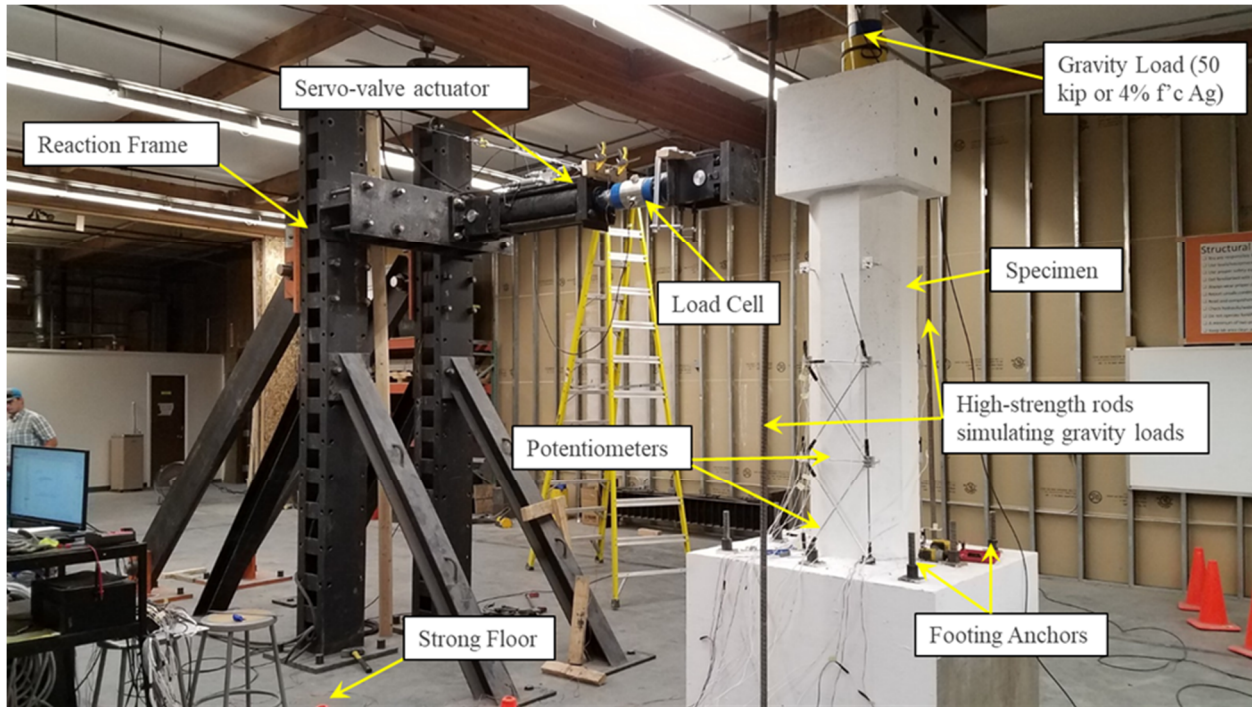


Figure 3.7: Typical test setup with load cells.

Lateral displacement at the top of the column is measured by string potentiometers shown as “IPC”, “OPC”, and “ASP” in Figure 3.6 and representing in-plane, out-of-plane, and actuator displacements, respectively. The spring potentiometers are mounted to a steel structure that is independent of the testing arrangement. Each of the instruments is connected to the column at the centerline of the actuator.

The lateral and vertical loads are measured using load cells. The lateral load cell is mounted between the hydraulic ram and the end of the actuator. The vertical load cell is mounted between a hydraulic jack and a steel beam which is resisting any vertical movement of the hydraulic jack. The footing displacement is monitored using horizontally and vertically mounted spring potentiometers shown as “FHI”, “FHO”, “FVN” and “FVS” in Figure 3.6 and representing footing horizontal in-plane, footing horizontal out-of-plane, footing vertical on the north end and footing vertical on the south end of the footing, respectively. The spring potentiometers are also mounted independently of the testing arrangement. Spring potentiometers are positioned on the

footing to measure any sliding or rocking of the footing that may occur. Data collected from these instruments are used to correct the lateral displacement at the top of the column.

The column deformation is obtained by using rod potentiometers, these are shown as “A”, “B”, and “C” symbols in Figure 3.6. The rod potentiometers are attached to the face and back of the column in three distinct zones: Zone A measured from the top of the footing to 18 in., Zone B measured from 18 in. to 36 in., and Zone C measured from 36 in. to 54 in. This deformation data is used to calculate the curvature of the section up the height of the column.

Elongation of the rebar within the column is monitored by strain gauges. The strain gauges are attached to the longitudinal rebar at the column to footing interface before pouring the concrete.

### 3.6 Material Properties

The 28-day compressive strength of concrete,  $f'_c$ , is designed to be 4 ksi. The yield strength of the longitudinal and transverse reinforcement of the rebar is 60 ksi with a modulus of elasticity of 29,000 ksi. The actual compressive strength of the concrete on the test day is summarized in Table 3.1.

Table 3.1: Actual  $f'_c$  values (ksi).

	Test 1	Test 2	Test 3	Test 4	Average
Footing	3.98	4.74	4.45	5.33	4.63
Column	5.28	4.68	4.97	4.46	4.85

### 3.7 Design of Cast-In-Place Specimen

Once the dimensions of the prototype structure have been established, the reinforcing steel is appropriately selected. The design of the reinforcing steel located in the column and footing is in

accordance with the 8<sup>th</sup> edition of AASHTO LRFD Bridge Design Specifications (AASHTO 2017).

The column base shear is selected so it does not exceed the capacity of the equipment in the SLAB. The base shear force has been selected to be 25-kip. Using this base shear, the longitudinal reinforcing has been determined to be twelve #6 rebars equally spaced in a circular pattern. For confinement purposes, a spiral having a pitch of 1.5 in. is used along the entire length of the column except where the footing reinforcing crosses the longitudinal bars. Where the footing reinforcement crosses the longitudinal bars, a mechanical splice is used on each side of the reinforcing bars. The minimum cover requirements of the spiral are 1.5 in. Guidelines on rebar hooks, bends, and development lengths are conservatively considered with all the rebar in the column.

The footing has reinforcing bars in each direction on both the top and bottom using #6 rebars. The rebar will have a spacing of roughly 3.5 in. between parallel bars and a minimum cover of 2 in. Guidelines on rebar hooks, bends, and development lengths are conservatively considered with all the rebar in the footing.

### **3.8 Column and Footing Capacities**

The moment capacity of the proposed cantilever column has been determined for a base shear of 25-kip. In the calculations, an 18 in. diameter column having 1.5 in. of cover, twelve #6 rebars, with #3 spirals are used. The compression strength of concrete,  $f'_c$ , is taken to be 4 ksi. The rebar properties are 60 ksi for the yield strength and 29,000 ksi for the modulus of elasticity. Using Response-2000 and SAP-2000 the yield moment capacity of the round column is calculated to be approximately 165 kip-ft without an axial load. Adding the 50-kip vertical axial force the moment capacity of the column increases to 187 kip-ft. A comparison of the two programs, before the axial

load, is shown in Figure 3.8. Using a moment arm of 6.5 ft., the shear demand from the moment capacity is approximately 25-kip which is the targeted base shear.

Referring to Figure 3.8, the reason why Response-2000 obtained a lower curvature is that the program does not have the capability to introduce spiral stirrups. Response-2000 thinks of the shear reinforcing as hoops compared to spirals which provide more confinement and ductility. In terms of capacity, the values from both programs are comparable. It should be noted that SAP-2000 uses a fiber model to compute the moment-curvature. A fiber model is a model with the capacity to perform an analysis with nonlinear behavior distributed across the cross-section of the element in the model.

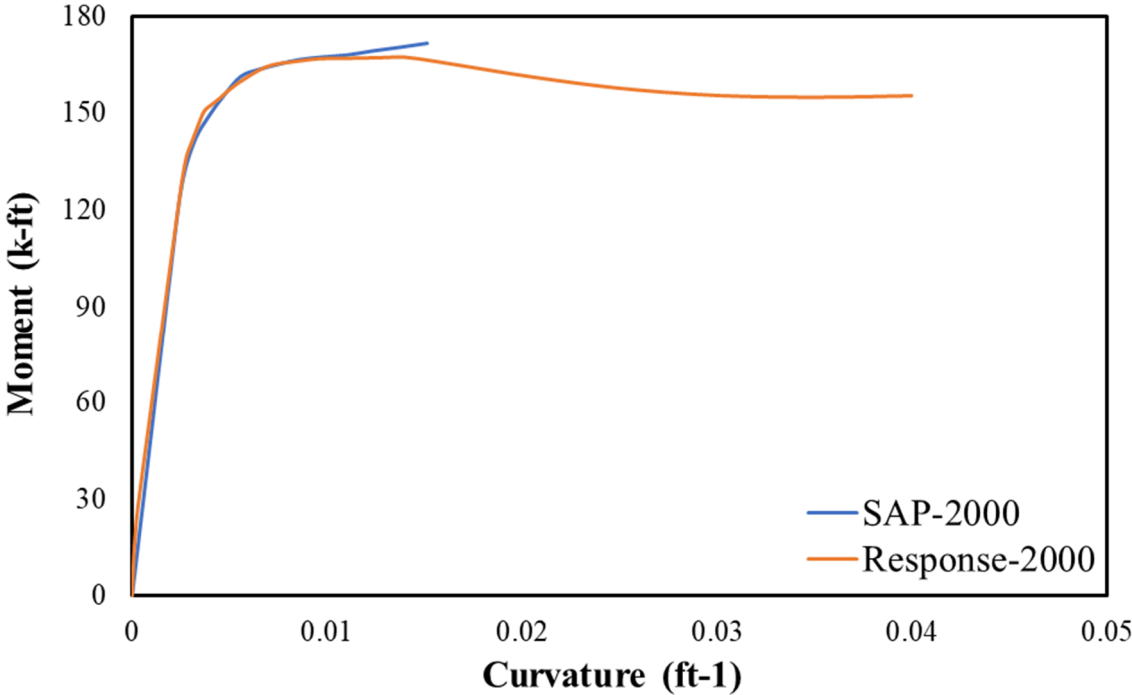


Figure 3.8: Comparison of Sap-2000 and Response-2000.

The parameters used to calculate the moment capacity of the footing are  $f'_c$  equal to 4 ksi, ten #6 rebars in both the top and bottom reinforcing layers with 2 in. of cover, rebar yield strength of 60 ksi, and a modulus of elasticity of 29,000 ksi. Using these values, the moment capacity is

calculated to be 1,000.2 and 998.5 kip-ft using SAP2000 and Response2000, respectively. An image depicting the footing is shown in Figure 3.9.

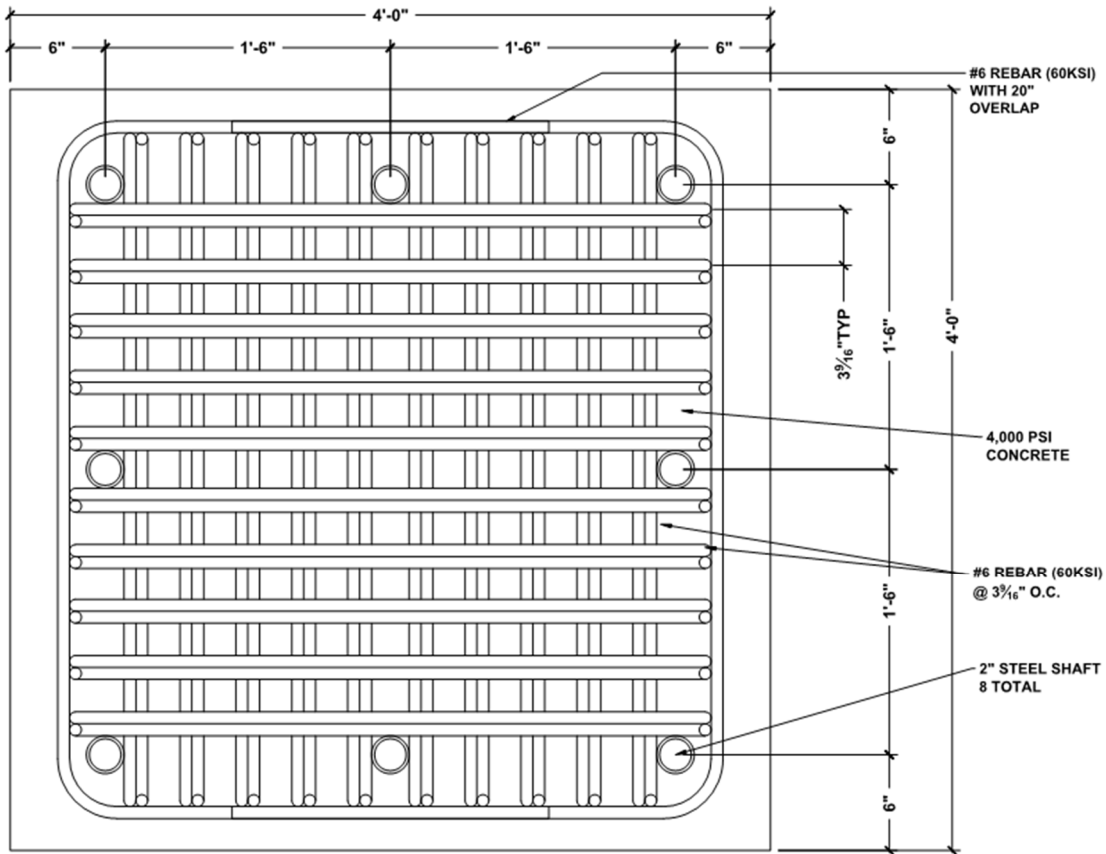


Figure 3.9: Cast-in-place footing reinforcing rebar layout.

In summary, the column is octagonal with a diameter of 18 in. The longitudinal reinforcement is comprised of twelve #6 rebars equally spaced and a #3 spiral having a pitch of 1.5 in. to confine the concrete. The calculated moment capacity of the column has been determined to be 165 kip-ft.

The footing is 4 ft. x 4 ft. x 3 ft. with ten #6 rebars reinforcing the top and bottom in each direction while maintaining a spacing of approximately 3.5 in. between the bars and 2 in. of cover. The moment capacity of the footing has been calculated to be roughly 1,000 kip-ft. Comparing the column moment capacity to the footing moment capacity, the column should reach its ultimate

strength before the footing is yielded. Figure 3.10 provides a visual representation of the test specimen.

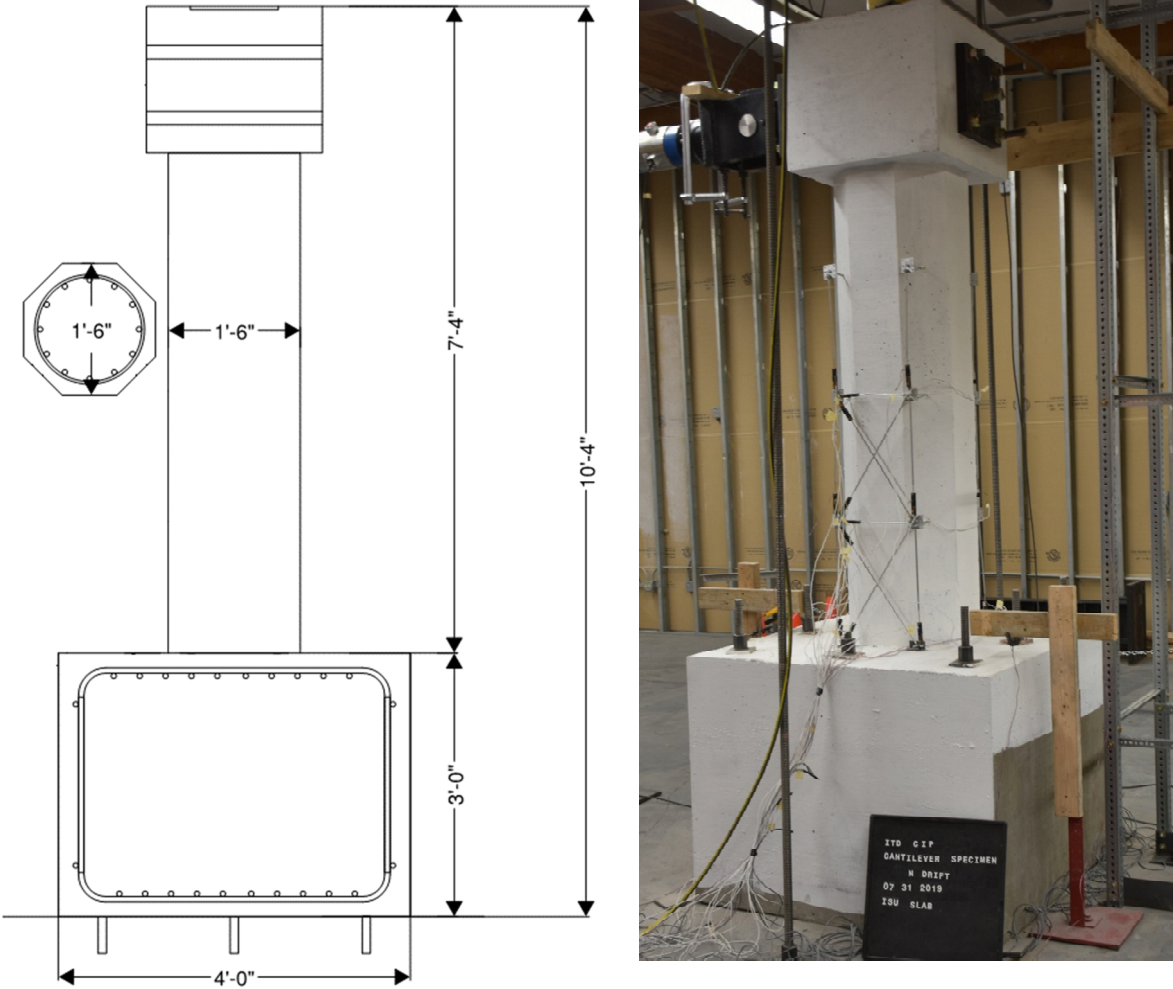


Figure 3.10: Cast-in-place test specimen.

### 3.9 Construction

Now that the design criteria have been determined, the construction of the cast-in-place cantilever column is next. To begin, the formwork is built. After the formwork is complete, rebar is cut to the required lengths and bent appropriately. Next, the rebar is tied together and the formwork is secured around the tied rebar (Figure 3.11a). Once the rebar and formwork are set, the concrete for the column footing is poured via Pocatello Ready Pour and ISU civil

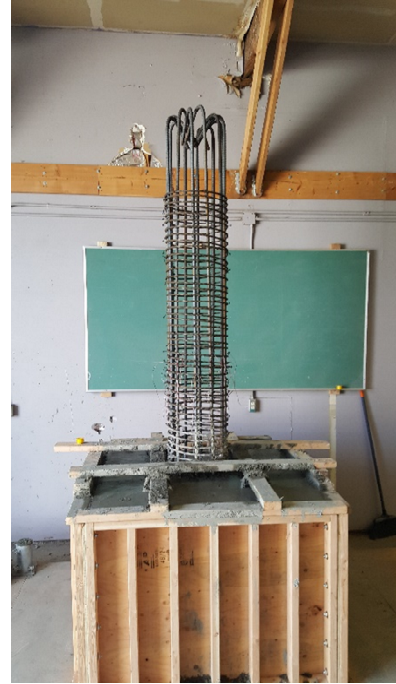
engineering students as shown in (Figure 3.11b). The footing is allowed to cure for three days before the formwork is removed. After the formwork is removed the concrete is covered with burlap and plastic and wetted daily to allow the concrete to continue curing in the most ideal conditions (Figure 3.11d). Once the footing reached seven days of curing, the footing is moved to the structural laboratory, the column formwork is assembled, column cap reinforcement is tied in place, then the column concrete is poured (Figure 3.11e). The column is allowed to cure for three days, then the formwork is removed. The column is then covered with burlap and plastic to ensure ideal curing conditions are present for 28 days. After the 28 days, the column is uncovered, painted, and instrumented in preparation to be tested. Images of the construction progress are shown in Figure 3.11.



a) Completed rebar cages



b) Pouring footing



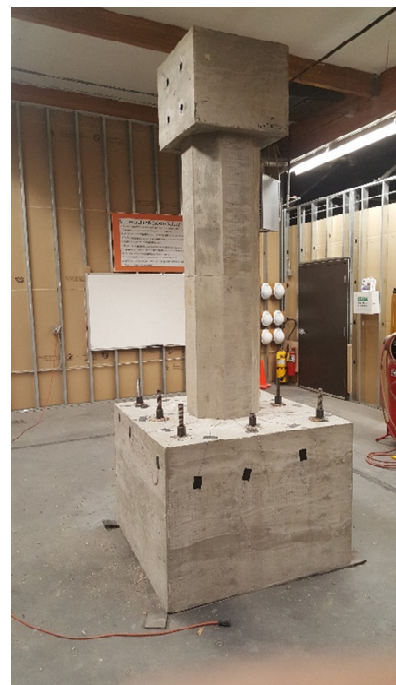
c) Finished footing



d) Footing curing



e) Column formwork set-up



f) Finished test specimen

Figure 3.11: Cast-in-place column construction images.

### 3.10 Experimental Testing

On the first cycle, hairline cracks appeared on the column within the first 0 – 18 in. from the base of the column where the plastic hinge is expected to form. During the second cycle, hairline cracks spread into the 18 – 36 in. of the column. By the third cycle, hairline cracks spread above the 36 in. mark and other lower cracks continued to spread and get larger. On the fourth cycle, a crack approximately 1mm wide developed at the column-footing interface. During the fifth and sixth cycles, cracking continued to develop with the base crack opening up to 4mm and the concrete began to spall. For the eighth, ninth, tenth, and eleventh cycles; all of the cracks continued to develop and the column concrete near the footing had all spalled off. During the twelfth cycle, there is a loud pop followed by a significant drop in lateral force, however, the drop in force is not significant enough to discontinue the test. The thirteenth cycle resulted in two additional loud pops which are followed by a significant drop in lateral force. The drop in lateral force is significant enough to terminate the testing procedure. The loud pops are a result of a longitudinal rebar breaking and the locations where they occurred are shown in Figure 3.12. Figure 3.13 shows images of the lower half of the column during the testing procedure. Throughout the testing procedure, the programmed displacement is not the actual displacement of the column. As a result of this, there is a cycle missing between cycles eight and nine to achieve the desired displacement. One of the reasons why the programmed displacement values are not the same as the actual values is because during the testing procedure the reaction frame is deflecting. Another reason is that the footing is sliding a little throughout the testing procedure. The sliding of the footing is documented via the instruments placed on the footing before the testing procedure. Using the collected data, the sliding of the footing is removed from the

column displacement to obtain the column displacement relative to the footing. A summary of the loading protocol is shown in Table 3.2.

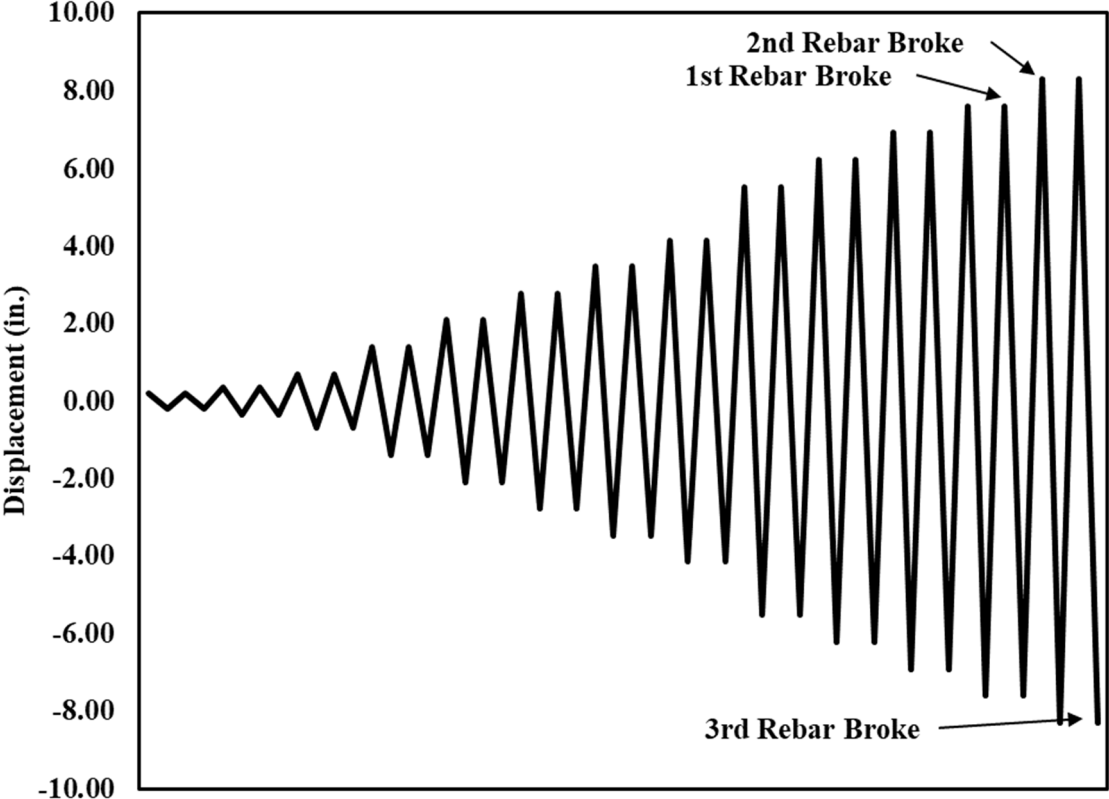


Figure 3.12: Loading protocol for the cast-in-place column.

Table 3.2: Summary of the cast-in-place loading protocol.

Cycle	Programed values		Actual pull values	
	Displacement (in.)	Drift (%)	Displacement (in.)	Drift (%)
1	0.20	0.26	0.16	0.20
2	0.35	0.45	0.26	0.33
3	0.69	0.88	0.46	0.59
4	1.38	1.77	0.86	1.10
5	2.08	2.67	1.50	1.93
6	2.77	3.55	2.15	2.76
7	3.46	4.44	2.84	3.64
8	4.15	5.32	3.50	4.49
9	5.54	7.10	4.86	6.23
10	6.23	7.99	5.54	7.10
11	6.92	8.87	6.23	7.99
12	7.61	9.76	6.94	8.90
13	8.30	10.64	7.71	9.89



### **3.11 Test Results**

After the testing procedure has concluded the data is analyzed. The maximum displacement of the column during the testing procedure is 7.7 in. The maximum load applied to the column during the testing procedure is 37.8 kip which corresponds to a 245.7 kip-ft moment capacity. Plots showing the Force vs. Displacement and Drift during the test are shown in Figure 3.14 and Figure 3.15, respectively. These plots show the yield displacement of the column and the corresponding base shear. The column reached its design flexural capacity of 25-kip and behaved in a ductile manner. Rebar ruptures can be spotted on the plots in Figure 3.14 and Figure 3.15 as a sudden reduction in capacity in the first quadrant. The backbone curve is also shown in Figure 3.16. Table 3.3 and Table 3.4 shows significant values from the cast-in-place column testing procedure.

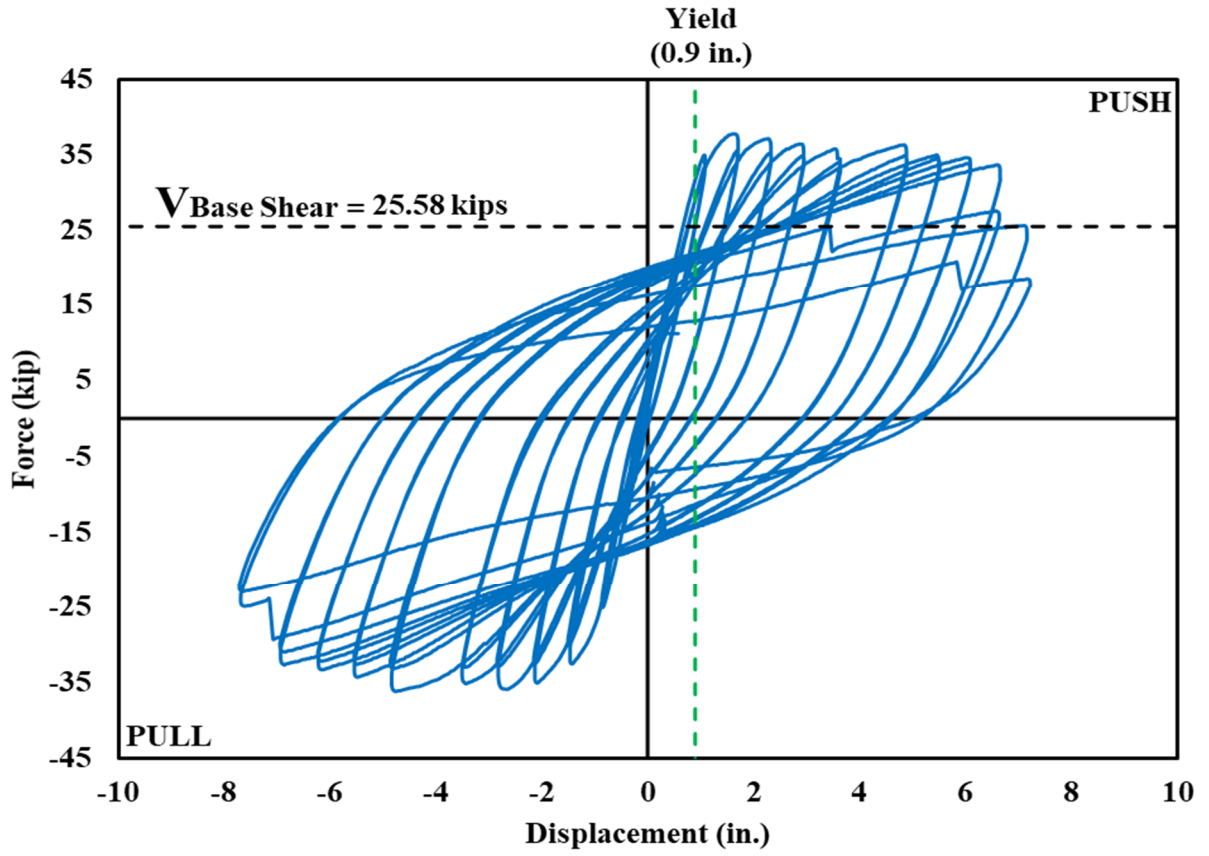


Figure 3.14: Force vs. Displacement plot for the cast-in-place column.

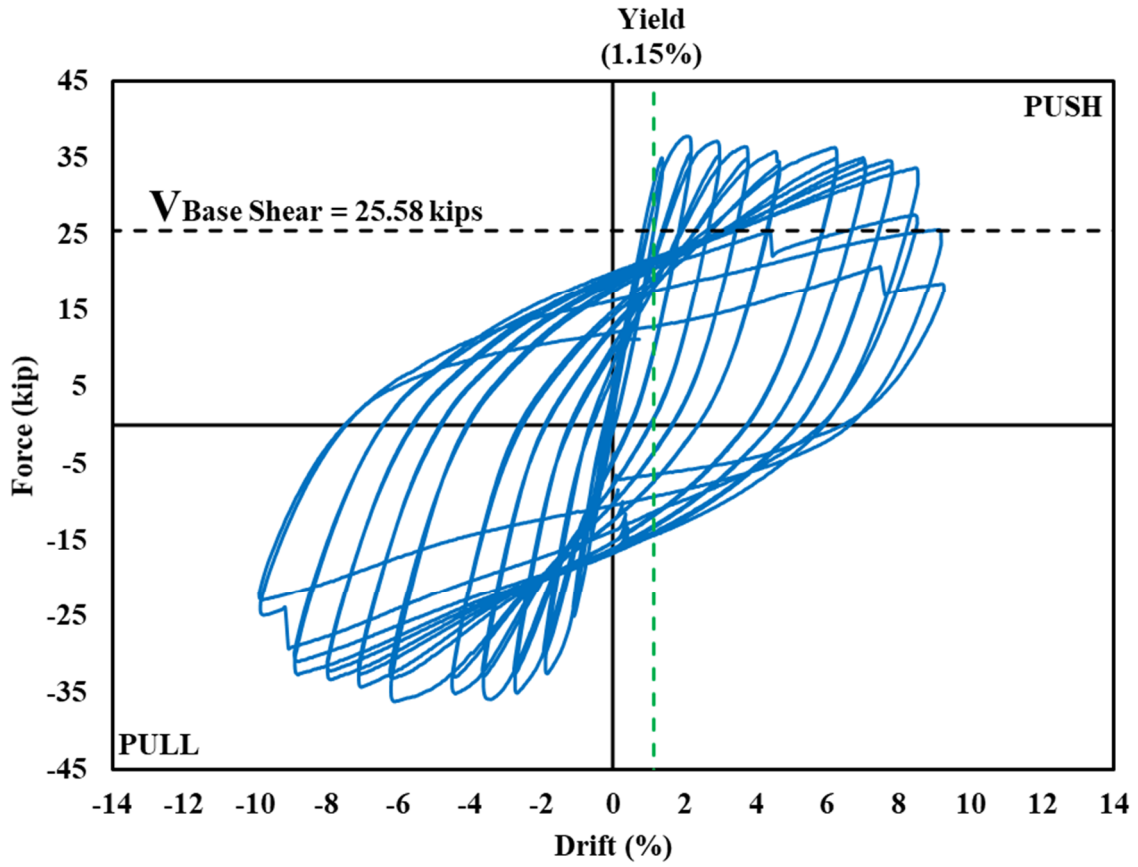


Figure 3.15: Force vs. Drift plot for the cast-in-place column.

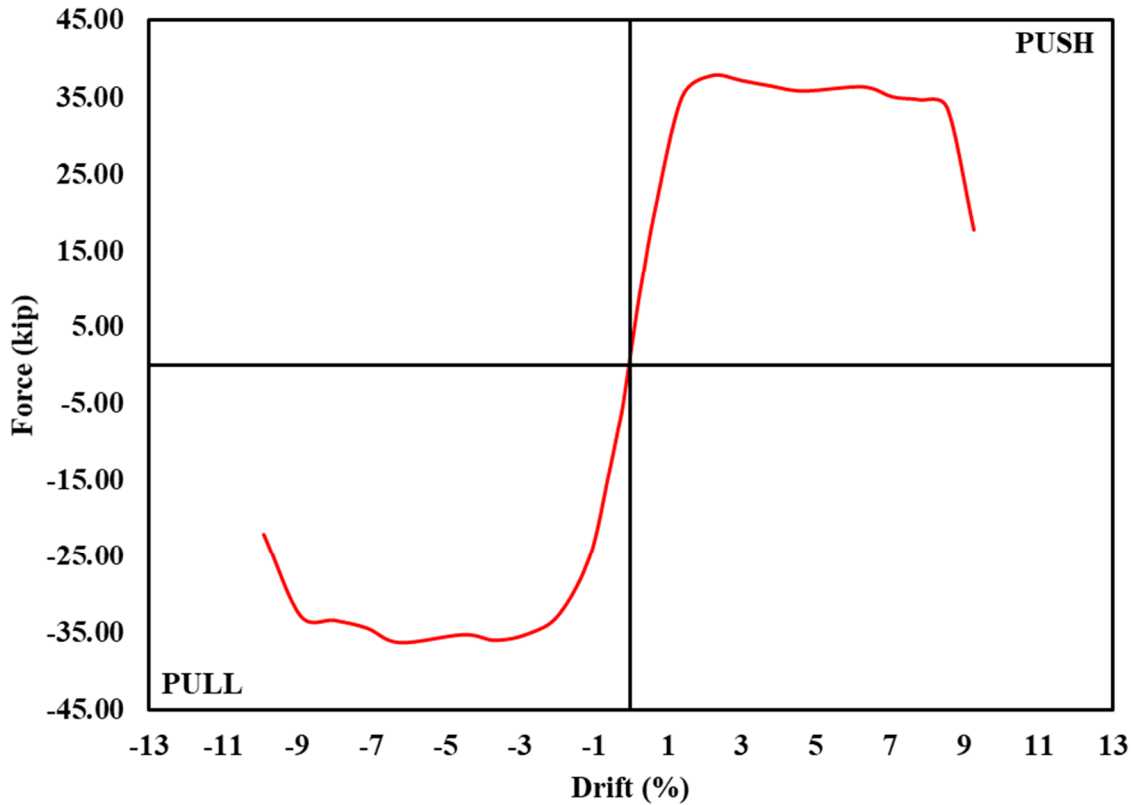


Figure 3.16: Backbone curve for the cast-in-place column.

Table 3.3: Damage observation from testing of the cast-in-place column.

Drift (%)					
Cracking	Spalling	Bar Rupture			End of testing
0.2	4.49%	1 <sup>st</sup>	2 <sup>nd</sup>	3 <sup>rd</sup>	9.89
		8.9	-9.89	9.89	

Table 3.4: Summary of the performance points from testing of the cast-in-place column.

Yielding				Ultimate Strength		
Predicted		Experimental		Experimental		
Drift (%)	Base Shear (kips)	Drift (%)	Base Shear (kips)	Drift (%)	Base Shear (kips)	Ductility*
0.88	25.58	1.15	35.1	9.89	37.8	7.4

\*Displacement ductility ( $\mu$ ) was 7.4 at the end of testing

The distribution of curvature along the height of the first 54 in. of the column is shown in Figure 3.17. The column is expected to yield and fail within the plastic hinge of the column. The plastic hinge is calculated by the following equation from Priestley et al. (2007):

$$L_p = 0.08H + l_{sp}$$

Where H is the column height and  $l_{sp}$  is the strain penetration. Strain penetration can be calculated using the following equation from Priestley et al. (2007):

$$l_{sp} = 0.15F_{ye}d_{bl} \quad 4$$

Where  $F_{ye}$  equals 1.1 times the longitudinal bar yield strength and  $d_{bl}$  is the diameter of the longitudinal bar. Using a yield strength of 60 ksi and a bar diameter of 0.75 in, the strain penetration becomes 7.4 in. Using a column height of 78 in. the plastic hinge can be calculated to be 13.7 in. Figure 3.17 shows that yielding occurred in the bottom 18 in. of the column. From 18" to 36 in. the column approached the yield point but never reached it. Because the region from 18 in. to 54 in. never reached the yield point, this region essentially remained elastic throughout the testing procedure.

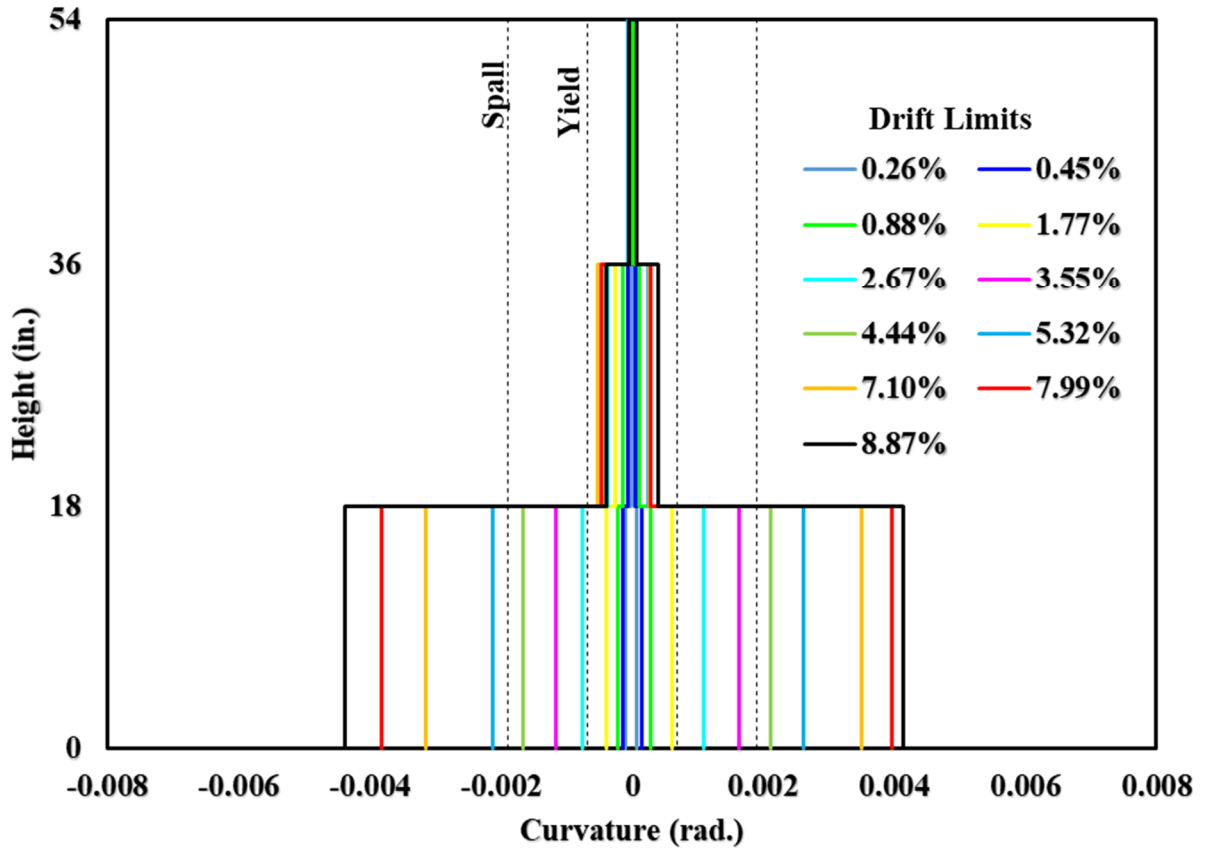


Figure 3.17: Cast-in-place curvature distribution.

The dissipated energy plot is shown in Figure 3.18. The dissipated energy is obtained by finding the area of each loop. The area is obtained using a MATLAB program. Each of the loops represents the total energy dissipated in a single cycle. Using input units of newtons and meters, the output energy units are of joules. For each drift cycle, the first loop dissipated more energy than the second because the column becomes weaker with each push-pull cycle. The largest difference in dissipated energy occurred during the 12<sup>th</sup> and 13<sup>th</sup> cycles which corresponds to the longitudinal rebars rupturing. The total dissipated energy during the testing procedure is 456 kJ.

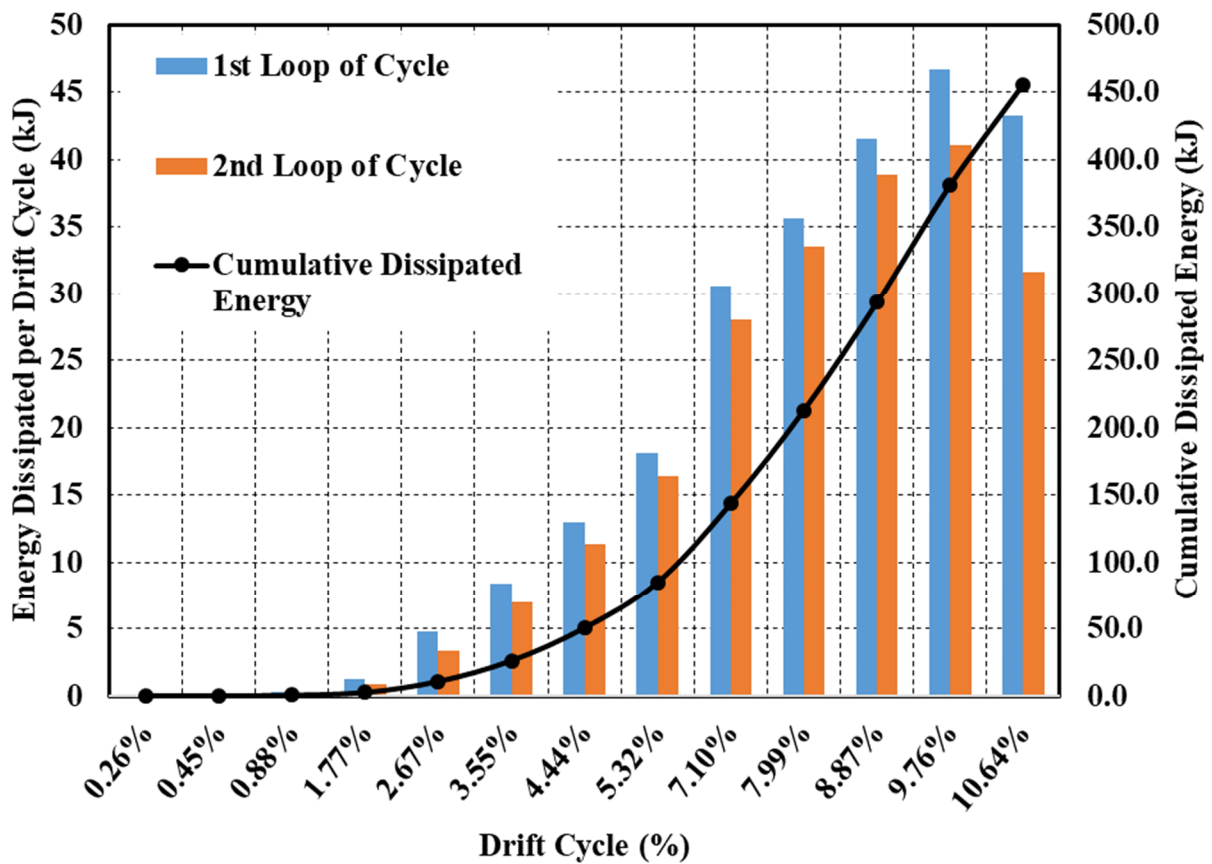


Figure 3.18: Dissipated energy plot for the cast-in-place column.

The area-based hysteretic damping is calculated using the following equation from Chopra (2017):

$$\xi_{area-based} = \frac{A_h}{2\pi F_m \delta_m} \quad (5)$$

Where  $A_h$  is the area of a loop in the force vs. displacement plot (N-m),  $F_m$  is the maximum force in the loop (N), and  $\delta_m$  is the maximum displacement in the loop (mm). To compare the hysteretic damping values to a theoretical model, a correction factor should be applied to convert the values to an equivalent time-history-calibrated hysteretic damping. The equation used to convert the area-based damping values to the time-history-calibrated hysteretic damping values is shown below from Priestley et al. (2007).

$$\xi_{hyst} = \xi_{area-based}[-0.018\xi_{area-based} + (0.0875\mu + 0.723)] \quad (6)$$

Displacement ductility is used to characterize the seismic response of a structure (Vielma and Mulder 2017) and is calculated using the following equation from Priestley et al. (2007):

$$\mu = 0.01(\%Drift) \frac{H}{\Delta_y} \quad (7)$$

Where  $H$  is the height of the column (m) and  $\Delta_y$  is the yield displacement (m).

A corrected area-based hysteretic damping plot is shown in Figure 3.19. As a comparison, the Takeda Fat, Takeda Thin, Elastic-Perfectly Plastic (EPP), and Ramberg-Osgood (RO) models have also shown in Figure 3.19. The Takeda Fat model represents a ductile reinforced concrete frame structure. The Takeda Thin model represents a ductile reinforced concrete wall or column structure. The Elastic-Perfectly Plastic (EPP) model represents an elastic model and the Ramberg-Osgood (RO) model represents a ductile steel structure (Priestley et al. 2007). The

equivalent viscous damping coefficients used are summarized Table 3.5 which are used in the following equation to obtain the hysteretic damping models from Priestley et al. (2007):

$$\xi_{hyst} = a \left( 1 - \frac{1}{\mu^b} \right) \left( 1 + \frac{1}{(T_e + c)^d} \right) \quad (8)$$

Where  $T_e$  is equal to the effective period, and  $\mu$  is the displacement ductility.  $T_e$  is taken to be equal to one to represent a column.

Table 3.5: Equivalent viscous damping coefficients for hysteretic damping component (courtesy of Priestley et al. 2007)

Model	a	b	c	d
EPP	0.224	0.336	-0.002	0.250
Takeda Thin	0.215	0.642	0.824	6.444
Takeda Fat	0.305	0.492	0.790	4.463
Ramberg-Osgood	0.289	0.622	0.856	6.460

Figure 3.19 shows the cast-in-place column having a relatively linear trend between the displacement ductility and the hysteretic damping. The hysteretic damping is approximately equal to the Takeda Thin model until a displacement ductility of 3.5. The cast-in-place column hysteretic damping curved achieved a value of 24.7% when the testing procedure is terminated.

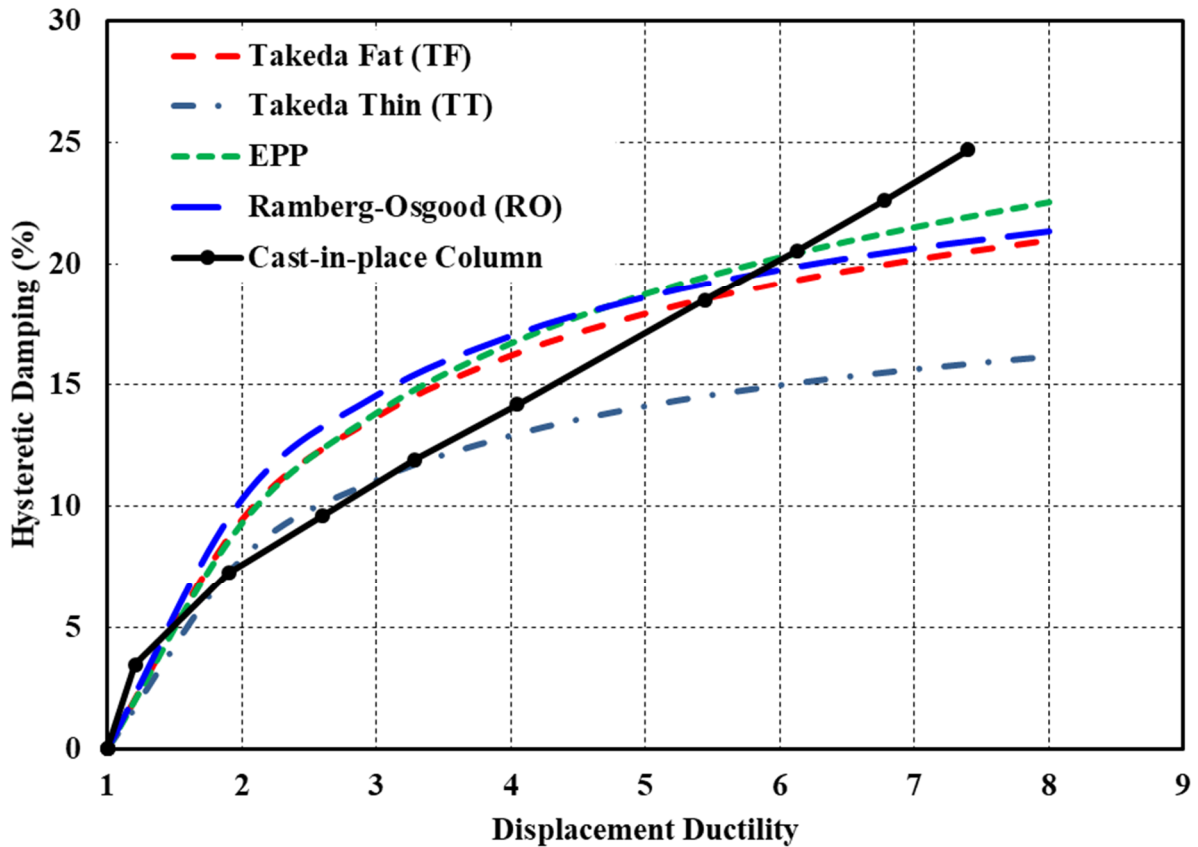


Figure 3.19: Corrected area-based hysteretic damping for the cast-in-place column.

### 3.12 Conclusions

The cast-in-place specimen is intended to be the benchmark for the precast solution that is explained in Chapter 4. The cast-in-place column is designed following the latest version of the AASHTO LRFD Bridge Design Specifications. The footing and column are constructed using traditional methods and materials. The column is tested under quasi-static loading until failure. The column behaved in a ductile manner. The column achieved its design base shear of 25-kip. The maximum base shear obtained during the testing procedure is 37.8-kip. The maximum displacement achieved is 7.7 in. which corresponded to a ductility of just below 7.5. Damage to the column during the test is within the first 18 in. of the column which is the expected plastic

hinge length for a well detailed and confined section. The total energy dissipated during the testing procedure is 456 kJ. A hysteretic damping plot showed that the column had similar values to a Takeda-Thin model up to a displacement ductility of slightly lower than 3.5. Above that, the column had higher values of hysteretic damping compared to a Takeda-Thin model

## **Chapter 4: Precast Cantilever Pier System**

### **4.1 Introduction**

This chapter presents the design, construction, and testing of a precast cantilever column. The precast cantilever column is intended to have the same capacity as the cast-in-place column in terms of resisting lateral force and drift capacity. Using precast elements will increase the rate of construction and reduce overall construction costs. One of the foreseeable issues is with regards to the proper alignment of the hollow structural section (HSS) made from steel that is incorporated into the design of the column. Proper alignment is crucial because small errors can have a significant impact during the assembly of the precast members. The design discussed in this chapter closely follows the 2019 WSDOT Bridge Design Manual (WSDOT 2019). The overall structural dimensions, testing arrangement, and instrumentation are identical to the cast-in-place column.

### **4.2 Connection Overview**

The pipe connection incorporates two HSS members. One of the HSS members is installed at the end of the precast column. Approximately half of the HSS is extending out of the precast column and with centering fins welded to the outside edge of the pipe and provides flexural capacity, shear capacity, and confinement for the concrete at the plastic hinge zone. The centering fins are for inserting the column into the footing and are not structurally important. Headed rebars are used to develop the strength of the rebar during a seismic event. Inserting the precast column into the footing is made possible by the second HSS member. The second HSS member will remain hollow until the column is inserted into it. An unbonded length on the HSS member is provided to reduce the stresses in the HSS member and emulate a cast-in-place behavior. An elastomeric bearing pad is placed between the column and footing to eliminate any undesired concentrated

loading between the two elements and allows the column to rock during smaller earthquakes to prevent cracking. After the protruding HSS column member has been inserted into the column HSS member, the remaining voids between the two elements are filled using a non-shrinkage grout via PVC pipes strategically placed to allow the grout to fill all of the desired voids without compromising the integrity of the footing or column before the grouting procedure. The grout is poured or pumped into the grout inlet pipe while the grout vent provides an escape for air that would otherwise be trapped. The gap between the two HSS members is approximately 1 in. to ensure the grout performs properly. Any of the rebars in the footing that are impeded by the HSS member in the footing are terminated using a welding bar coupler. Figure 4.1 shows an accurate representation of the pipe connection assembly. The column and footing design that is not impeded by the HSS members follows the AASHTO LRFD Bridge Design Specifications (AASHTO 2017).

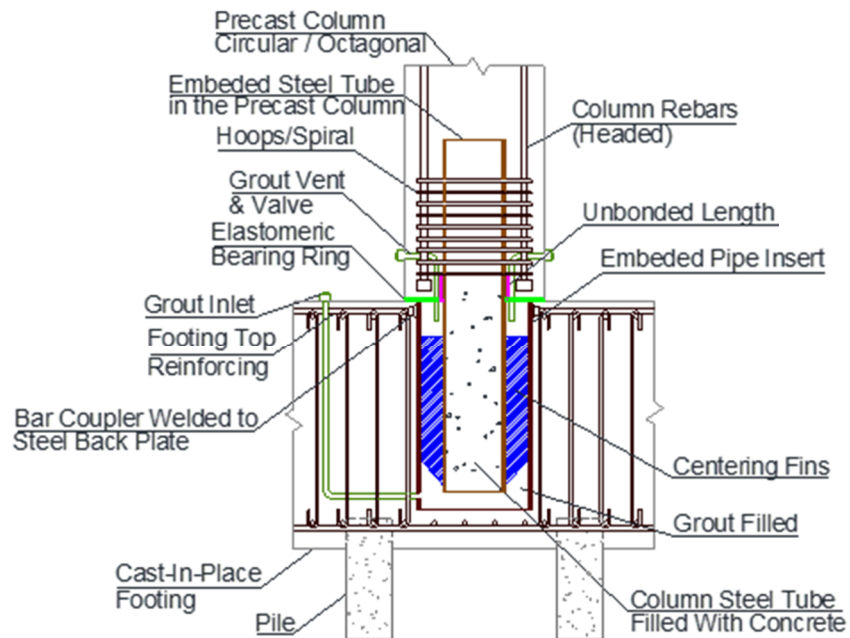


Figure 4.1: Pipe connection assembly.

### 4.3 Material Properties

The WSDOT design manual (WSDOT 2019) specifies materials to be used in the design of the concrete-steel tube members. First, the concrete should be class 5000P which is 5 ksi concrete.

The second material specification is to use ASTM A 709 GR 50 steel. ASTM A 709 GR 50 steel has a tensile strength of 65 ksi and a yield strength of 50 ksi (Chapel Steel 2018).

In this study, the 28-day compressive strength of concrete ( $f'_c$ ) is 4 ksi. Through trial and error, the HSS member selected to obtain a moment capacity approximately equal to the cast-in-place member is HSS8.625x0.625. The properties of an HSS8.625x0.625 member is 42 ksi yield strength ( $F_y$ ), 58 ksi ultimate strength ( $F_u$ ), and a modulus of elasticity ( $E$ ) of 29,000 ksi. The dimensions of the HSS member are 8.625 in. for the outside diameter and a pipe thickness of 0.581 in. The actual compressive strength of the concrete and grout on the test day is summarized in Table 3.1.

Table 4.1: Actual  $f'_c$  values for the precast column (ksi).

Element	Test 1	Test 2	Test 3	Average
Footing/Column	3.80	4.18	3.93	3.97
Grout	5.41	5.42	5.37	5.40

#### 4.4 Design of Precast Specimen

The Concrete Filled Steel Tube (CFST) at the interface of the column and footing (e.g. where the CFST is unbonded) is the ductile link. This section is designed to provide flexural and shear capacities as well as confinement for the plastic hinge. The footing and the section of the column above the unbonded region are designed to remain elastic. For a simplified approach, the contribution of the unconfined cover concrete towards the flexural resistance of the CFST section is ignored. The size of the CFST for the ductile link was selected to closely match the flexural capacity of the cast-in-place specimen (e.g. similar base shear).

The flexural design procedure for CFST has several resistance factors to use for a variety of situations. The resistance factor used in this design is equal to one, which is used for an extreme event limit state. To ensure the pipe is not subject to local buckling before developing the strength of the pipe, the WSDOT (2019) advises the use of the following equation for members subject to plastic forces:

$$\frac{D}{t} \leq 0.15 \frac{E}{F_y} \quad (9)$$

Where  $D$  is the outside diameter and  $t$  is the wall thickness of the HSS member. For the selected HSS member the  $D/t$  is equal to 14.85 and  $0.15E/F_y$  is equal to 103.57. In common practice, both  $D$  and  $t$  should be adjusted for corrosion but due to the short life of the testing timeline, this is considered irrelevant. The nominal compressive strength of the concrete-filled HSS member is determined by using the following equation:

$$P_0 = 0.95f'_c A_{concrete} + F_{y,steel} A_{steel} \quad (10)$$

For the selected HSS member  $P_0$  has been calculated to be 949 kips. The equation used to determine the nominal moment capacity is shown below:

$$M_n(y) = \left( c(r_i^2 - y^2) - \frac{c^3}{3} \right) * 0.95f'_c + 4ct \frac{r_m^2}{r_i} F_y \quad (11)$$

Where c is equal to one half the chord length of the tube in compression and is calculated using

$$c = r_i \cos \theta \quad (12)$$

Where  $r_i$  is equal to the radius to the inside of the steel tube and  $\theta$  is calculated using:

$$\theta = \sin^{-1} \left( \frac{y}{r_m} \right) \quad (13)$$

Where y is the distance from the centroid of the specimen to the neutral axis during a seismic event and  $r_m$  is the radius to the center of the steel tube. Because the neutral axis is expected to be equal to the centroid the variable y is taken equal to zero. Once y is determined, the variables  $\theta$  and c are calculated to be  $0^\circ$  and 3.73 in., respectfully. The nominal moment capacity is calculated then calculated to be 1842 kip-in. or 142.5 kip-ft.

The variable y can be used if the centroid and neutral axis are not equal to each other. If this is the case, the column is not perfectly vertical. Determining the variable y is difficult if the column is not vertical and is more of a guess. Figure 4.2 shows the plastic stress distribution of the steel and concrete when the variable y is not equal to zero. Material forces can be obtained by solving the following equations simultaneously.

$$\sum F_x = P + T_s - C_c - C_s = 0 \quad (14)$$

$$\sum M_o = \frac{(C_c + C_s)(r + y)}{2} - \frac{T_s(r - y)}{2} = 0 \quad (15)$$

$$A_s = A_{sc} + A_{st} \quad (16)$$

$$T_s = A_{st} F_y \quad (17)$$

$$C_c = 0.95 A_{cc} f'_c \quad (18)$$

$$C_s = A_{sc} F_y \quad (19)$$

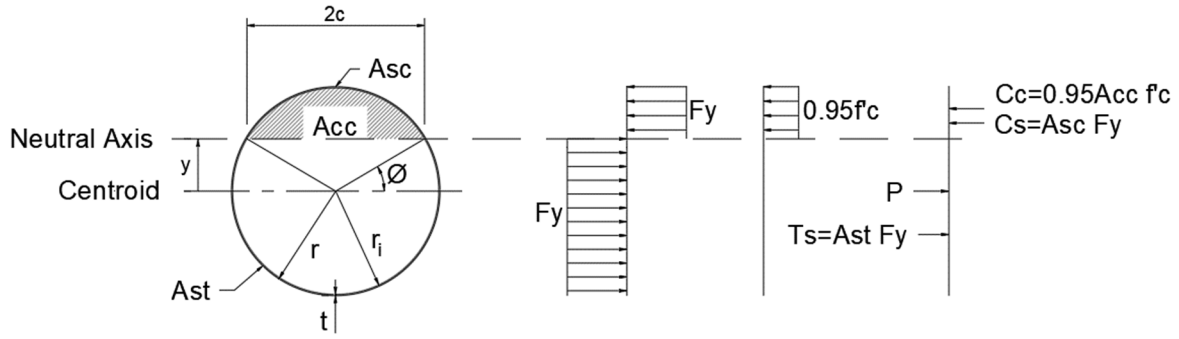


Figure 4.2: Plastic Stress Distribution.

Where  $P$  is the axial load.  $A_{st}$ ,  $A_{cc}$ , and  $A_{sc}$  are the area of steel in tension, area of concrete in compression, and the area of steel in compression, respectively. The first equation sums the forces in the x-direction where  $P$  is the axial load,  $T_s$  is the resultant force of the steel in tension,  $C_c$  and  $C_s$  are the resultant compressive concrete and steel forces, respectively. The second equation sums the moments about the centroid where  $r$  is equal to the radius of the pipe measured to the outside of the pipe. The third equation ensures the area of steel in compression and area of steel in tension is equal to the total area of steel.

To calculate the base shear, the following equations were used:

$$\phi V_n = \phi(V_c + V_s) \quad (20)$$

Where  $\phi$  is the capacity reduction factor equal to 0.75,  $V_n$  is the net shear,  $V_c$  is the shear in the concrete, and  $V_s$  is the shear in the HHS steel member.  $V_c$  is calculated using the following equation from McCormac (2014):

$$V_c = 2\lambda\sqrt{f'_c}b_wd \quad (21)$$

Where  $\lambda$  is a modification factor equal to one,  $f'_c$  is the compressive strength of concrete, and  $b_wd$  is the area of concrete. Using appropriate values, the equation becomes:

$$V_c = 2(1)\sqrt{4000}(43.74) = 5,532 \text{ lb}$$

$V_s$  is calculated using the following equation from AISC (2011):

$$V_s = 0.6F_y A_g / 2 \quad (22)$$

Where  $F_y$  is the yield strength of the steel and  $A_g$  is the gross cross-sectional area of the member.

Using the appropriate values, the equation becomes:

$$V_s = \frac{0.6(42,000)(14.68)}{2} = 184,968 \text{ lb}$$

And the net shear equation becomes:

$$\phi V_n = 0.75(5,532 + 184,968) = 142,875 \text{ lb}$$

Two methodologies are considered to determine the embedment of the pipe into the column and footing. The methodologies used are proposed by WSDOT and Edward P. Wasserman (Wasserman and Walker 1996). The WSDOT equation includes an annular ring, as shown in Figure 4.3, and is used to ensure full plastic behavior of the concrete-filled steel tube is as follows:

$$l_e \geq \sqrt{\frac{D_o^2}{4} + \frac{5.27DtF_u}{\sqrt{f'_c}}} - \frac{D_o}{2} \quad (23)$$

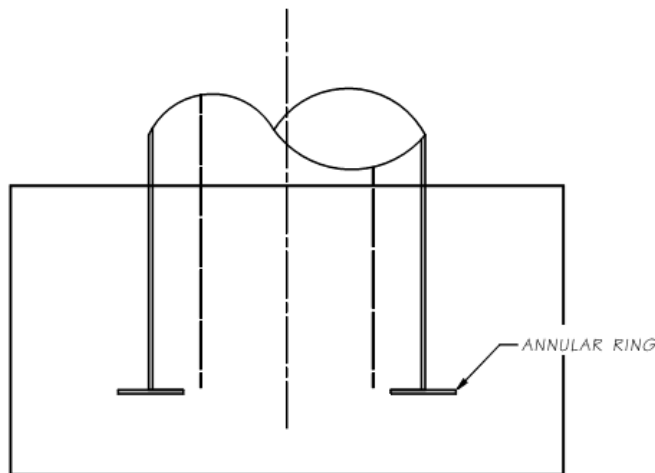


Figure 4.3: Embedment length with embedded ring.  
(courtesy of WSDOT)

Where  $l_e$  is the calculated embedment length,  $D_0$  is the outside diameter of the annular ring,  $D$  is the diameter of the embedded pipe,  $t$  is the wall thickness of the embedded pipe,  $F_u$  is the ultimate strength of the embedded pipe, and  $f'_c$  is the compression strength of the concrete with all variables in terms of kip and inches. Eliminating the annular ring from the equation, e.g.  $D_0 = 0$ , the equation becomes:

$$l_e \geq \sqrt{\frac{5.27DtF_u}{\sqrt{f'_c}}} \quad (24)$$

Incorporating the appropriate values into the equation an embedment length of 27.7 in. is adequate.

For the embedment length proposed by Wasserman, the following equations are used:

$$l_e = \frac{2F_y Z}{\sqrt{700f'_c b}} \quad (25)$$

$$b = \frac{d\sqrt{\pi}}{2} \quad (26)$$

Where  $F_y$  is the yield strength of the embedded pipe,  $Z$  is the plastic section modulus of the embedded pipe,  $f'_c$  is the compressive strength of the concrete, and  $d$  is the outside diameter of the embedded pipe. Incorporating these values into the equations an embedment length of 23.7 in. As a result of these two equations an embedment length of 2 ft-3 in. is used as the HSS embedment length.

The column longitudinal reinforcing is comprised of twelve #6 headed rebar equally spaced in a circular pattern. For confinement purposes, a spiral having a pitch of 1.5 in. is used along the entire length of the column with a mechanical splice located at each end of the spiral. The spiral should maintain 1.5 in. of cover.

A portion of the HSS member just inside the concrete column is left unbonded. The unbonded length is a way to force the HSS over a certain length above the footing and encourage a rocking

type (gap opening) motion at the base of the column during smaller movements (i.g. small earthquakes) without yielding of the CFST. Also, during larger movements/earthquakes, the unbonded length distributes the inelastic strain over a longer length of the CFST which enhances the low-cycle fatigue performance and ultimate displacement ductility of the connection.

The unbonded length of the HSS member is determined using PRESSS Design Handbook (Pampanin 2010). All of the equations from the PRESSS Design Handbook are in metric units. To begin the elongation of the mild steel from the cast-in-place column testing procedure is determined to be roughly 0.88 in. (22.4 mm). The strain penetration is then calculated using the following equation:

$$l_{sp} = 0.022F_y d_{bl} \quad (27)$$

Where  $F_y$  is equal to the yield strength and  $d_{bl}$  is equal to the diameter of the reinforcing bars. Using a value of 60 ksi (413.7 MPa) for  $F_y$  and 0.75 in. (19.05 mm) for  $d_{bl}$ , the strain penetration is calculated to be 6.83 in. (173.4 mm). Strain in the steel is then calculated using the following equation:

$$\varepsilon_s = \frac{\Delta}{l_{ub} + 2l_{sp}} \quad (28)$$

Where  $\Delta$  is the elongation of the rebars and  $l_{ub}$  is the unbonded length. The elongation of the rebars during the cast-in-place testing procedure was determined to be 0.81 in., from the data collected at a 8.87% drift. Using a value of 0 for the unbonded length and 0.81 in. (22.4 mm) for the elongation of the rebars, the strain is calculated to be 5.90% for the cast-in-place column. Using  $\Delta = 0.81$  in. (22.4 mm),  $F_y = 42$  ksi (289.6 MPa),  $d_{bl} = 0.581$  in. (14.76 mm) or the pipe thickness, and an unbonded length of 3 in. (76.2 mm), the strain in the HSS member is determined to be 7.75%. As a result of this calculation, the unbonded length is determined to be 3 in. Figure 4.4 shows the details of the precast column.

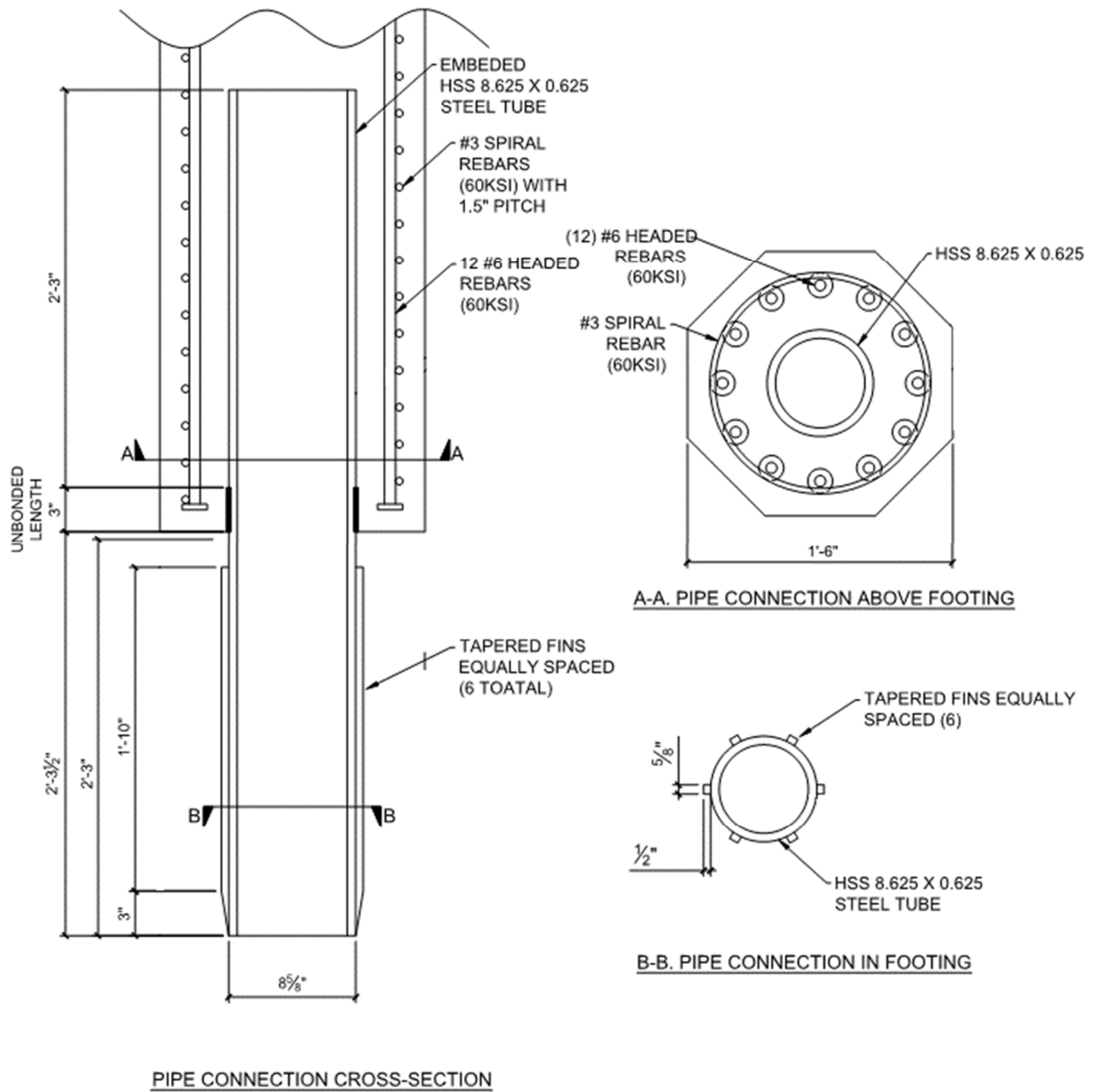


Figure 4.4: Precast column detail.

After the precast testing procedure, the gap opening for the precast column is measured to be 0.55 in. (13.97 mm) on cycle 10 or 5.96 in. (7.64% drift) after which the instruments were removed from the column. Using the values previously discussed, the actual strain in the HSS member is determined to be 5.29%.

The elastomeric bearing pad is designed according to the AASHTO LRFD Bridge Design Specifications (AASHTO 2017). The elastomeric bearing pad is designed for a column with a diameter of 18 in., 50-kips axial load, and has a 10.5 in. diameter hole through the center of the bearing pad. Using these parameters and shear modulus of 0.13 ksi, a plain elastomeric bearing pad with a thickness of 0.5 in. is determined to be sufficient.

The footing for the precast column was designed to remain elastic throughout testing. The footing design is similar to the cast-in-place column. The changes that are made to the footing are to accommodate for assembling the column to the footing. An HSS10.75x0.5 having a length of 28 in. is installed into the top of the footing such that the top of the HSS member is level with the top of the footing. All of the footing reinforcing rebars that are affected by the HSS member are adjusted by incorporating a 90° bend with an appropriate amount of development length to accommodate this change. Guidelines on rebar hooks, bends, and development lengths are conservatively considered with all the rebar in the footing. An image depicting the precast column assembly to the footing is shown in Figure 4.5.

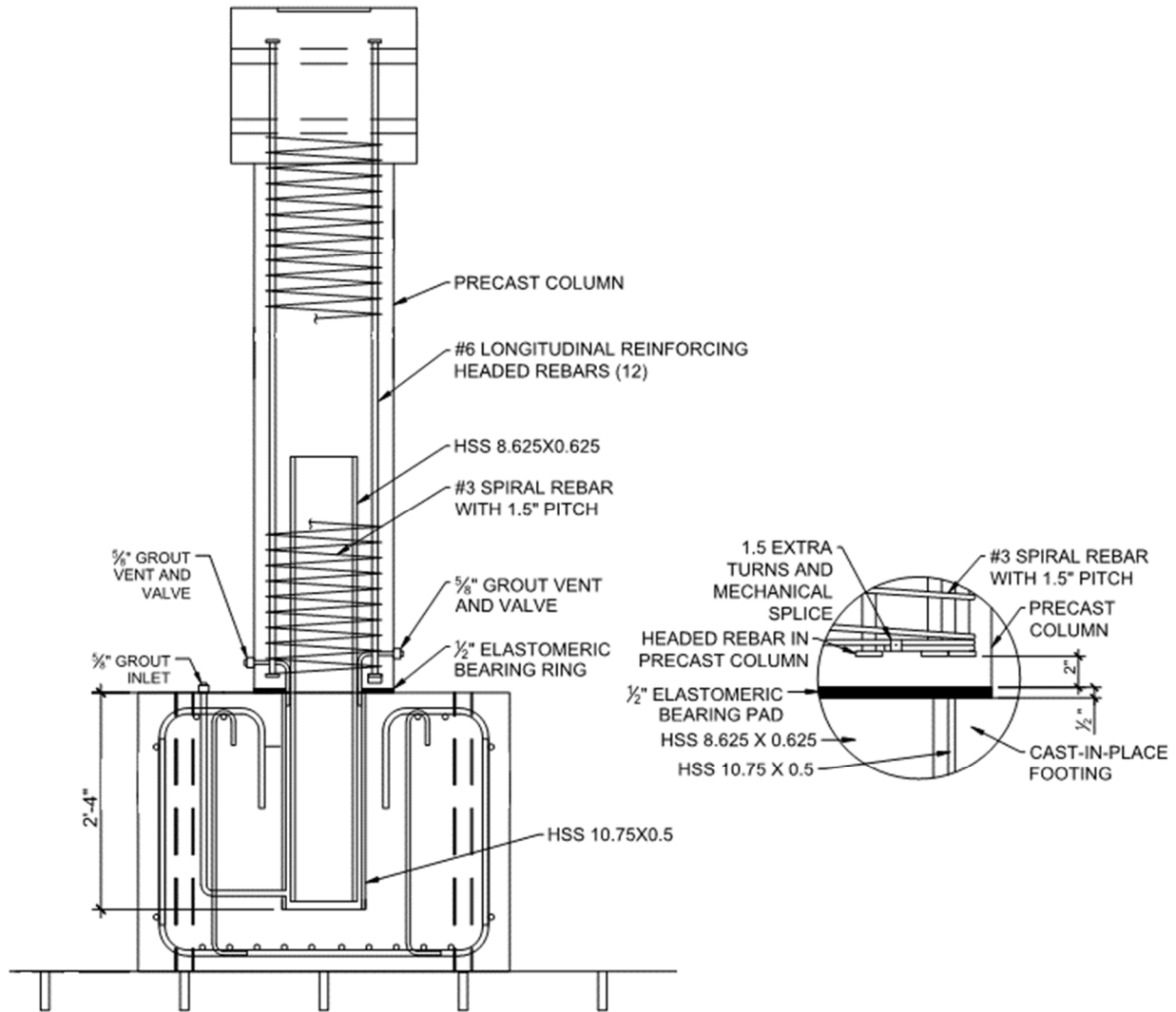


Figure 4.5: Precast column to footing assembly.

In summary, the precast column is octagonal with a diameter of 18 in. The longitudinal reinforcement is comprised of twelve #6 headed rebar equally spaced with a #3 spiral having a pitch of 1.5 in. to confine the concrete. The HSS8.625x0.625 has a development length of 2 ft-3 in. into the column and footing with 3 in. of un-bonded length at the footing to column interface. The calculated moment capacity of the concrete-filled HSS member is 142.5 kip-ft This corresponds to a base shear of 21.9-kips for a cantilever height of 6.5ft. The footing is 4 ft. x 4 ft. x 3 ft. with ten #6 rebar reinforcing the top and bottom in each direction while maintaining a spacing of approximately 3.5 in. between the bars and 2 in. of cover. An

HSS10.5x0.5 member is embedded into the footing to receive the precast column. The moment capacity of the footing is expected to be roughly 1,000 kip-ft. Comparing the column's plastic hinge moment capacity to the footing moment capacity, the CFST at the interface of the column and footing is designed to be the ductile link with inelastic deformation.

#### **4.5 Construction**

For the construction of the precast specimen, the formwork from the cast-in-place test specimen is modified slightly to accommodate for the HSS members and is reused. Rebar is cut to the required lengths and bent appropriately. Next, the rebar is tied together and the formwork is secured around the tied rebar (Figure 4.6a). Before installing the HSS members, the exposed surfaces are sandblasted to remove paint and roughen the surface to obtain a better bond with the concrete. The precast column is poured horizontally because of the restrictions over dropping height for concrete as well as difficulty in keeping the column standing upright with a pipe protruding from the end (Figure 4.6b). Once the HSS members, rebar, and formwork are set, the concrete for the column and footing is poured (Figure 4.6c-d). Both the footing and column are allowed to cure for three days before the formwork is removed. After the formwork is removed the concrete is covered with burlap and plastic and wetted daily to allow the concrete to continue curing in the most ideal conditions. Once the concrete reached seven days of curing, the concrete footing is moved to the Structural LAB (SLAB). After another seven days, the column is also moved to the structural laboratory and grouted into place, painted, and instrumented in preparation to be tested. Images of the construction progress are shown in Figure 3.11. Before the column assembly, the exposed surfaces of the HSS member embed in the footing is roughened and lightly wetted in preparation for the grouting process. The grout used to fill the void between the two HSS elements is SikaGrout®-328. After mixing the grout per the grout

mixing instructions, the mixture is promptly poured into a Polyvinyl Chloride (PVC) pipe that extended from the top of the column to the footing grout inlet pipe. After a few moments grout is observed to be pouring out of both of the grout outlet pipes (Figure 4.6e). The grout is allowed to flow freely through the grout ducts for approximately 30 seconds to remove any air pockets that may be trapped. Once the grout had flowed for approximately 30 seconds the PVC pipe connecting to the footing grout inlet is removed and the grout is allowed to cure for 7 days before the testing protocol is initiated. Figure 4.6f shows the completed precast specimen.



a) Footing rebar cages



b) Column rebar assembly



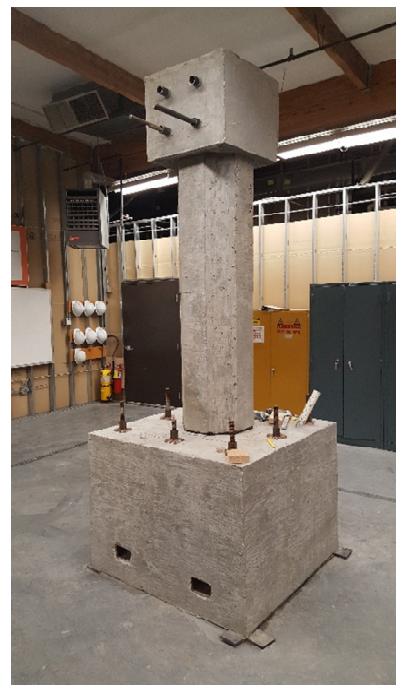
c) Finished footing



d) Finished column



e) Grout flowing out of grout vent



f) Finished test specimen

Figure 4.6: Precast column construction images.

#### 4.6 Experimental Testing

The testing protocol and arrangement for the precast column is similar to that of the cast-in-place column. The instrumentation of the precast column is similar to the cast-in-place; however, the precast column had a total of four strain gauges, two on each side, located on the column HSS member at the extreme push and pull locations. On each extreme location of the HSS member, a strain gauge is placed on the exposed surface about one inch from the surface of the concrete and the other was placed approximately one inch inside of the concrete surface as shown in Figure 4.7. Arranging the strain gauges in this manner makes so each of them is one inch from the column to footing interface.

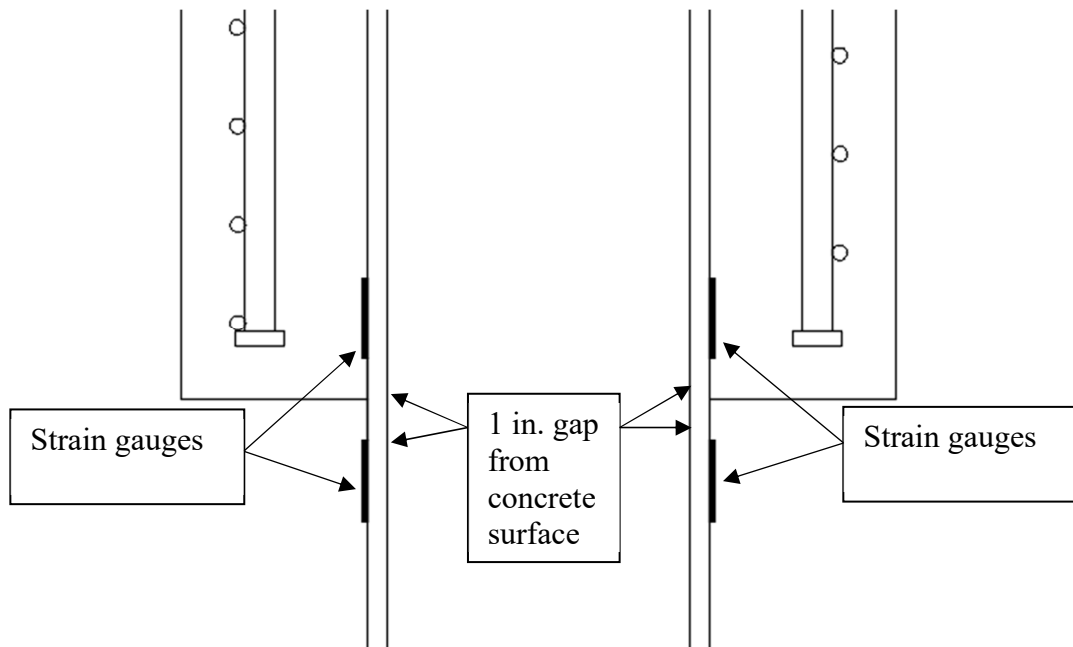


Figure 4.7: Location of strain gauges on the HSS member.

After testing began, for the first two cycles, there are no visible hairline cracks. On the third cycle, hairline cracks are visible below the first 0 – 36 in. of the column which continued to develop into the fourth cycle. During the fifth cycle, concrete spalling began to occur on the north face of the column and by the seventh cycle, spalling occurred on the south face as well. Cracking and spalling continued to develop until the 11<sup>th</sup> cycle. On the 11<sup>th</sup> cycle, the unbonded length of the pipe is visible on both the north and south faces of the column. On the 13<sup>th</sup> cycle, an elephant leg behavior is observed on the exposed HSS member. During the 15<sup>th</sup> cycle, approximately 10 kips of lateral force is lost as a result of the pipe beginning to degrade. On the 16<sup>th</sup> cycle, another significant drop in lateral force is observed due to a fracture of the pipe on one side and the testing procedure was terminated due to safety reasons. The fracture is located very close to the interface, the buckling of the pipe is obvious on the other side as shown in Figure 4.8.



Figure 4.8: Pipe failure during the testing procedure.

Figure 4.9 shows the loading protocol used during the testing procedure. Similar to the cast-in-place column, the programmed displacement is not the actual displacement due to the actuator frame deflecting and the footing sliding. The actual deflection of the column for the push and pull cycles are within 0.05 in. of each other. To keep the same loading protocol as the cast-in-place there is a missing cycle between cycles eight and nine as shown in Figure 4.9. The same

procedure is followed to correct the column displacement data which is summarized in Table 4.2.

Figure 4.10 shows images of the lower half of the column during the testing procedure.

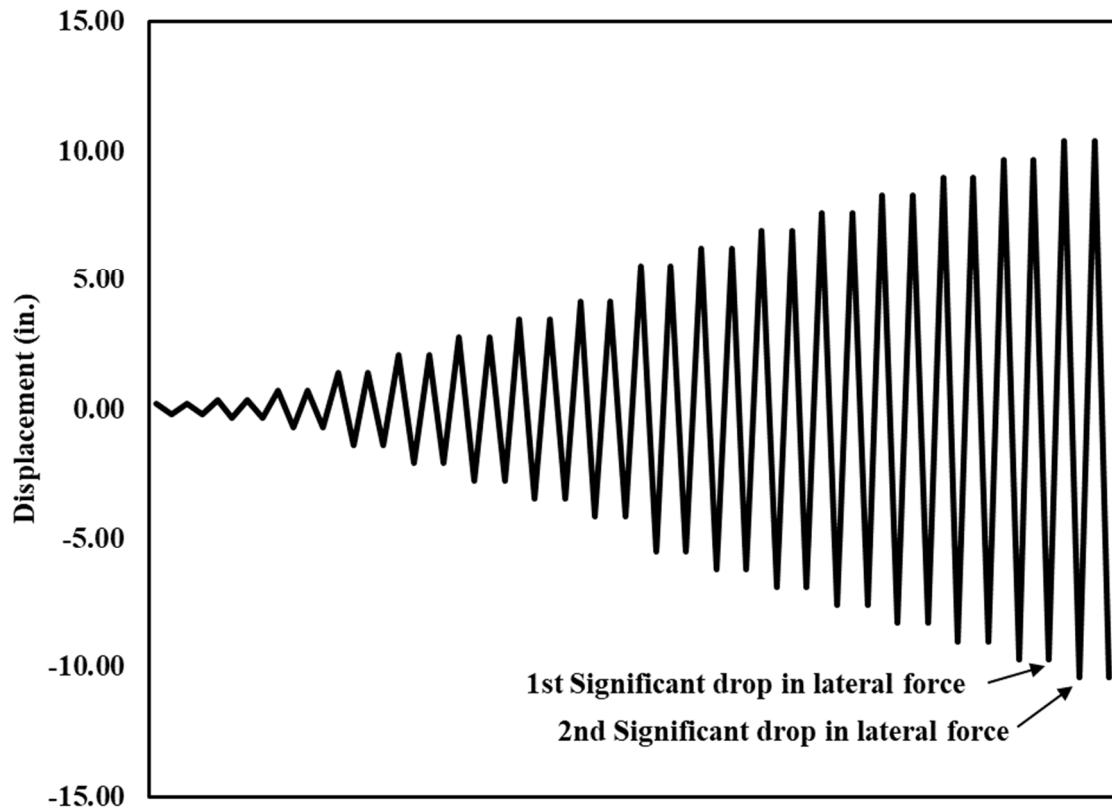


Figure 4.9: Loading protocol for the precast column.

Table 4.2: Summary of performance values from testing of the precast column.

Cycle	Programed values		Actual pull values	
	Displacement (in.)	Drift (%)	Displacement (in.)	Drift (%)
1	0.20	0.26	0.14	0.18
2	0.35	0.45	0.23	0.29
3	0.69	0.88	0.47	0.60
4	1.38	1.77	0.92	1.19
5	2.08	2.67	1.53	1.96
6	2.77	3.55	2.15	2.75
7	3.46	4.44	2.82	3.62
8	4.15	5.32	3.36	4.30
9	5.54	7.10	4.87	6.24
10	6.23	7.99	5.37	6.89
11	6.92	8.87	6.09	7.80
12	7.61	9.76	6.78	8.69
13	8.30	10.64	7.45	9.55
14	9.00	11.54	8.14	10.44
15	9.69	12.42	8.87	11.37
16	10.38	13.31	9.57	12.27



a) 0.45% drift



b) 2.67% drift



c) 5.32% drift



d) 8.87% drift



e) 13.27% drift



f) Failed HSS member

Figure 4.10: Images from the precast testing procedure.

#### 4.7 Test Results

After the testing procedure has concluded the data is analyzed. The maximum displacement of the column during the testing procedure is 9.57 in. which corresponds to a 12.27% drift ratio. The maximum load applied to the column during the testing procedure is 41.2 kip which corresponds to a 267.8 kip-ft moment capacity. The column showed a stable response with significant energy dissipation. When the column reached the peak load, a reduction in the lateral load is observed as a result of the column engaging the cover concrete. The lateral load continues to slowly decrease with each cycle because the HSS pipe is experiencing cyclic fatigue. As the testing procedure progresses a significant drop in lateral force is observed which is a result of the pipe buckling or “Elephant Leg” behavior. On the next cycle the lateral force approaches the same lateral force then decreases as the pipe fails. Plots showing the Force vs. Displacement and Drift during the test are shown in Figure 4.11 and Figure 4.12, respectively. These plots show the yield displacement of the column and the design base shear of the column which was reached before the pipe failed. The backbone curve is also shown in Figure 4.13. The initial kink in the backbone curve is a decompression point or point at which a gap began to open as a result of the column rocking. Table 4.3 and Table 4.4 shows significant values from the precast column testing procedure.

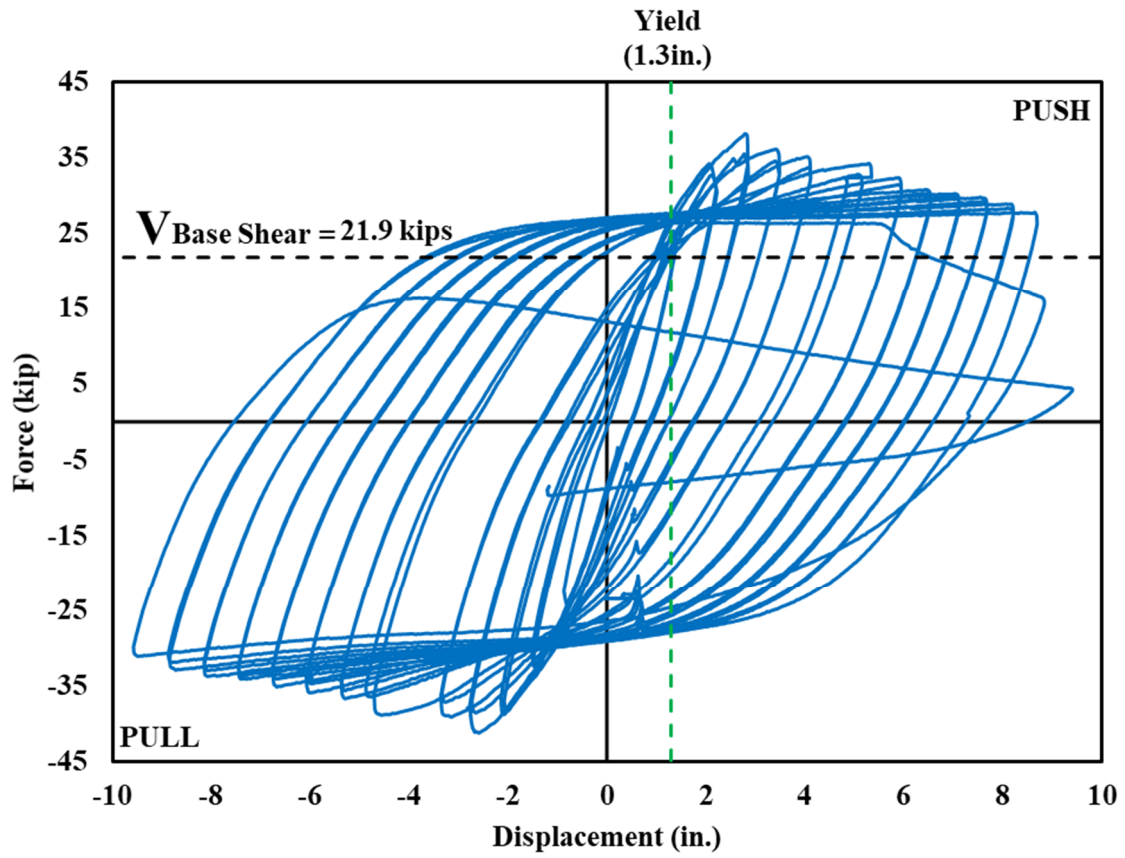


Figure 4.11: Force vs. Displacement plot for the precast column.

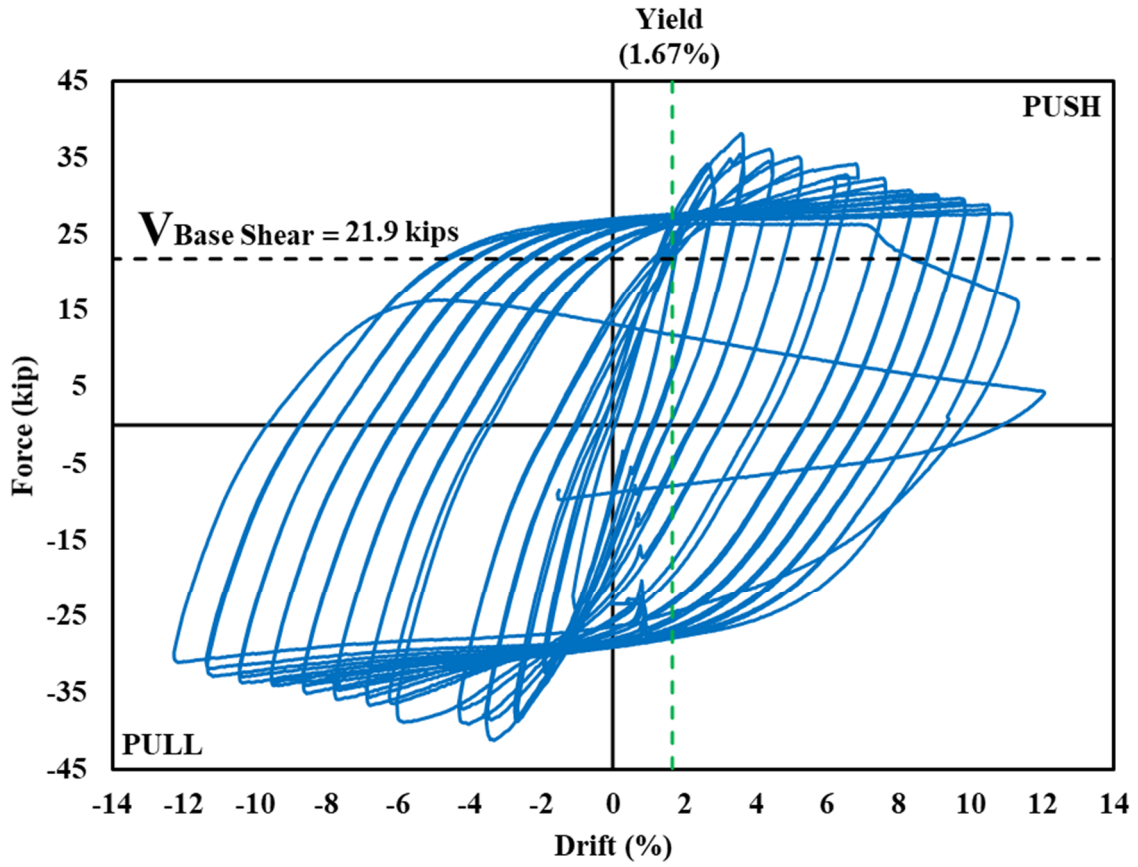


Figure 4.12: Force vs. Drift plot for the precast column.

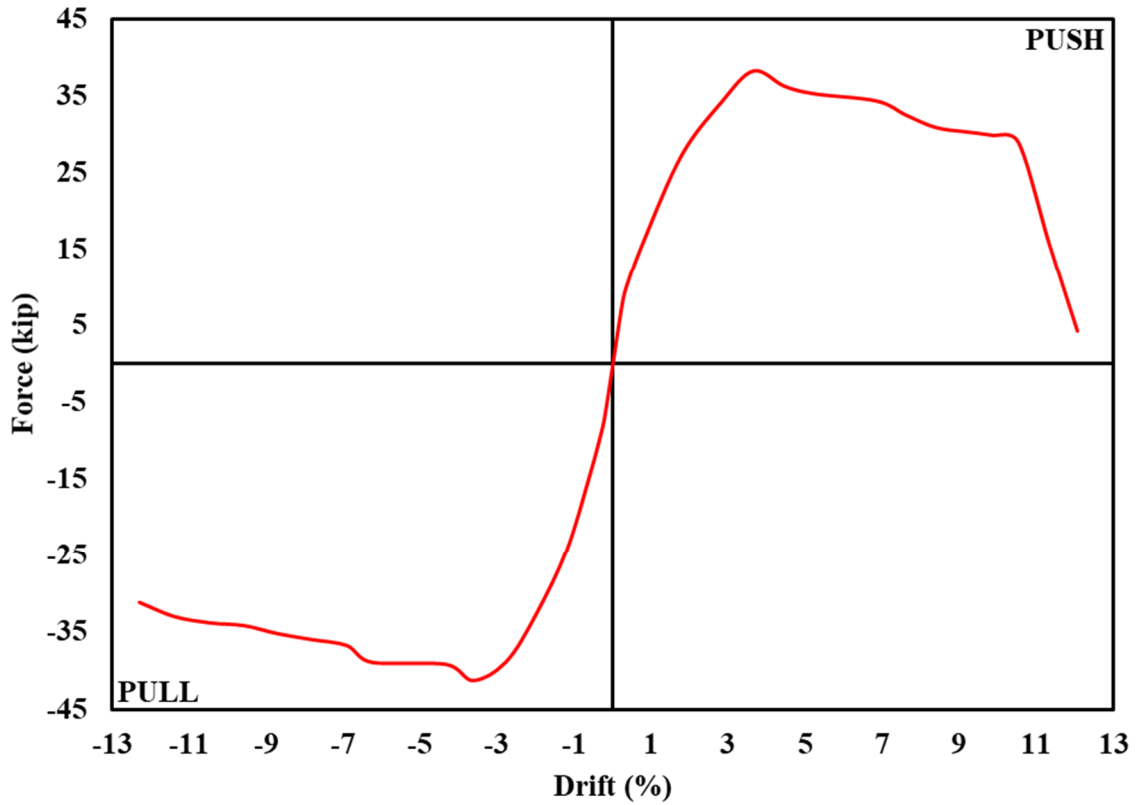


Figure 4.13: Backbone curve for the precast column.

Table 4.3: Damage observation from testing of the precast column.

Drift (%)				
Cracking	Spalling	Significant Elephant-Leg Buckling	Fracture of the Pipe	End of testing
0.6	4.42%	8.7	10.5	12.27

Table 4.4: Summary of the performance points from testing of the precast column.

Yielding				Ultimate Strength		
Predicted		Experimental		Experimental		
Drift (%)	Base Shear (kips)	Drift (%)	Base Shear (kips)	Drift (%)	Base Shear (kips)	Ductility*
0.88	21.9	1.7	27.2	12.27	41.2	6.3

\*Displacement ductility ( $\mu$ ) was 6.3 at the end of testing

The distribution of curvature along the height of the first 54 in. of the column is shown in Figure 4.14 Like the cast-in-place column, the column is expected to yield and fail within the plastic hinge of the column. The plastic hinge for the precast column can be calculated using the same equation as the cast-in-place column from Priestley et al. (2007):

$$L_p = 0.08H + l_{sp} \quad (29)$$

Using the strain penetration discussed earlier in this chapter and column height of 78 in. the plastic hinge is calculated to be 13.07 in. Figure 3.17 shows that yielding occurred in the bottom 18 in. of the column. From 18 in. to 36 in. the column approached the yield point but never reached it. Because the region from 18 in. to 54 in. never reached the yield point, this region essentially remains elastic throughout the testing procedure.

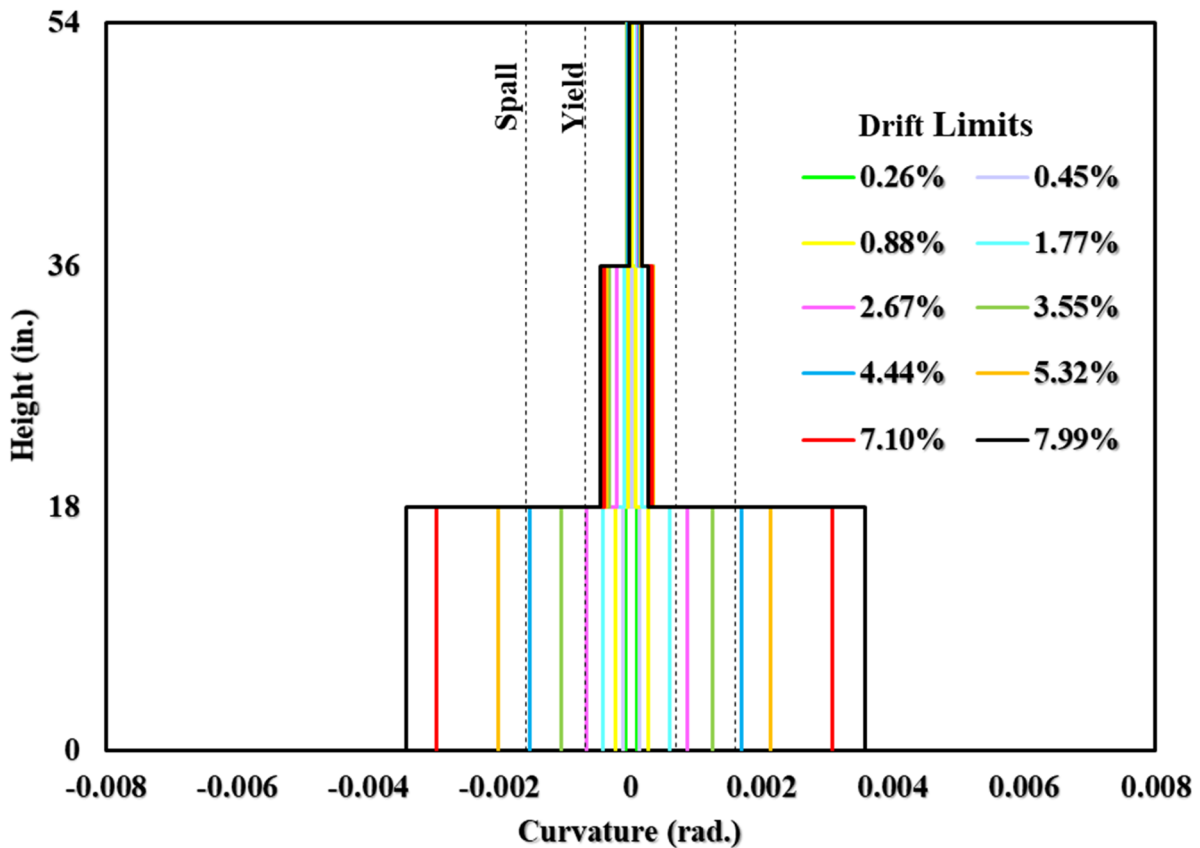


Figure 4.14: Precast curvature distribution.

The dissipated energy plot is shown in Figure 4.15. The dissipated energy is obtained using the same procedure as the cast-in-place column. The largest difference in dissipated energy occurred during the 15<sup>th</sup> and 16<sup>th</sup> cycles which corresponds to the HSS member located in the column buckling and fracture. The total dissipated energy during the testing procedure is 1025 kJ.

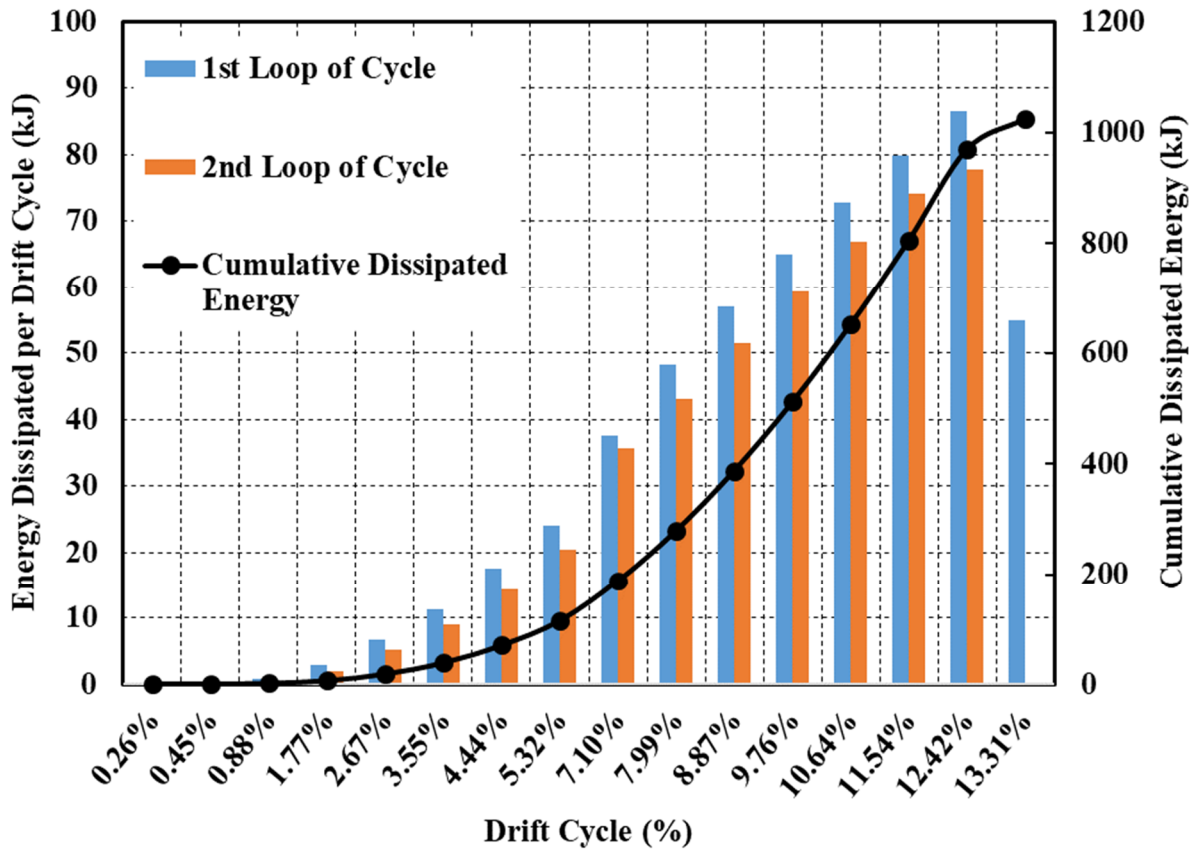


Figure 4.15: Dissipated energy plot for the precast column.

An area-based hysteretic damping plot is shown in Figure 4.16. The area-based hysteretic damping is calculated using the same procedure as the cast-in-place column. Figure 3.19 shows the precast column having a relatively parabolic trend for the majority of the testing procedure. The column had higher hysteretic damping at the beginning of the testing procedure as a result of the elastomeric damping pad (e.g. contact damping) allowing the column to move without significantly increasing the load at the top of the column. The precast column hysteretic damping is just below the Takeda Fat model after the capability of the elastomeric bearing pad is exceeded, then approximately equal to the Takeda Fat model from a displacement ductility of 4 to 5.5 after which the column hysteretic damping approached the Ramberg-Osgood model until the testing procedure was ended.

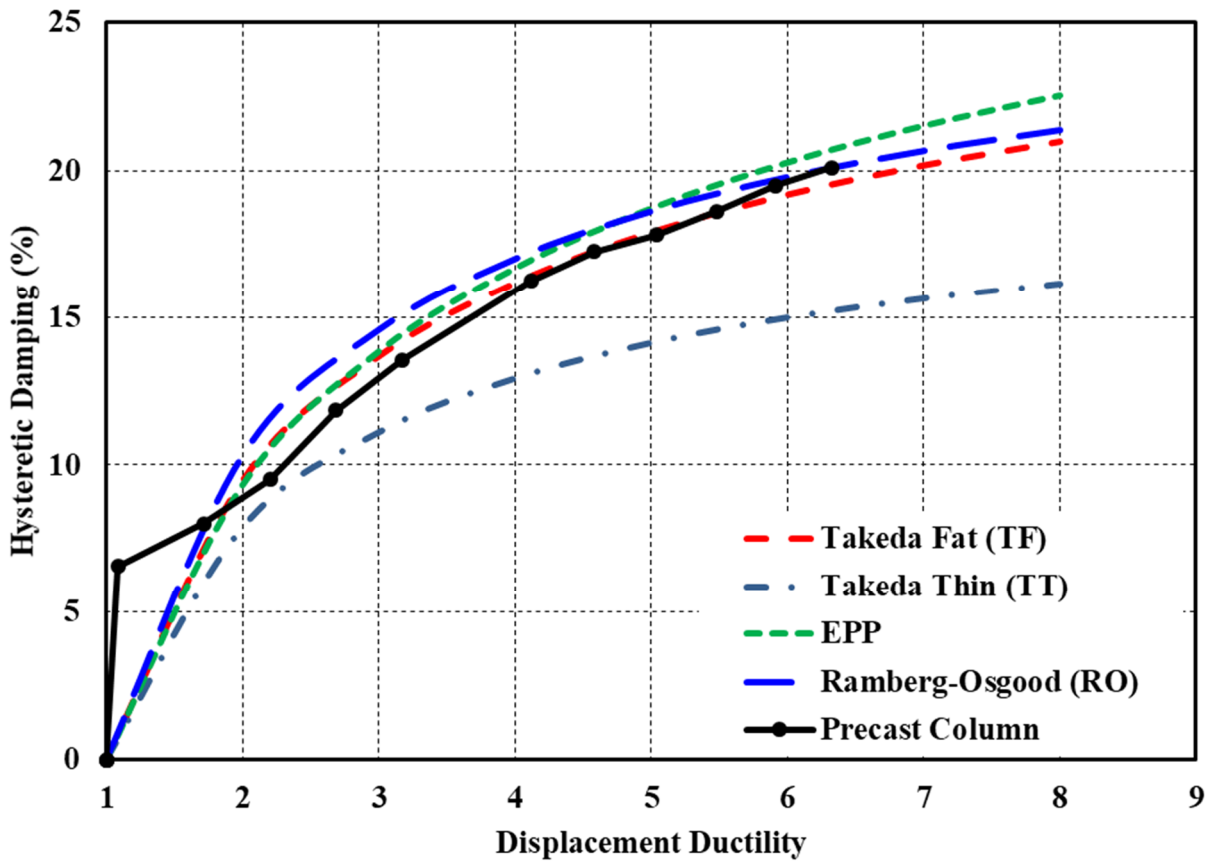


Figure 4.16: Area-based hysteretic damping for the precast column.

## 4.8 Conclusions

The precast specimen is designed to match the capacity and ductility of the cast-in-place benchmark. The precast footing and column are constructed incorporating HSS members. The Concrete Filled Steel Tube (CFST) at the interface of the column and footing provides flexural and shear resistance as well as confinement. The specimen is designed using the CFST equations provided in the WSDOT Bridge Design Manual and the latest version of AASHTO LRFD Bridge Design Specifications. The contribution of the unconfined concrete cover at the interface was ignored for the flexural design of the column. An elastomeric pad is provided at the column and footing interface to prevent cracking during smaller drift ratios and allow rocking of the column. The embedment length of the pipe is selected such to develop the plastic capacity of the column pipe without any premature failure or pullout. An unbonded length of the pipe is provided to distribute inelastic strain during larger drift ratios and to improve the low-cycle fatigue performance of the pipe. The unbonded length region was designed to be the ductile link in the specimen. The footing and other parts of the column are designed to be capacity protected regions. Testing results show good performance of the precast column with enhanced energy dissipation. Damage to the column during the test was observed to be within the first 18 in. of the column which thought to be the plastic hinge region. The loss of the cover concrete occurred during the 4.42% drift ratio. This was later than what was observed in the testing of the cast-in-place benchmark. The failure mechanism for the connection started with an “Elephant-Leg” buckling of the pipe over the unbonded region, followed by the fracture of the pipe on one side. There was a rapid decrease in the lateral capacity of the column when the buckling increased. The maximum force obtained during the testing procedure was 41.2-kip which was approximately 10% higher compared to the cast-in-place benchmark. The maximum

displacement achieved was 9.4 in. which is about 20% higher compared to the cast-in-place benchmark. The ultimate displacement ductility is just below 6.5. The lower value of ductility compared to cast-in-place (7.5) was the fact that the precast column had a higher yield point compared to cast-in-place. The total energy dissipated during the testing procedure was 1,025 kJ. This was 2.25 times of the cast-in-place benchmark. The hysteretic damping plot showed that the precast column, overall, had similar values of hysteretic damping of Takeda-Fat and Ramberg-Osgood models. This is thought to be due to enhanced confinement (e.g. Concrete Filled Steel Tube) and detailing considerations. The precast column reached a hysteretic damping of 20% at the failure point.

## **Chapter 5: Comparison of Cast-In-Place and Precast Cantilever Pier Systems**

### **5.1 Introduction**

This chapter presents both the cast-in-place and precast test results. Each of the plots previously discussed are viewed side-by-side. Each of the hysteresis curves are compared first. After the hysteresis plots, the backbone plots are compared followed by the curvature distribution, dissipated energy, and area-based hysteretic damping plots.

Both columns are designed from the same prototype structure and as a result, are designed and built with the same overall dimensions. The columns had a height of 7 ft-4 in. and a diameter of 18 in. The designed moment capacity of the cast-in-place column is 165 kip-ft, after the AASHTO LRFD Bridge Design Specifications (AASHTO 2017), and the moment capacity of the precast column is 143 kip-ft, after the WSDOT LRFD Bridge Design Manual (WSDOT 2019).

### **5.2 Loading Protocol**

The testing setup and procedures are identical for each of the columns except the precast column endured through more cycles to reach its failure point. The cast-in-place column reached the 50% degradation of the highest observed lateral force on the 13<sup>th</sup> cycle, which corresponds to 7.7 in. of displacement and 9.9% drift after the displacement of the footing is removed from the data. The precast column reached the 50% degradation of the highest observed lateral force on the 16<sup>th</sup> cycle, which corresponds to 9.57 in. of displacement and 12.3% drift after the displacement of the footing is removed from the data. The loading protocol for the cast-in-place and precast columns is shown in Figure 5.1 and Figure 5.2, respectively. Figure 5.3 and Figure 5.4 show images of the cast-in-place and precast columns, respectively during the testing procedure at approximately the same displacements.

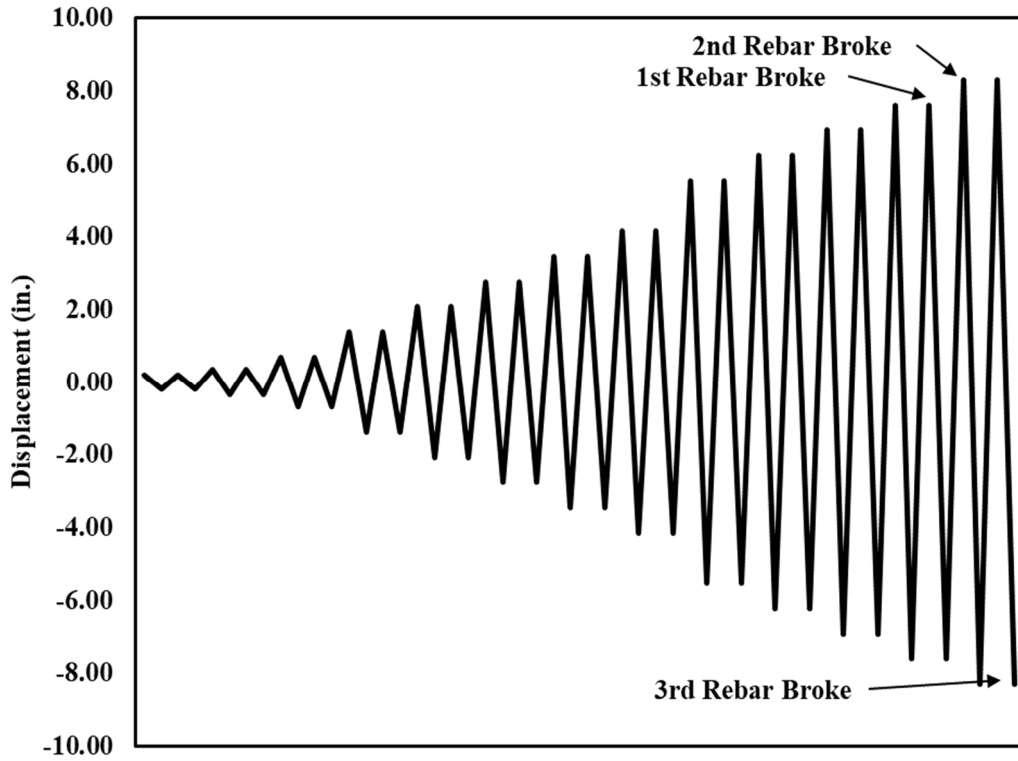


Figure 5.1: Loading protocol for the cast-in-place column.

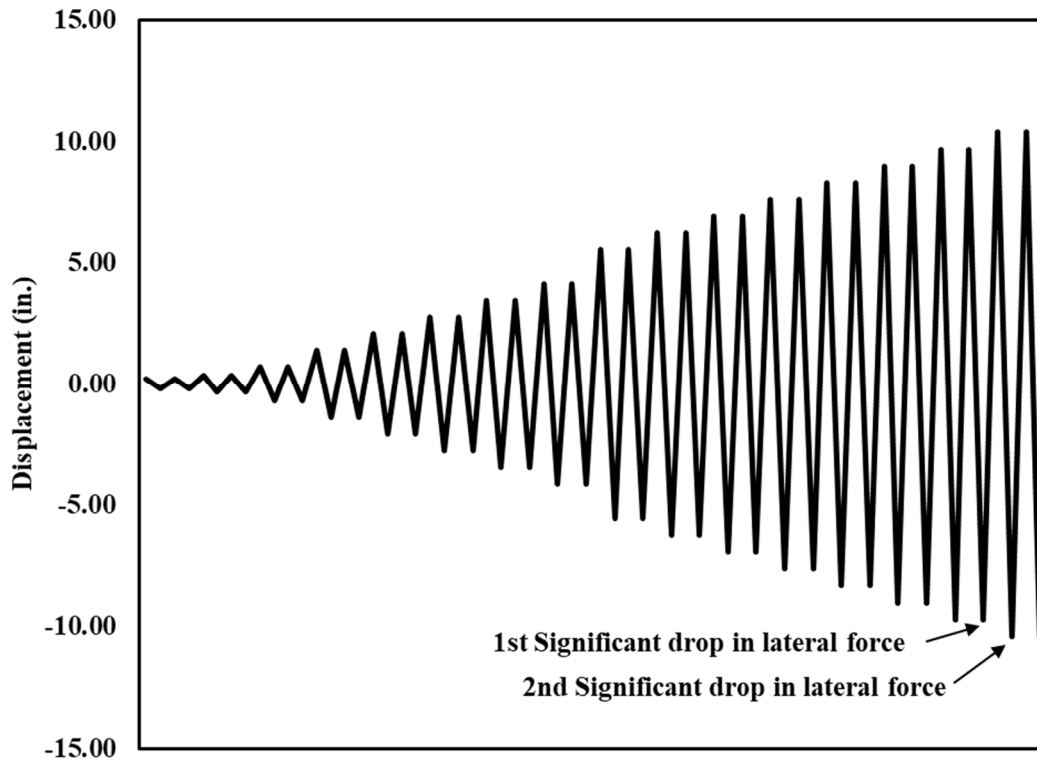


Figure 5.2: Loading protocol for the precast column.





a) 0.45% drift



b) 2.67% drift



c) 5.32% drift



d) 8.87% drift



e) 13.27% drift



f) Failed HSS member

Figure 5.4: Images from the precast testing procedure.

### 5.3 Hysteresis Test Results

The cracking drift ratio for the cast-in-place and precast columns are 0.2% and 0.6%, respectively. The precast column exhibited flexibility during smaller drift ratios to prevent cracking to the column.

The maximum displacement of the cast-in-place column during the testing procedure is 7.7 in. which corresponds to a 9.9% drift. The maximum load applied to the cast-in-place column during the testing procedure is 37.8 kip which corresponds to a 245.7 kip-ft moment capacity.

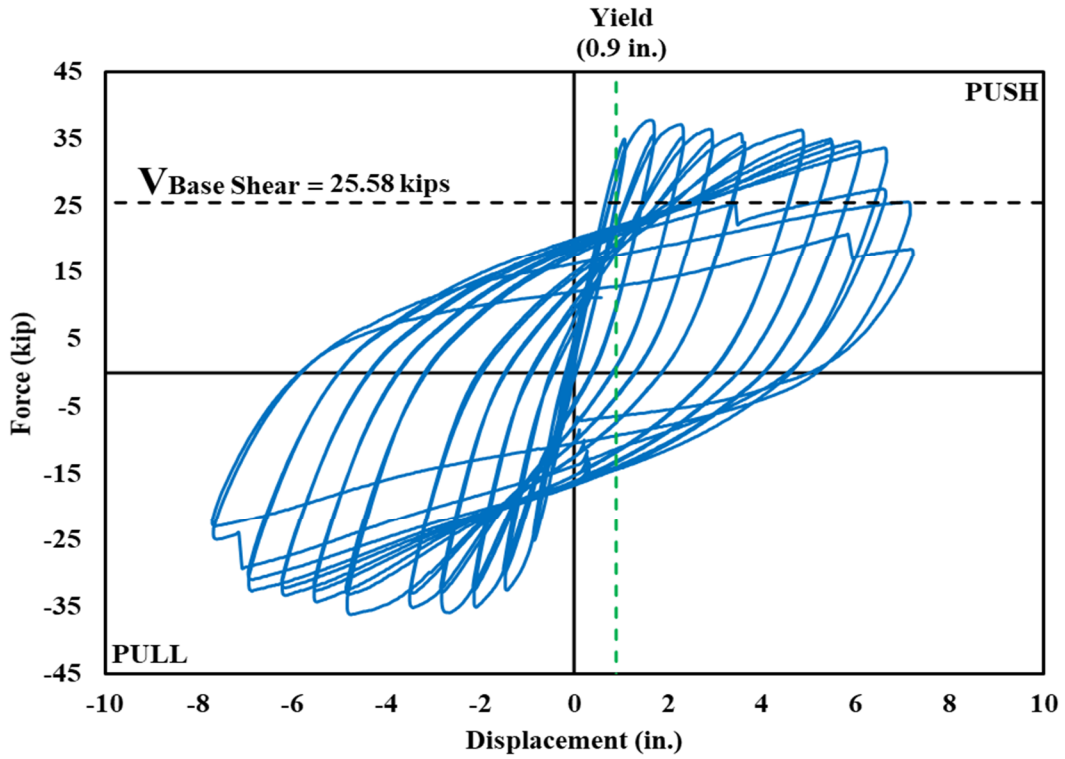
The maximum displacement of the precast column during the testing procedure is 9.6 in. which corresponds to a 12.3% drift. This is 20% higher compared to the cast-in-place benchmark. The maximum load applied to the precast column during the testing procedure is 41.2 kip which corresponds to a 267.8 kip-ft moment capacity. This is 9% higher compared to the cast-in-place benchmark. The Force vs. Displacement plots for the cast-in-place and precast testing procedures are shown in Figure 5.5 and Figure 5.6, respectfully. The Force vs. Drift plots are shown in Figure 5.7 and Figure 5.8 for the cast-in-place and precast testing procedures, respectively.

Looking at each of the hysteresis plots, it is obvious that the area of the loops for the precast column is larger compared to the cast-in-place column. In each of the plots, the enclosed area values are larger for the precast column than the cast-in-place column. It can be observed that the cast-in-place column yielded sooner compared to the precast column. The precast column had a yield drift which was 30% higher compared to the cast-in-place column.

The backbone curve for both testing procedures is also shown in Figure 5.9. It can be observed that the precast column has a lower stiffness compared to the cast-in-place column. The cast-in-place column had a consistent stiffness of 36.7 kips/in. The precast column begins with a stiffness of 42.4 kips/in., transitions to 16.44 kip/in., then has a stiffness of 8.5 kips/in. before

achieving the maximum lateral load. Comparing the values, the precast column initially has a stiffness 16% higher, then 45% lower, next 23% lower compared to the cast-in-place benchmark column. However, the precast column reached the capacity of the cast-in-place column at about a 3% drift ratio. The lower stiffness of the precast column is due to the rocking movement to allow flexibility and prevent concrete cracking at lower drift ratios. The ultimate displacement ductility for the precast column was nearly 6.5 which was slightly lower than the cast-in-place (e.g. 7.5) This was mainly due to larger yield drift for the precast column.

Table 5.1 and Table 5.2 shows significant values from the cast-in-place testing procedure while Table 5.3 and Table 5.4 show significant values for the precast column testing procedure.



+ Figure 5.5: Force vs. Displacement plot for the cast-in-place column.

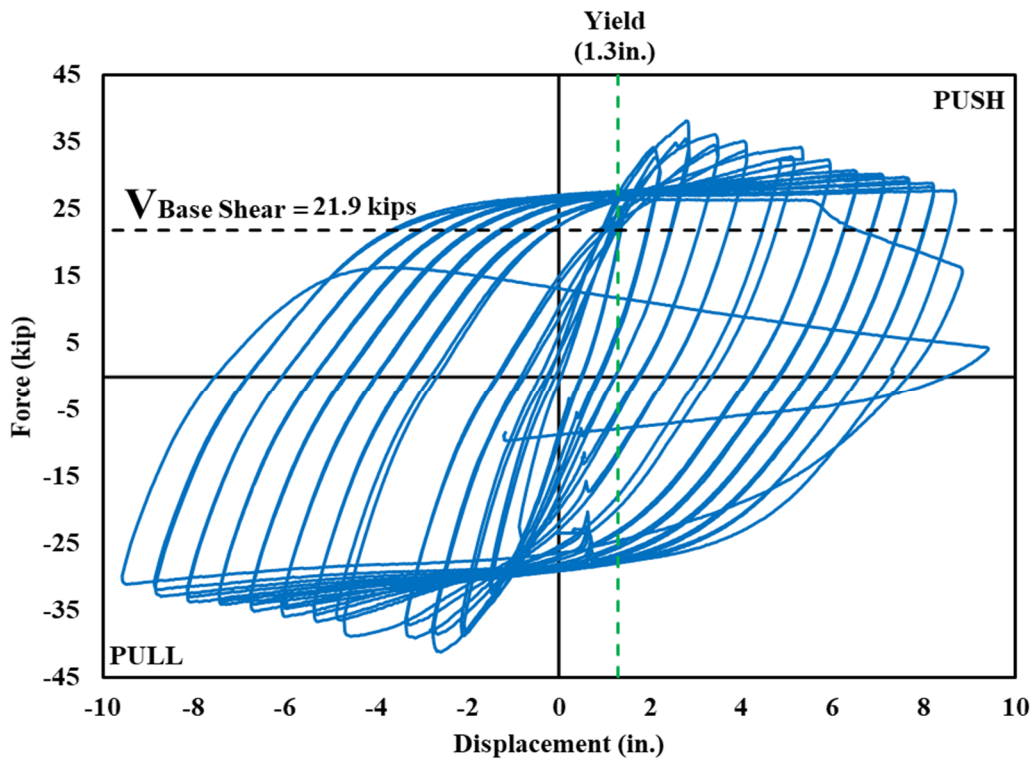


Figure 5.6: Force vs. Displacement plot for the precast column.

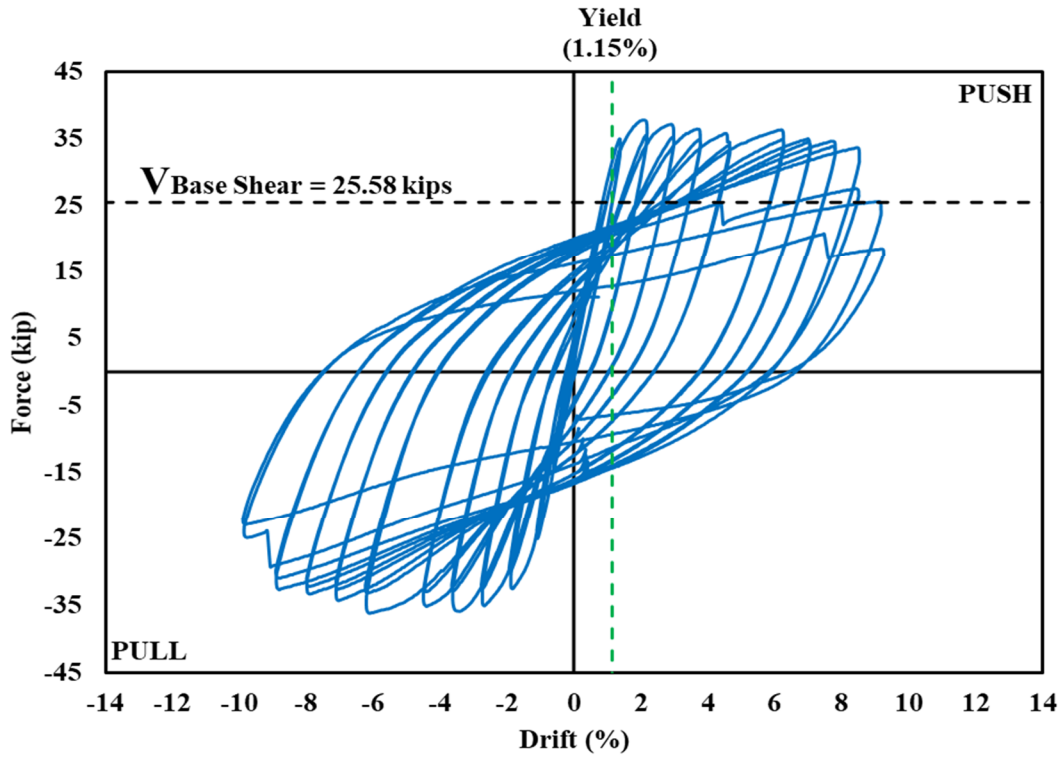


Figure 5.7: Force vs. Drift plot for the cast-in-place column.

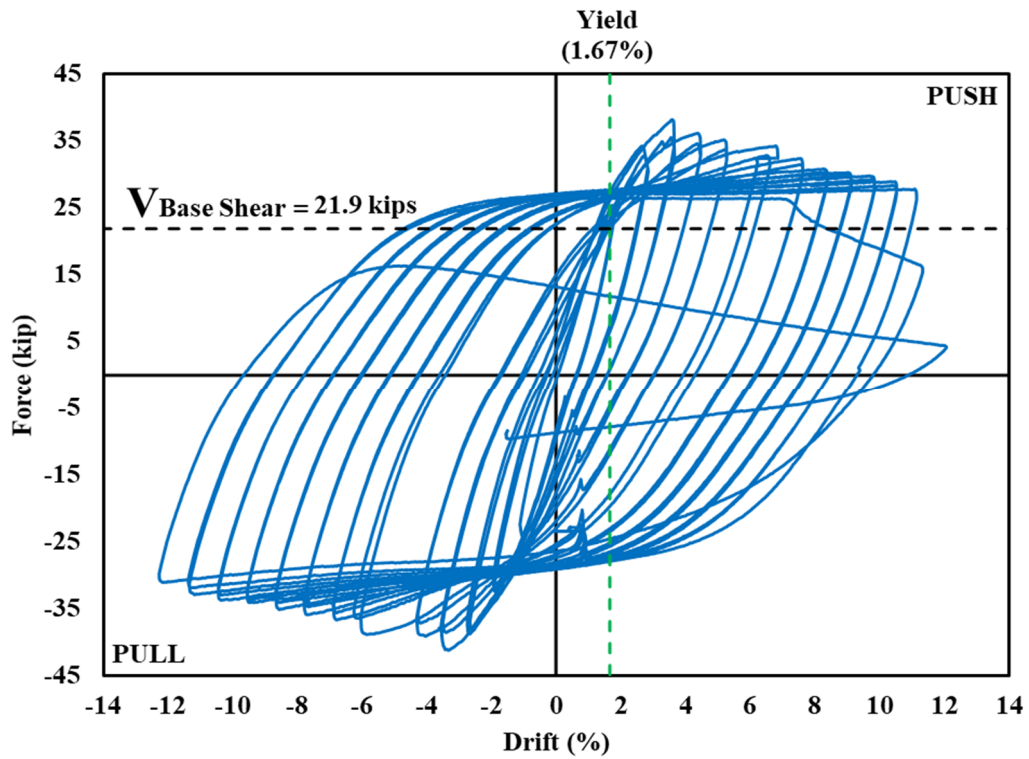


Figure 5.8: Force vs. Drift plot for the precast column.

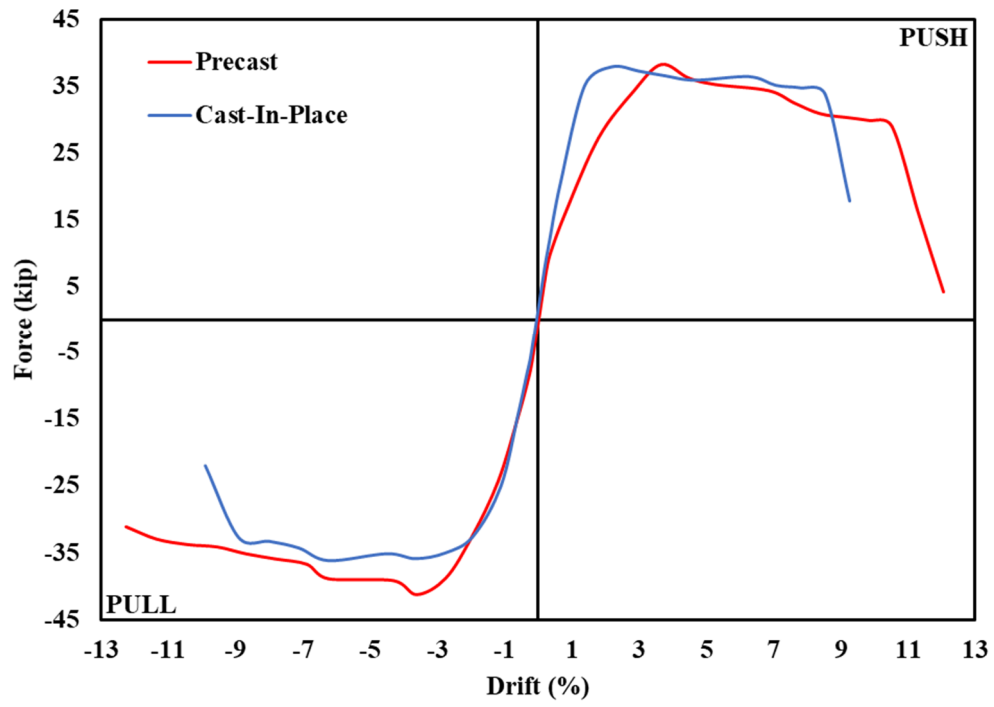


Figure 5.9: Backbone curve for the cast-in-place and precast columns.

Table 5.1: Damage observation from testing of the cast-in-place column.

Drift (%)						
Cracking	Spalling	Bar Rupture			End of testing	
0.2	4.49%	1 <sup>st</sup>	2 <sup>nd</sup>	3 <sup>rd</sup>	9.89	
		8.9	-9.89	9.89		

Table 5.2: Summary of the performance points from testing of the cast-in-place column.

Yielding				Ultimate Strength		
Predicted		Experimental		Experimental		
Drift (%)	Base Shear (kips)	Drift (%)	Base Shear (kips)	Drift (%)	Base Shear (kips)	Ductility*
0.88	25.58	1.15	35.1	9.89	37.8	7.4

\*Displacement ductility ( $\mu$ ) was 7.4 at the end of testing

Table 5.3: Damage observation from testing of the precast column.

Drift (%)				
Cracking	Spalling	Significant Elephant-Leg Buckling	Fracture of the Pipe	End of testing
0.6	4.42%	8.7	10.5	12.27

Table 5.4: Summary of the performance points from testing of the precast column

Yielding				Ultimate Strength		
Predicted		Experimental		Experimental		
Drift (%)	Base Shear (kips)	Drift (%)	Base Shear (kips)	Drift (%)	Base Shear (kips)	Ductility*
0.88	21.9	1.7	27.2	12.27	41.2	6.3

\*Displacement ductility ( $\mu$ ) was 6.3 at the end of testing

#### 5.4 Test Results for Curvature Distribution

The curvature distribution along the height of the first 54 inches of the cast-in-place and precast columns are shown in Figure 5.10 and Figure 5.11, respectively. Each of the columns is expected to yield and fail within the plastic hinge of the column. The plastic hinge of the cast-in-place column, as discussed in Chapter 3, is 13.7 in. The plastic hinge for the precast column, as discussed in Chapter 4, is 13.07 in.

Each of the curvature figures shows that yielding occurred in the bottom 18 inches of the column. From 18 inches to 36 inches, the columns approached the yield point but never reached it. Because the region from 18 inches to 54 inches never reached the yield point, this region deformed elastically throughout of the testing procedures. The maximum calculated curvature the cycle corresponding to the 10<sup>th</sup> cycle or 7.99% drift for the cast-in-place column is 0.0038 radian compared to 0.0036 radians for the precast column. These values are nearly identical.

There were several large cracks in the plastic hinge length of the cast-in-place column. However, for the precast column, there was essentially one large crack (e.g. gap opening) in the beginning until the spalling of the cover concrete.

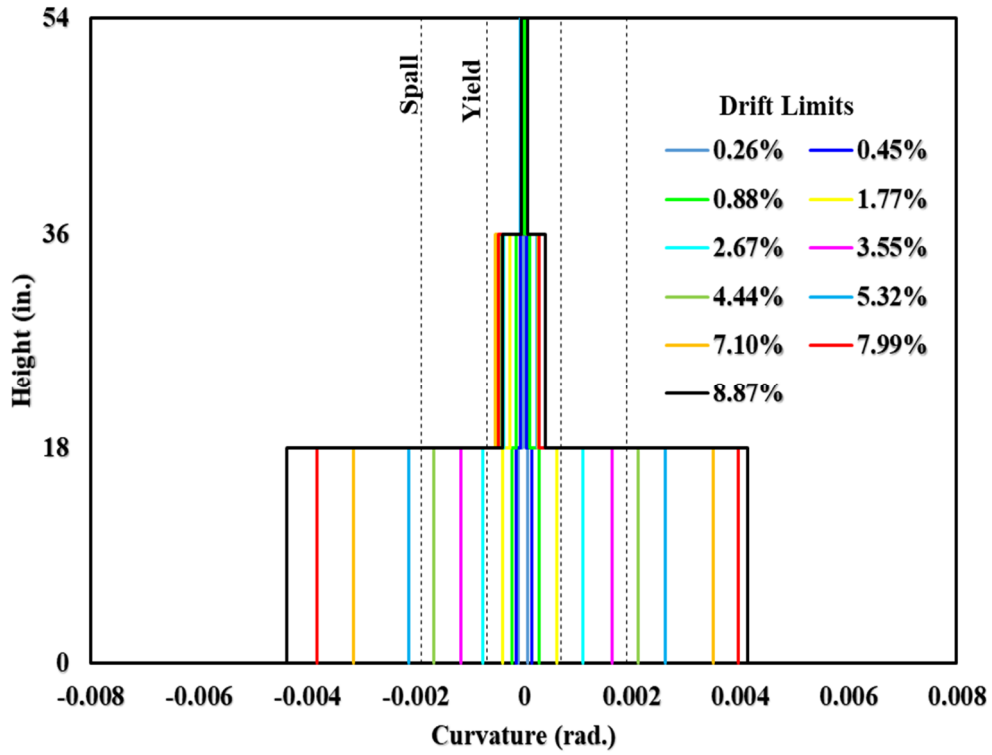


Figure 5.10: Cast-in-place curvature distribution.

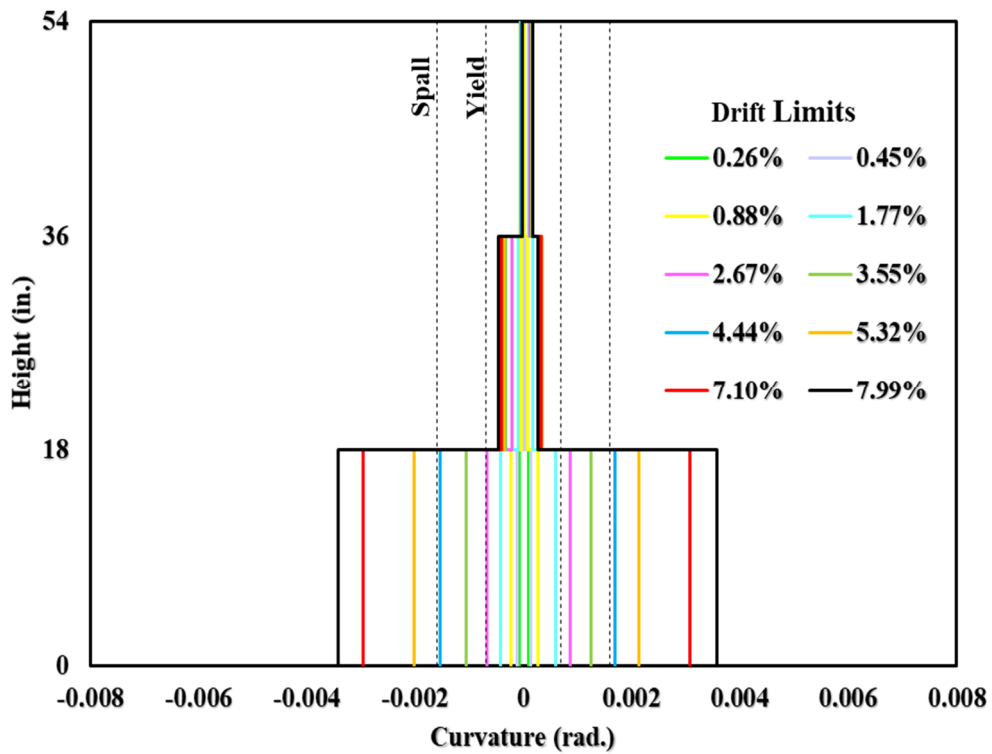


Figure 5.11: Precast curvature distribution.

## 5.5 Dissipated Energy Test Results

The dissipated energy is obtained by finding the area of each loop in the Force vs. Displacement plot after the units are converted to newtons and meters. The area of each loop represents the total energy dissipated in units of joules. The total dissipated energy during the cast-in-place testing procedure is 456 kJ. The total dissipated energy during the precast testing procedure is 1025 kJ which is more than 2.2 times the cast-in-place column. However, comparing the cumulative dissipated energy plots at the end of the cycle just before the cast-in-place column's first rebar break, 8.87% drift, the cast-in-place column dissipated 293 kJ compared to 388 kJ for the precast column. Figure 5.12 and Figure 5.13 show the dissipated energy for both the columns. One reason why the dissipated energy is higher for the precast column is that there is more steel in the column which makes the column more ductile and able to absorb more energy. Also, the precast column had better confinement (e.g. presence of a steel shell) compared to the cast-in-place benchmark.

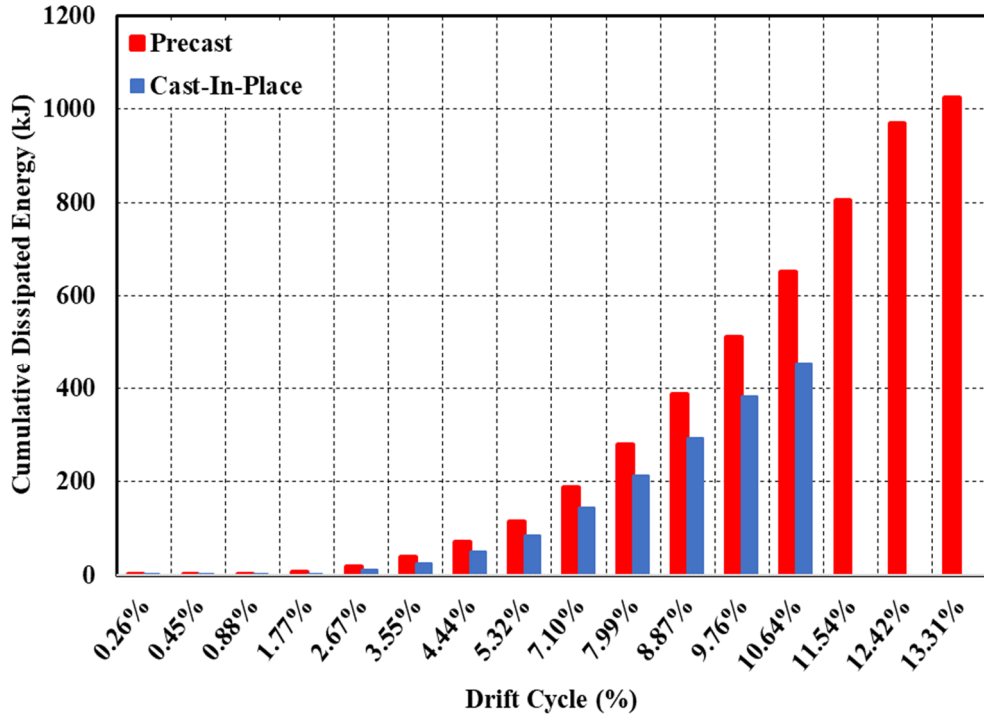


Figure 5.12: Cumulative dissipated energy for both columns.

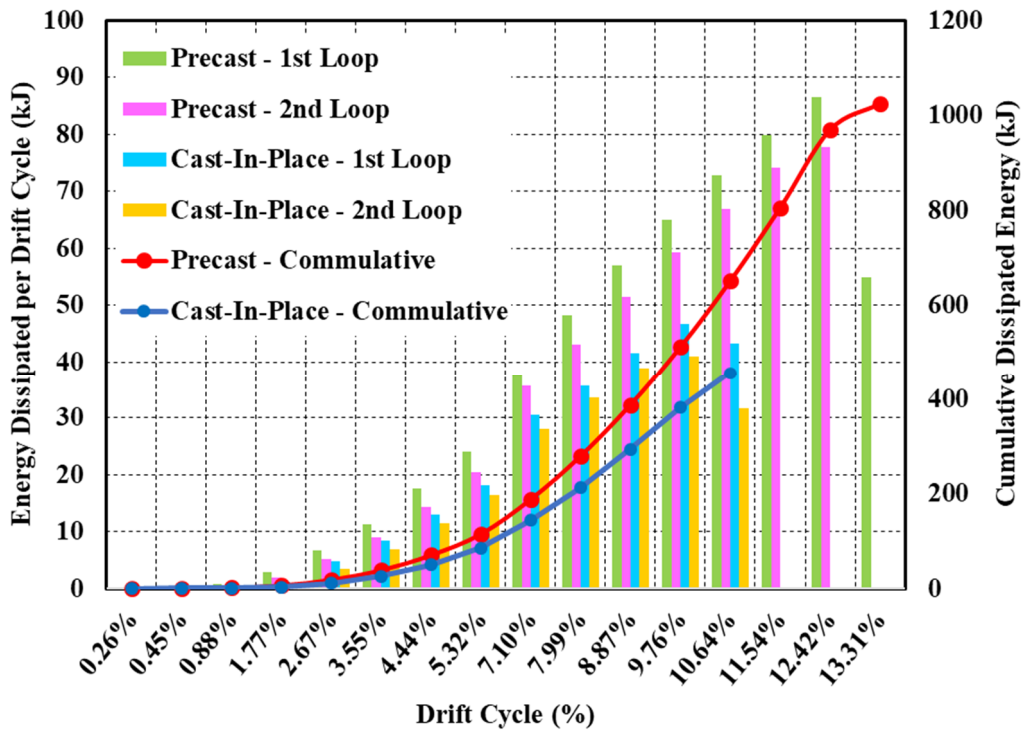


Figure 5.13: Dissipated energy for each cycle for both columns.

## 5.6 Area-Based Hysteretic Damping Test Results

Figure 5.14 shows the corrected area-based hysteretic damping plots for both the cast-in-place and precast columns. It can be observed that the precast column had higher values of hysteretic damping compared to the cast-in-place column up until a ductility of nearly 5.5. The initial jump in the hysteretic damping plot of the precast column is due to contact damping provided by the elastomeric pad. The effects reduce as the pipe starts yielding with increasing displacement ductility.

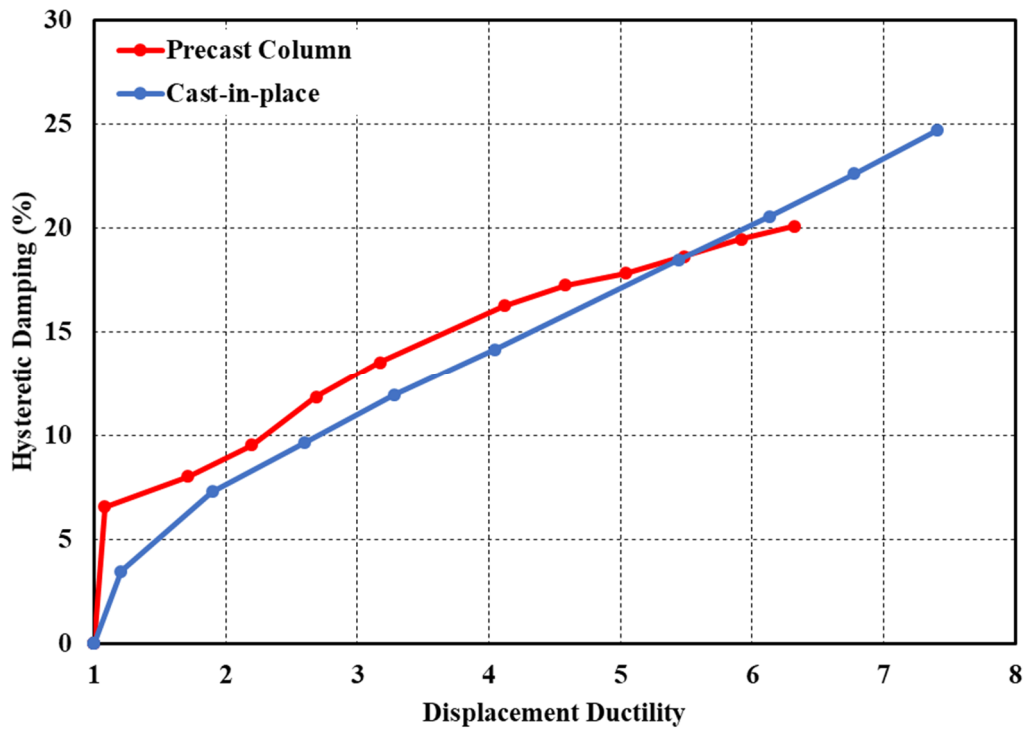


Figure 5.14: Corrected area-based hysteretic damping for both columns.

## 5.7 Residual Drift

Figure 5.15 shows the residual drift for the cast-in-place and precast columns. Looking at the image, the two columns follow a similar trend line throughout their testing procedures. The residual drift of the cast-in-place column on the last cycle of the testing procedure is 6.64% compared to the 9.27% drift that the column was pushed. This corresponds to the column maintaining 70% of the displacement applied to the column when the lateral force was equal to zero. The residual drift of the precast column was 10.91% compared to the 12.08% drift that the column was pushed or 90% of the displacement of the column was maintained when the column lateral force was equal to zero. If the cast-in-place column could continue through more of the test cycles, the residual drift results are expected to continue following the precast cast column results.

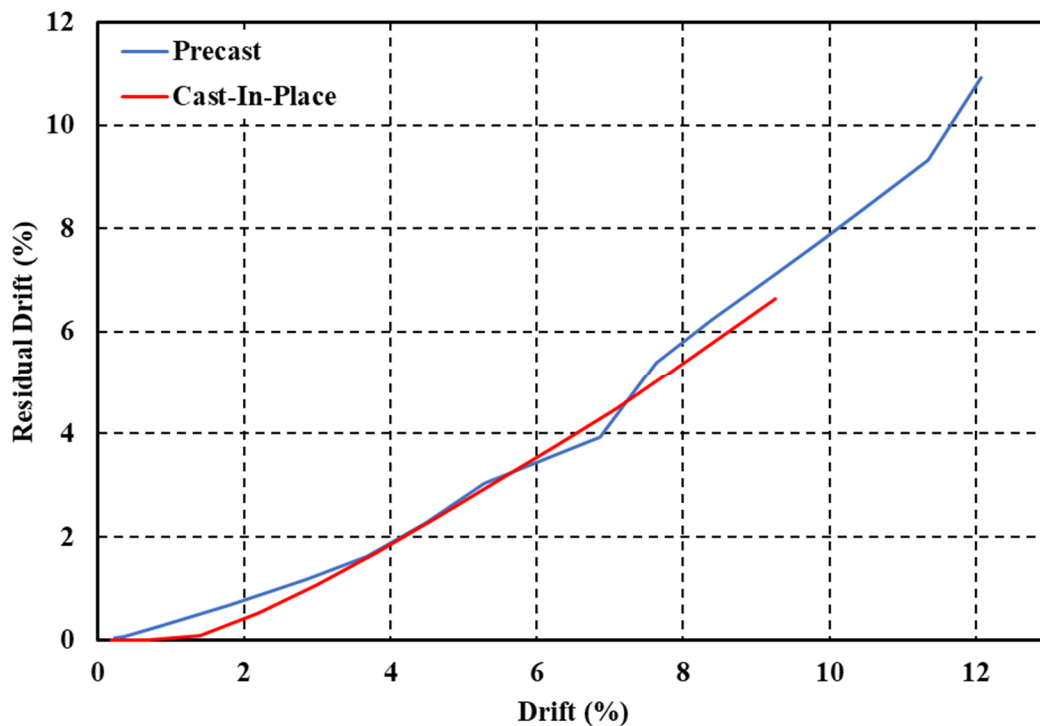


Figure 5.15: Residual drift for the cast-in-place and precast columns.

## 5.8 Conclusions

Each of the cantilever columns is designed and constructed having the same overall dimensions and approximately similar capacities. The cast-in-place and precast columns are tested using identical loading protocols and displacement progression for each cycle. The columns perform similarly throughout the testing procedures. The precast column, however, continued through more loading cycles and as a result, achieved higher deflections and cumulative dissipated energy. Overall testing shows better performance of the precast column compared to the cast-in-place column. It reached higher displacements with good strength. The residual deformation for both columns is comparable.

Table 5.5 summarizes some of the key data from the testing of the two columns.

Table 5.5: Summary of performance factors for the cast-in-place and precast columns.

Performance Factors	Cast-in-place column	Precast column
Yield Displacement	0.9 in. (1.2% Drift Ratio)	2.6 in. (3.3% Drift Ratio)
Base Shear at Yield	33 kip	37.5 kip
Maximum Curvature at 7.99% Drift Ratio	0.0038 radian	0.0036 radian
Ultimate Displacement Ductility	7.4	6.3
Ultimate Displacement Capacity	7.7 in. (9.9% Drift Ratio)	9.6 in. (12.3% Drift Ratio)
Ultimate Base Shear	37.8 kip	41.2 kip
Total Energy dissipated	456 kJ	1025 kJ

## **Chapter 6: Design, Detailing Considerations, and Repair Methodologies for the Precast Pier System**

### **6.1 Introduction**

This chapter discusses a variety of aspects used in the design, construction, and repair of the precast column. Design and detailing considerations are discussed first. After the design considerations, the construction and assembly of the precast element are briefly explained. Next, the limitations of the precast connection and repair strategies are discussed.

This chapter also discusses the development and use of an interaction diagram as a quick way to select pipe diameter and wall thickness based on the desired moment capacity and compression strength of concrete.

### **6.2 Design and Detailing Considerations**

Throughout the design of the precast column, there are three different resources used. The resources used to design the precast column are AASHTO LRFD Bridge Design Specifications (AASHTO 2017), WSDOT Bridge Design Manual (WSDOT 2019), and Integral Abutments for Steel Bridges (Wasserman and Walker 1996). The AASHTO LRFD Bridge Design Specifications are used as a basis for all footing and column reinforcement. The WSDOT Bridge Design Manual is used to determine the capacity and size the HSS member used to connect the column to the footing. The WSDOT Bridge Design Manual and Integral Abutments for Steel Bridges are used to determine the embedment length of the HSS member.

#### **6.2.1 Selecting Size of the HSS Member**

The first step is to design the column as cast-in-place and identify the required nominal capacity. In the next step, the size of the HSS for the precast solution is identified. The WSDOT Bridge

Design Manual provides several equations to select an appropriate HSS member. Appendix C of this report provides a variety of different pipe sizes as a means to quickly determine if a pipe will work and to estimate the moment capacity of an HSS pipe having a yield strength of 42 ksi, ultimate strength of 58 ksi, and compression strength of concrete of either 4 or 8 ksi.

WSDOT (2019) provides equations to check the diameter to pipe thickness ratio and to determine the moment capacity of a CFST. The following equation is used to ensure the pipe is not subject to local buckling before developing the strength of the pipe:

$$\frac{D}{t} \leq 0.15 \frac{E}{F_y} \quad (30)$$

Where D is the outside diameter and t is the wall thickness of the HSS member. In appendix C, this formula is checked and is indicated as “Good” or “Bad.” According to WSDOT (2019), the pipe thickness should be reduced as a result of corrosion over a 75-year minimum design life.

The corrosion rates vary according to the environment as described in Table 6.1 and assumes that the soil is not highly corrosive. The minimum corrosion reduction shall be taken as 1/16 in. The interaction diagrams and tables in this report do not incorporate the corrosion reduction factor.

Table 6.1: Common corrosion rates from WSDOT Bridge Design Manual

Soil embedded zone (undisturbed soil)	0.001 in./year
Soil embedded zone (fill or disturbed soils)	0.003 in./year
Immersed zone (freshwater)	0.002 in./year
Immersed and tidal zone (saltwater)	0.004 in./year
Splash zone (saltwater)	0.006 in./year
Atmospheric zone	0.004 in./year

The equation WSDOT provided to determine the nominal moment capacity is shown below:

$$M_n(y) = \left( c(r_i^2 - y^2) - \frac{c^3}{3} \right) 0.95f'_c + 4ct \frac{r_m^2}{r_i} F_y \quad (31)$$

Where  $c$  is equal to one half the chord length of the tube in compression and is calculated using

$$c = r_i \cos\theta \quad (32)$$

Where  $r_i$  is equal to the radius to the inside of the steel tube and  $\theta$  is calculated using:

$$\theta = \sin^{-1}\left(\frac{y}{r_m}\right) \quad (33)$$

Where  $y$  is the distance from the centroid of the specimen to the neutral axis during a seismic event and  $r_m$  is the radius to the center of the steel tube. Because the neutral axis is expected to be approximately equal to the centroid when the structure is assembled, the variable  $y$  is equal to zero. If the column is not plumb when the column is assembled to the footing, the variable  $y$  is used to reduce the column capacity.

To select the column receiving pipe use a size that will allow a tolerance gap. The gap needs to be large enough to allow the grout to easily flow between the two HSS members. This tolerance gap is larger compared to grouted ducts or similar connections. It is expected that the gap can be up to 2 in. on each side of the pipe without compromising the structural integrity of the connection. For gaps larger than 2 in. experimental and analytical testing should be performed to demonstrate the integrity of the connection. The gap used in this research was equal to 0.5 in. on each side of the pipe.

### **6.2.2 Embedment Length of the HSS Member**

Two methodologies are considered to determine the embedment of the pipe into the column and footing. The methodologies used are proposed by WSDOT Bridge Design Manual and (Wasserman and Walker 1996). The equation used in this research is shown below.

$$l_e \geq \sqrt{\frac{5.27DtF_u}{\sqrt{f'_c}}} \quad (34)$$

Where  $l_e$  is the calculated embedment length,  $D$  is the diameter of the embedded pipe,  $t$  is the wall thickness of the embedded pipe,  $F_u$  is the ultimate strength of the embedded pipe, and  $f'_c$  is the compression strength of the concrete with all variables in terms of kip and inches.

For the embedment length proposed by Wasserman, the following equations are used:

$$l_e = \frac{F_y Z}{\sqrt{700f'_c b}} \quad (35)$$

$$b = \frac{d\sqrt{\pi}}{2} \quad (36)$$

Where  $F_y$  is the yield strength of the embedded pipe,  $Z$  is the plastic section modulus of the embedded pipe,  $f'_c$  is the compressive strength of the concrete, and  $d$  is the outside diameter of the embedded pipe with all variables in terms of kip and inches.

To select the appropriate embedment length, simply follow the flow chart shown in Figure 6.1. A summary of embedment lengths for commercially available HSS and pipes are shown in Figure 6.2 and Figure 6.3, respectively with  $f'_c$  is 4 ksi,  $F_y$  is 46 ksi, and  $F_u$  is 62 ksi for both graphs.

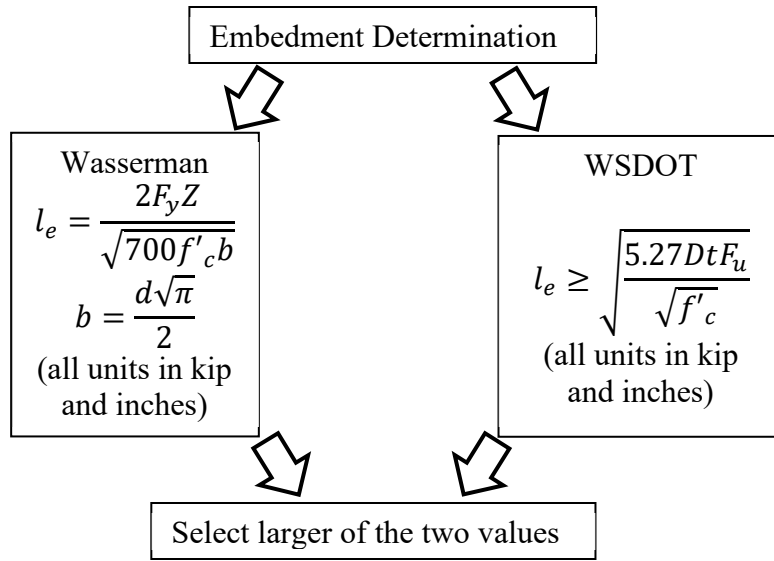


Figure 6.1: Embedment length determination flow chart

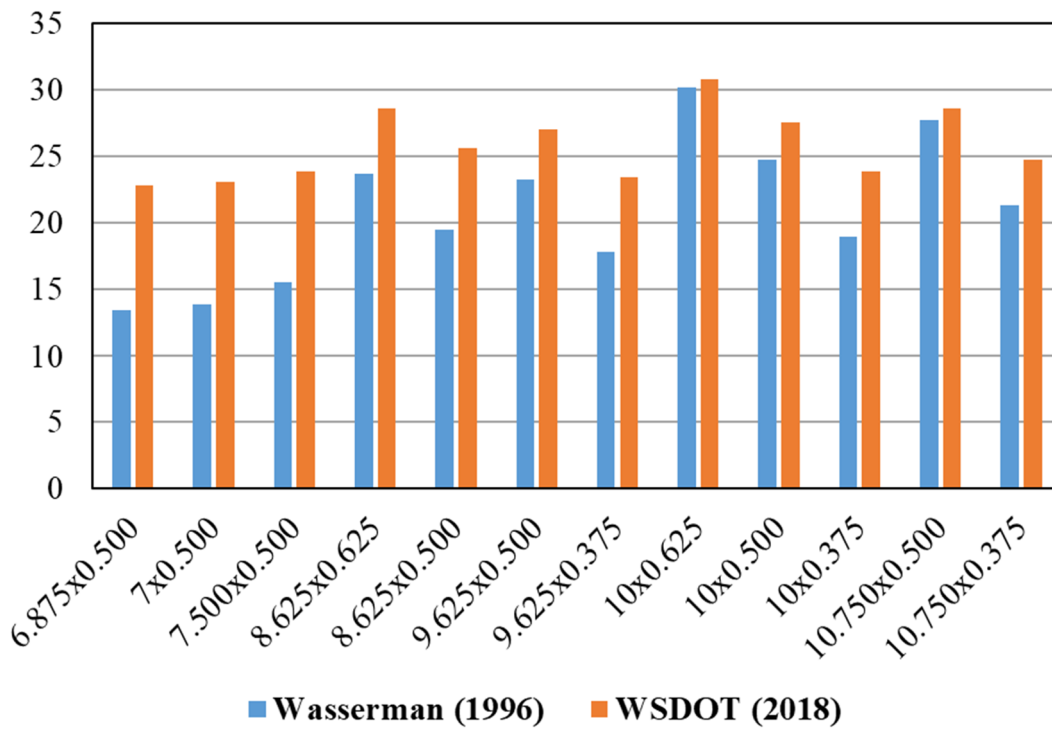


Figure 6.2: Embedment length comparison for HSS round (in.)

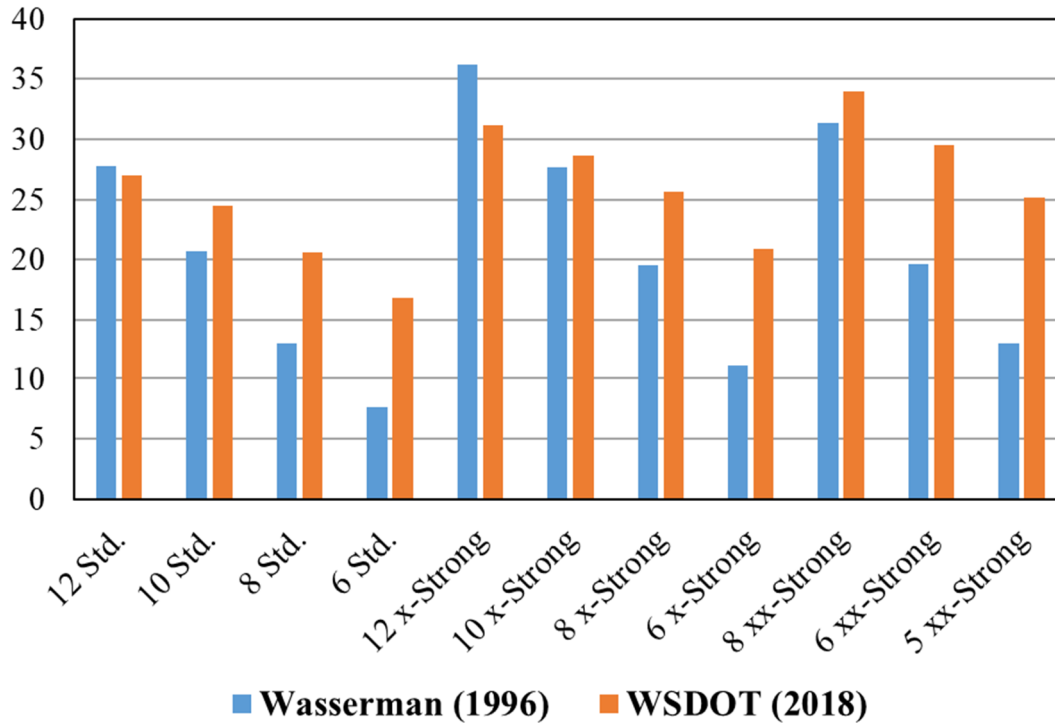


Figure 6.3: Embedment length comparison for pipe (in.)

### 6.2.3 Unbonded length

The unbonded length in the plastic hinge is a way to force the HSS to yield at a designated location (above the footing) that can be inspected following an earthquake. The unbonded length of the HSS member is determined using the methodology presented in the PRESSS Design Handbook (Pampanin et al. 2010). The unbonded length can be selected such that the strain in the HSS member would be approximately equal to a cast-in-place column or say 6% at the design level. To begin, the strain penetration needs to be calculated using the following equation:

$$l_{sp} = 0.022F_y d_{bl} \quad (37)$$

Where  $F_y$  is equal to the yield strength and  $d_{bl}$  is equal to the diameter of the reinforcing bars or thickness of HSS member. Once the strain penetration length is calculated, the strain in the HSS member can be calculated using the equation below.

$$\varepsilon_s = \frac{\Delta}{l_{ub} + 2l_{sp}} \quad (38)$$

Where  $\Delta$  is the elongation of the HSS member and  $l_{ub}$  is the unbonded length. It is important to estimate the elongation of the HSS member to determine an appropriate unbonded length. Data from the cast-in-place column is used to predict the elongation of the HSS member.

#### **6.2.4 Development of Interaction Diagrams**

The equations used to develop the interaction diagram are the same equations that are discussed in CH4 which are obtained from the WSDOT Bridge Design Manual (WSDOT 2019). To create the interaction diagram, a variety of different pipe thicknesses, pipe diameters, and two different compression strengths of concrete. The pipe thicknesses used are values found in the American Institute of Steel Construction Manual (AISC Committee 2010) and vary from 0.174 in. to 0.581 in. The Pipe diameters range from 10 in. to 60 in. The compression strength of the concrete used is 4 and 8 ksi and does not account for an axial load. The interaction diagram is shown in Figure 6.4 and displays the variables used to develop it. Looking at Figure 6.4, the moment capacity increases as the pipe diameter, pipe thickness, and compression strength of concrete increase. To determine the moment capacity of a specific HSS member, the user only needs to have predetermined the pipe diameter, pipe wall thickness, and the compression strength of concrete. For example, if a 36 in. diameter pipe having a thickness of 0.465 in. were to be selected to be embedded in concrete having a compression strength of 8 ksi, the resulting moment capacity can be determined from Figure 6.4 to be roughly 4500 kip-ft.

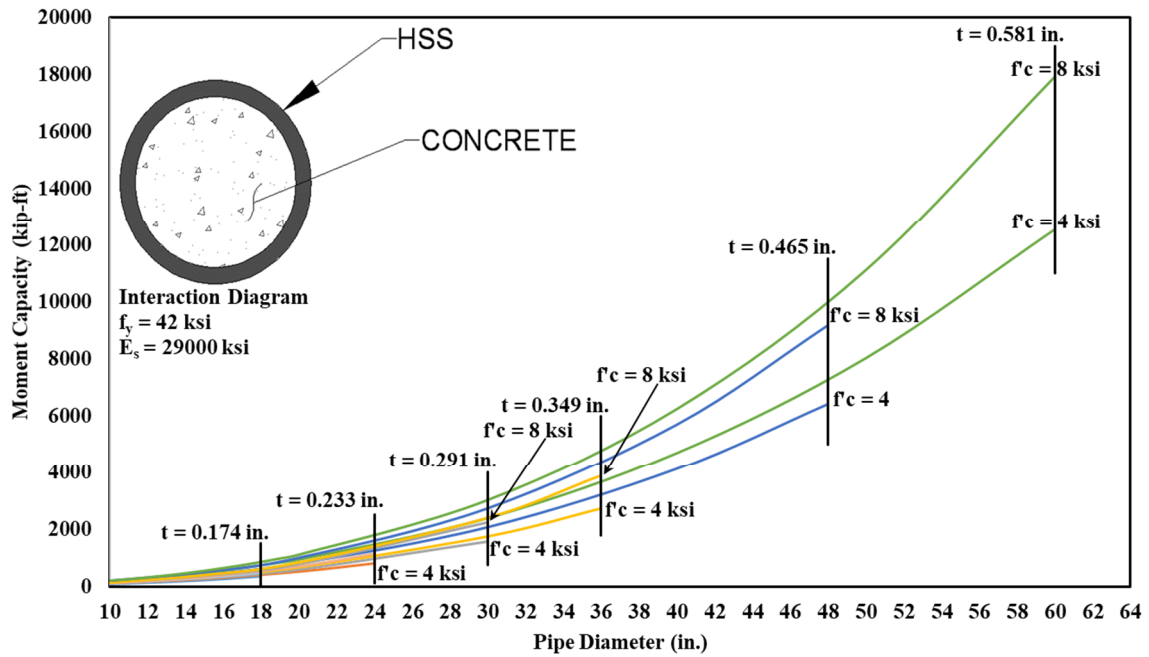


Figure 6.4: HSS member moment capacity interaction diagram.

### **6.3 Construction Technology and Assembly**

It is recommended that the materials used in this testing procedure be a minimum for practical applications. When constructing the footing, care should be taken to ensure the inside of the receiving HSS member remains clear of concrete. If concrete propagates into the receiving HSS member, the undesired concrete will need to be removed with a grinder before the assembly of the precast column. To keep concrete out of the footing HSS member, A  $\frac{3}{4}$  in. piece of plywood is sized and secured to the inside bottom edge of the HSS member and gorilla tape is placed at the top of the HSS member (Figure 6.5a-c). While the footing is curing, water should not be allowed to pool at the bottom of the receiving HSS member. Any rust that accumulates on the inside of the receiving HSS member should be removed before assembling the precast column and the grouting process.

The precast column is poured horizontally for ease of construction, the restrictions over dropping height for concrete, and to make sure it is not knocked over accidentally while the concrete is being poured or while the concrete is curing. The outside of the HSS pipe is sandblasted before pouring concrete to achieve a better bond between the HSS member to the concrete. The unbonded length of the pipe is accomplished by wrapping the desired unbonded pipe length with gorilla tape. The grout vents used is PVC pipe. The PVC pipes are sealed using gorilla tape while the concrete is being poured to ensure concrete does not enter and clog them. A level should be used to ensure the HSS member is oriented correctly in the formwork (Figure 6.5d). If the HSS member is not level before the concrete is being poured, then the column will not be plumb when the precast column is assembled to the cast-in-place footing. Once the concrete is poured, the column should be allowed to cure sufficiently so premature cracking does not occur. The

centering fins should be welded onto the protruding HSS member after it is removed from the formwork (Figure 6.5e). Refer to Chapter 4 of this report for more construction images.



a) Receiving HSS member



b) Footing reinforcement



c) Finished footing



d) Column reinforcement



e) Welded centering fins

Figure 6.5: Precast column construction images.

For assembly, the precast column needs to be rotated from the horizontal orientation to a vertical orientation. To rotate the column to a vertical orientation, care should be taken to ensure the HSS member that is protruding from the precast column is not damaged. A crane should be used at each end of the column, without coming in contact with the HSS member, until the column is vertical. The HSS member should not come in contact with the ground at any time to prevent any dents or scratches that could compromise the structural performance and long-term durability. Once the column is in a vertical position the precast column's protruding HSS member should be promptly inserted into the cast-in-place footing receiving HSS pipe and grouted into place. Non-shrinkage grouting should be used to fill the void between the two HSS members that has a higher compressive strength compared to the concrete used in the column and footing. The grout can be either pumped or gravity feed into the footing grout inlet pipe. Once all the voids between the two HSS members are filled, grout would flow out of the grout vents located on each side of the column. Allow the grout to flow unobscured out of each grout vent for approximately 30 seconds to ensure all air pockets are removed that may have been trapped. Refer to the grout literature, in Appendix D, for appropriate mixing and cure times. Once the grout has been sufficiently cured, the connection is complete.

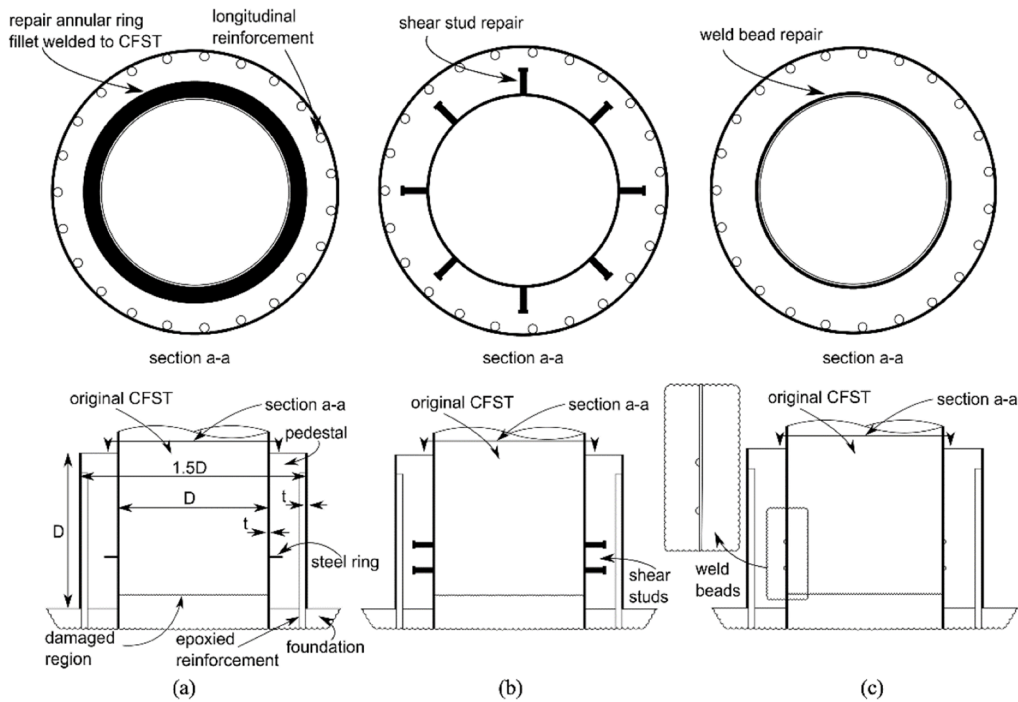
#### **6.4 Limitations of the Precast Column**

The limitations of the precast column connection are nearly the same as a traditional cast-in-place column. One of the limitations to the precast column that varies from a cast-in-place column is the column capacity. The capacity of the precast column is controlled by the compressive strength of concrete used, the size of the selected HSS member, and the material properties of the HSS member. Vertical pour of the precast column may not be possible due to concrete drop height restrictions as well as bracings for the formwork. Another limitation is the

ability to lift and rotate the column to a vertical position. Equipment capable of lifting the column is required to transport the column to its designated location. As the column height and diameter increase, the total weight of the column also increases, and as a result, larger equipment may be required. For precasting, it is recommended to stay with the available formwork sizes or standardizing the sections so multiple precast columns can be produced using the same formwork. This will help in reducing the cost of the precast columns.

### **6.5 Proposed Repair Methodologies**

If a seismic event were to occur that damaged the precast column, the precast column may be able to be repaired. (Bumstead et al. 2019) explored a variety of repair options for Concrete Filled Steel Tubes (CFST) after a major seismic event. Each of the repair methods used a concrete pedestal, 1.5 times the diameter of the steel tube, and a height equal to the steel tube, around the damaged section of the column. The concrete pedestal is encased in a steel tube to confine the concrete. The three methods are a welded embedded ring, the use of shear studs, and weld beads on the outside of the damaged pipe as shown in Figure 6.6. Using a finite element model, via ABAQUS software, the three repair methods are analyzed with a damaged concrete steel pipe as shown in Figure 6.7.



(a) Embedded ring repair, (b) Shear stud repair, and (c) Weld bead repair

Figure 6.6: Repair methods

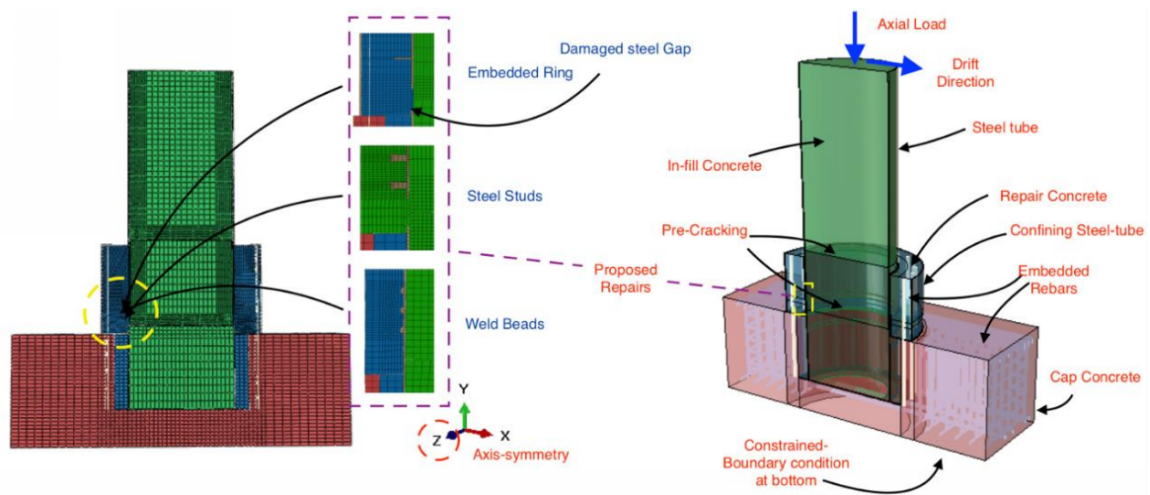


Figure 6.7: Finite element model for repair methods

The results from the analysis indicated that all of the repair methods are effective in restoring the column's original stiffness and strength. The welded bead repair is the most effective. The top four analysis results were: two embedded rings having a width of  $x4$  the pipe thickness (ER-

2x4t), four shear stud equally spaced (SS-x4), three welded bead equally spaced (WB-x3), and three welded beads with a thicker pedestal confinement tube (WB-x3-1). The graphical results of the described methods are shown in Figure 6.8 and Figure 6.9 while Figure 6.10 depicts the various repair methods that exhibited the highest results.

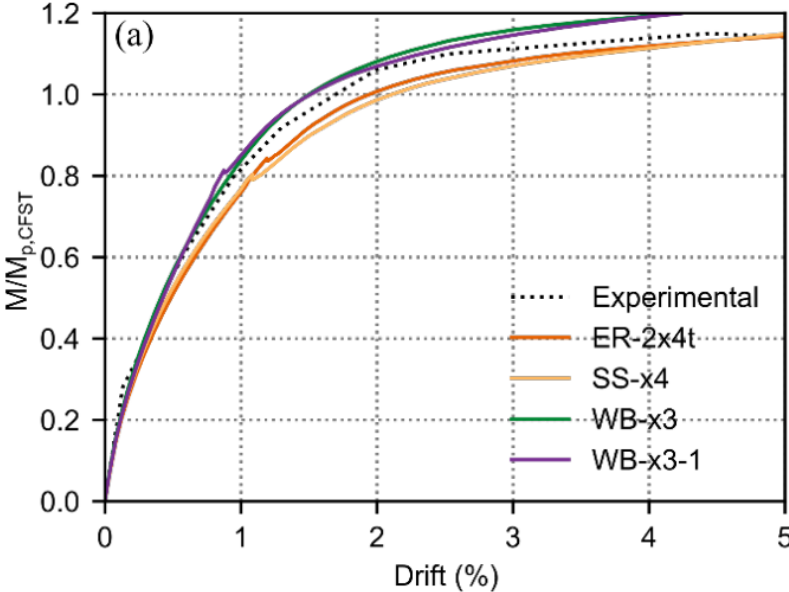


Figure 6.8: Moment vs. drift for repair methods

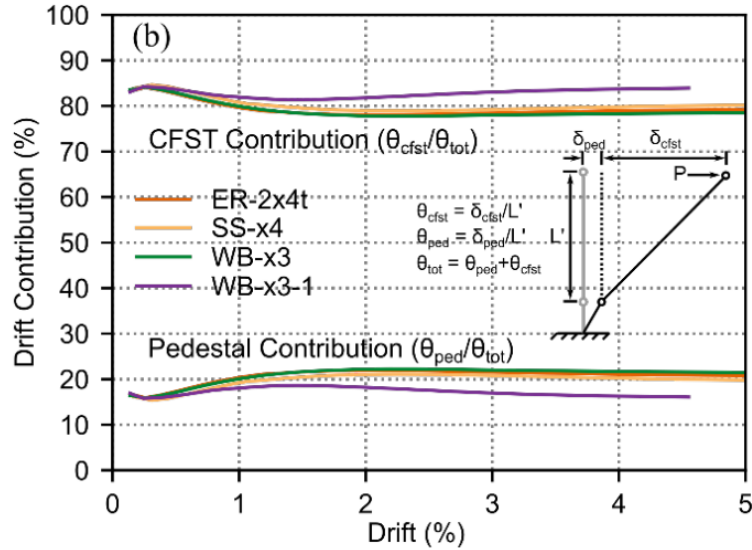


Figure 6.9: Pedestal rotation for repair methods

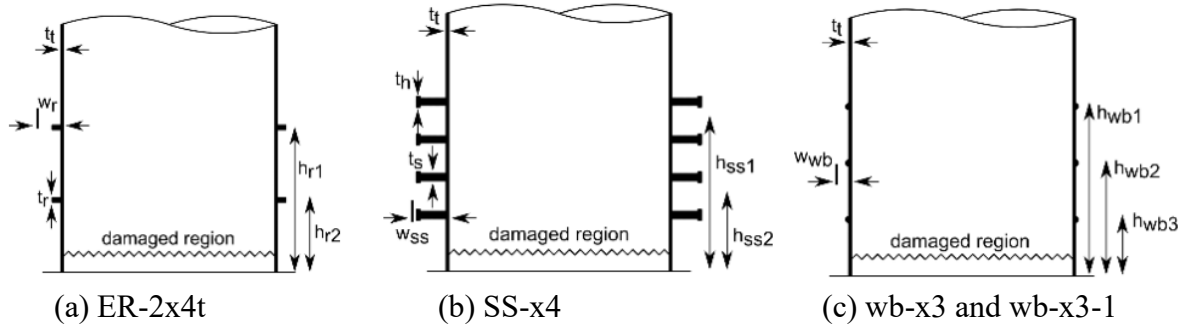


Figure 6.10: Repair methods with highest results

Some of the repair methods proposed by Bumstead (2019) may apply to the precast column connection investigated in this thesis, with some adjustments. Figure 6.11 presents a proposed repair methodology for the pipe connection based on existing literature. A concrete pedestal is cast around the base of the precast column. This repair methodology aims to push the plastic hinge further up the column and essentially transform the column behavior to a cast-in-place column. The plastic hinge is expected to form on top of the pedestal during a future earthquake. The diameter of the pedestal should be 1.5 times the diameter of the precast column. The height of the pedestal should be extended up until the termination point of the HSS member inside the

column as shown in Figure 6.11. The longitudinal rebars of the pedestal are epoxied or grouted to the drilled holes in the foundation. A combination of an embedded annular ring at the base and epoxied studs around the circumference of the column are used to connect the precast column to the pedestal.

To secure the threaded bars to the column and the pedestal rebars to the footing, the column and footing should be scanned to locate the existing rebars so the drill does not damage any rebars. The embedded ring should be welded to the exposed headed rebars instead of the HSS member because of the difficulty of welding in a confined area. An alternative to welding the embedded ring to the column after a seismic event is to weld the embedded ring before the precast column is poured. The embedded ring will not provide any support to the column until after the column has been damaged and a pedestal is poured. Testing should be carried out to validate the proposed repair methodology in Figure 6.11.

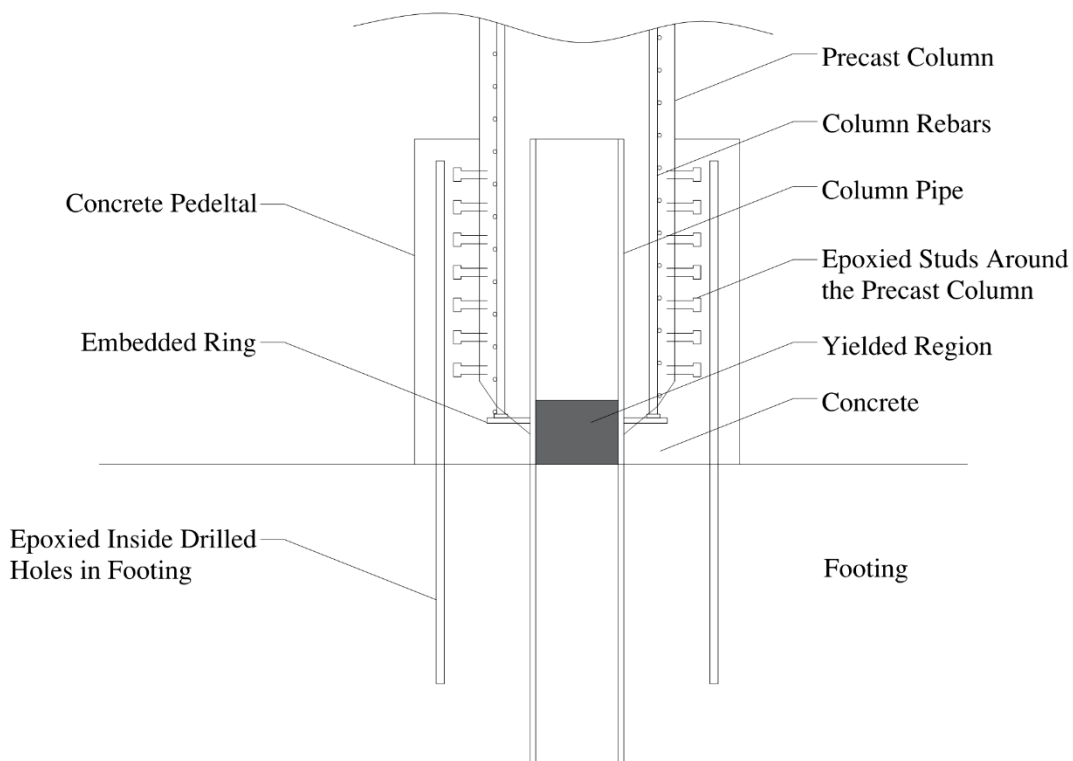


Figure 6.11: Proposed repair method for the precast column connection.

## **6.6 Conclusions**

The design, detailing, construction, assembly, and repair methods and procedures used in this research should be used as a minimum for the design of the precast column. The interaction diagrams were created using the WSDOT Bridge Design Manual. The interaction diagrams show the moment capacity increasing as the HSS member diameter and wall thickness increase. The interaction diagrams do not account for an axial load. Caution should be taken when orienting the column vertically. The limitations of the precast column are presented with the capacity of the connection, precasting technology, and the weight of the precast element. A potential repair method is the use of an embedded ring and epoxied studs made of high-strength threaded bars encased in a concrete pedestal surrounding the damaged region of the column. This repair method should be experimentally tested to verify its effectiveness.

## Chapter 7: Conclusions and Recommendations

### 7.1 Introduction

According to the 2017 ASCE infrastructure report card, approximately 4 in 10 of the bridges are 50 years old or older and 56,007 of the nation's bridges are considered structurally deficient in the year 2016. One of the ways the bridges can be replaced quickly and efficiently is by incorporating ABC methods (ASCE 2017). Some of these bridges are located in seismic zones, therefore before deploying any ABC method, it is important to investigate the seismic performance of the proposed connection between precast elements.

This research investigated the use of a precast column with a pipe connection as an alternative to the cast-in-place solution. The precast column used in this research incorporated an HSS member filled with concrete also known as a "Concrete Filled Steel Tube" CFST. Using a precast column in place of a cast-in-place column can reduce the duration of disruptions to traffic, increase the speed of construction, reduce formwork and equipment costs, increase safety on the construction site, and reduce the environmental impact to the surrounding area. The objectives of this research are as follows:

- 1) Review current ABC technologies and connections for seismic regions
- 2) Testing of a benchmark cast-in-place specimen under quasi-static cyclic loading
- 3) Outline the design procedure and detailing considerations for the proposed pipe connection
- 4) Experimentally validate the pipe connection via large-scale testing of a cantilever test specimen with similar dimensions and capacity to the cast-in-place benchmark
- 5) Compare the seismic performance of the pipe connection against the traditional cast-in-place column

- 6) Provide recommendations regarding repair considerations for the proposed pipe connection.

The first objective is accomplished in Chapter 2. The second objective is accomplished in Chapters 3, 4, and 5. Chapter 6 completed objective 3.

## **7.2 Conclusions from Research**

Both the cast-in-place and precast columns are designed with nearly the same materials properties, flexural capacity, overall shape, and dimensions. The only material that varied is the HSS member. The cast-in-place column is determined to have a moment capacity of 165 kip-ft compared to the precast column which had a moment capacity of 143 kip-ft. Although the cast-in-place column is designed to have a larger moment capacity, its overall seismic performance is lower compared to the precast column.

The precast column endured through more drift cycles 16 cycles compared to the 13 cycles that the cast-in-place column endured. The maximum displacement of the cast-in-place column during the testing procedure is 7.7 in. which corresponds to a 9.9% drift. The maximum load applied to the cast-in-place column during the testing procedure is 37.8 kip which corresponds to a 245.7 kip-ft moment capacity. The maximum displacement of the precast column during the testing procedure is 9.6 in. which corresponds to a 12.3% drift. This is 20% higher compared to the cast-in-place benchmark. The maximum load applied to the precast column during the testing procedure is 41.2 kip which corresponds to a 267.8 kip-ft moment capacity. This is 9% higher compared to the cast-in-place benchmark. The precast column also dissipated more energy 1025 kJ compared to 456 kJ for the cast-in-place column which is just below half of what the precast column dissipated.

Based on the results above, several conclusions can be made when comparing a precast column and cast-in-place column having identical overall dimensions and moment capacities.

- The precast column pipe connection offers ABC advantages as well as better tolerances and performance compared to other connections such as grouted ducts.
- During a seismic event, the precast column can absorb more of the energy released by an earthquake. The precast column can absorb more energy because there is more steel located at the column to footing interface as a result of the HSS pipe which makes the connection more ductile.
- The precast column has better confinement and shear resistance.
- The precast column connection will stay intact longer and maintain its structural integrity during a major seismic event. This is evident because the precast column was able to endure through more of the cyclic loads during the testing procedure.
- Based on the observations during each of the testing procedures, the precast column does not get damaged during smaller seismic events due to lower initial stiffness and flexibility to accommodate small displacements at the top. This provides better performance for the serviceability of the bridge. Testing showed that cracks on the cast-in-place column after the first cycle (0.16 in. of displacement or 0.2% drift) compared to the third cycle (0.47 in. of displacement or 0.6% drift) for the precast column.
- Overall, the precast column performs better during a seismic event compared to the cast-in-place column.
- It is possible to repair the precast column using traditional methodologies such as concrete jacketing after an earthquake.

### 7.3 Future Research Suggestions

Additional research can be conducted on the following topics:

- The embedment length of the pipe should be refined based on experimental pull out tests and analytical Finite Element modeling. Two embedment lengths were calculated to determine an appropriate length. The two calculations were from the WSDOT LRFD Bridge Manual (WSDOT 2019) and Integral Abutment for Steel Bridges (Wasserman and Walker 1996). Additional research should be conducted to not only verify the methods but also to close the gap between the two.
- The appropriate gap between the column and footing pipes should be refined and optimized for tolerance and structure performance through experimental and analytical work.
- Experimental and analytical work should be performed to quantify the accurate unbonded length of the pipe. More information is needed on this topic to understand the effects of the unbonded length of a pipe embedded into the concrete. Leaving an unbonded length is not common practice and needs to be understood to clarify its use in CFST.
- The repair methods discussed in the previous chapter should also be tested to prove whether or not they should be used as adequate repair methods. The literature regarding CFST is a good resource, but the proposed repair method has not been tested.
- The performance of the proposed pipe connection in this thesis should be experimentally investigated in a frame/bent structure.
- Bi-directional quasi-static cyclic, shake table testing, and consideration of soil-structure interaction for the proposed pipe connection will provide valuable data about its performance for a wider application and various seismic hazard/ground motion type.

## References

- AASHTO. (2017). *AASHTO LRFD Bridge Design Specifications*. American Association of State Highway and Transportation Officials, 8th Edition.
- ACI Committee 374. (2013). *Guide for testing reinforced concrete structural elements under slowly applied simulated seismic loads (ACI 374.2R-13)*. American Concrete Institute, Farmington Hills, MI.
- AISC Committee. (2010). *Steel Construction Manual American Institute of Steel Construction*. Chicago, Ill
- Al-Kaseasbeh, Q., and Mamaghani, I. H. P. (2019). "Performance of Thin-Walled Steel Tubular Circular Columns with Graded Thickness under Bidirectional Cyclic Loading." *ASCE Structures Congress 2019*.
- Ameli, M. J., Brown, D. N., Parks, J. E., and Pantelides, C. P. (2016). "Seismic column-to-footing connections using grouted splice sleeves." *ACI Structural Journal*.
- ASCE. (2017). "Infrastructure Report Card." ASCE's Infrastructure Report Card, <<https://www.infrastructurereportcard.org/cat-item/bridges/>> (Jan. 8, 2020)
- ASCE. (2018). *Report Card for Idaho's Infrastructure*. ASCE's Infrastructure Report Card, <<https://www.infrastructurereportcard.org/cat-item/bridges/>> (Jan. 8, 2020)
- Bumstead, J., Korat, J., and Stephens, M. T. (2019). "Repair Strategies for Earthquake-Damaged CFST Bridge Columns." *ASCE Structures Congress 2019*, 154–164.
- Chapel Steel. (2018). *Structural, Carbon & HSLA Steel Plate*. <<https://www.chapelsteel.com/a709-grade50-grade-345.html>> (Feb. 22, 2020).
- Chopra, Anil K. (2017). *Dynamics of Structures: Theory and Applications to Earthquake Engineering*. Pearson Education Limited.
- Collins, M. P., and Mitchell, D. (1991). *Prestressed Concrete Structures*. Prentice-Hall. Englewood Cliffs, NJ.
- Galvis, F., and Correal, J. F. (2017). "Characterization of the seismic behavior of a column-foundation connection for accelerated bridge construction."
- Kim, C. S., Lim, W. Y., Park, H. G., and Oh, J. K. (2016). "Cyclic loading test for cast-in-place concrete-filled hollow precast concrete columns." *ACI Structural Journal*.
- Marsh, L. P. (2018). "Seismic Design and Accelerated Bridge Construction (ABC)." <<http://onlinepubs.trb.org/onlinepubs/webinars/180711.pdf>>. (Jan. 10, 2020)
- Marsh, M. L. et al. (2011). *Application of Accelerated Bridge Construction Connections in*

*Moderate-to-High Seismic Regions.*

- Mashal, M., and Palermo, A. (2019a). "Low-damage seismic design for accelerated bridge construction." *Journal of Bridge Engineering*.
- Mashal, M., and Palermo, A. (2019b). "Emulative seismic resistant technology for Accelerated Bridge Construction." *Soil Dynamics and Earthquake Engineering*, Elsevier Ltd, 124(December 2018), 197–211.
- Mashal, M., White, S., and Palermo, A. (2016). "Quasi-static Cyclic Testing of Emulative Cast-in-place Connections for Accelerated Bridge Construction in Seismic Regions." *Bulletin of the New Zealand Society for Earthquake Engineering*, 49(3).
- McCormac, J.C., and Brown, R.H. (2014) *Design of Reinforced Concrete*. Wiley, Hoboken, NJ
- Mehraein, M., and Saiidi, M. S. (2016). *Seismic Performance of Bridge Column-Pile-Shaft Pin Connections for Application in Accelerated Bridge Construction*. Reno, NV.
- Ou, Y. C., Alrasyid, H., Haber, Z. B., and Lee, H. J. (2015). "Cyclic behavior of precast high-strength reinforced concrete columns." *ACI Structural Journal*.
- Pampanin, S. et al. (2010). *PRESSS Technology Design Handbook*. NZCS, Auckland N.Z.
- Priestley, M. J. N., Calvi, G. M., and Kowalsky, M. J. (2007). *Displacement-Based Seismic Design of Structures. Earthquake Spectra*, IUSS Press.
- Tazarv, M., and Saiidi, M. S. (2015a). *Design and Construction of Precast Bent Caps with Pocket Connections for High Seismic Regions*. Reno, NV.
- Tazarv, M., and Saiidi, M. S. (2015b). *Design and Construction of Bridge Columns Incorporating Mechanical Bar Splices in Plastic Hinge Zones*. Reno, NV.
- U.S. Department of Transportation/Federal Highway Administration. (2019). "Accelerated Bridge Construction." <<https://www.fhwa.dot.gov/bridge/abc/>> (Jan. 8, 2020).
- Vielma, J. C., and Mulder, M. M. (2017). "Procedure for Assessing the Displacement Ductility Based on Seismic Collapse Threshold and Dissipated Energy Balance." *16th World Conference on Earthquake Engineering*, (January).
- Wasserman, E. P., and Walker, J. H. (1996). *Integral Abutments for Steel Bridges*. American Iron and Steel Institute, Chicago, Ill
- WSDOT. (2019). "*Bridge Design Manual (LRFD)*." Engineering and Regional Operations Bridge and Structures Office
- Zaghi, A. E., and Saiidi, M. S. (2010). *Seismic Design of Pipe-Pin Connections in Concrete Bridges*. Reno, NV.

Zollman, C. C., Depman, F., Nagle, J., and Hollander, E. F. (1992). "Building and Rebuilding of Philadelphia's Walnut Lane Memorial Bridge." *PCI Journal*, 37(4), 66–82.

## Appendix A: Construction Drawings

### A.1 Cast-in-place Column Drawings

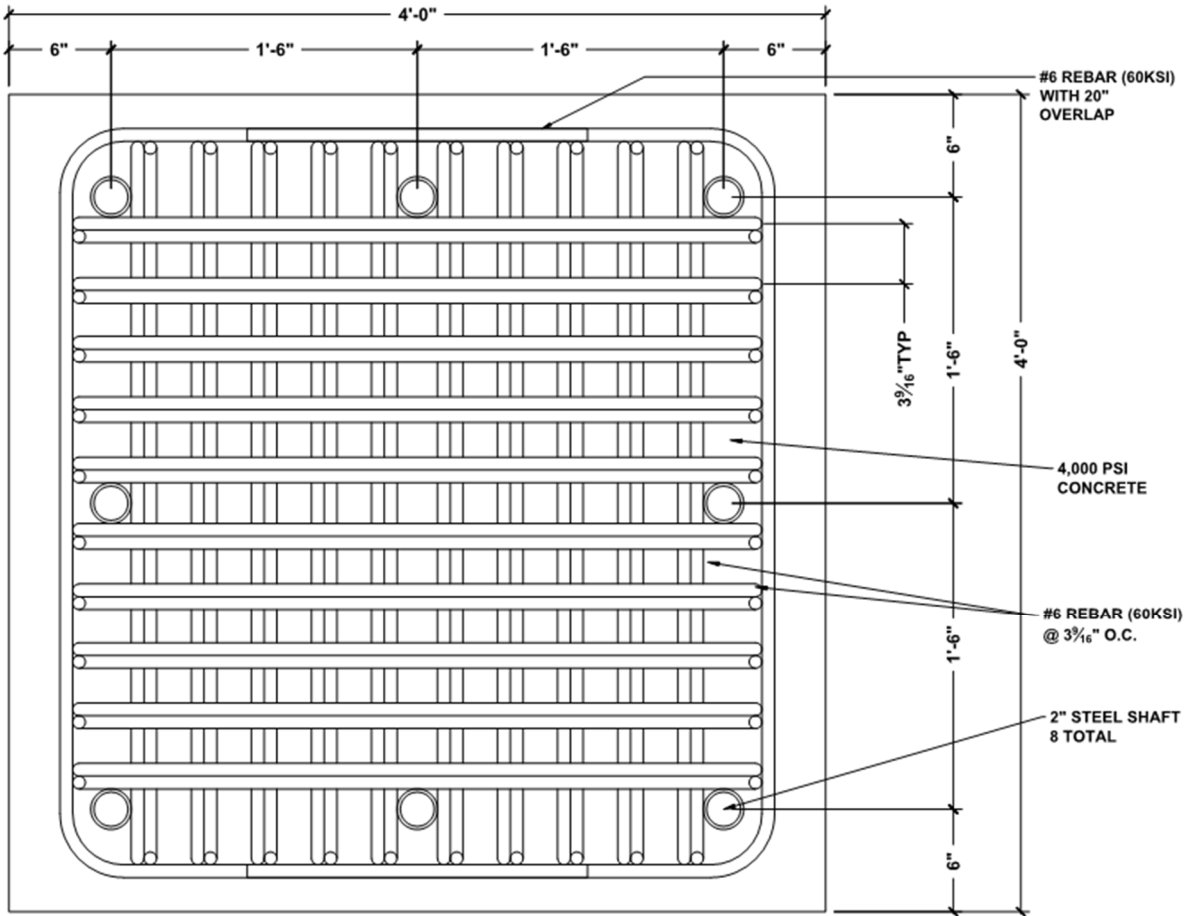


Figure A.1: Cast-in-place footing details.

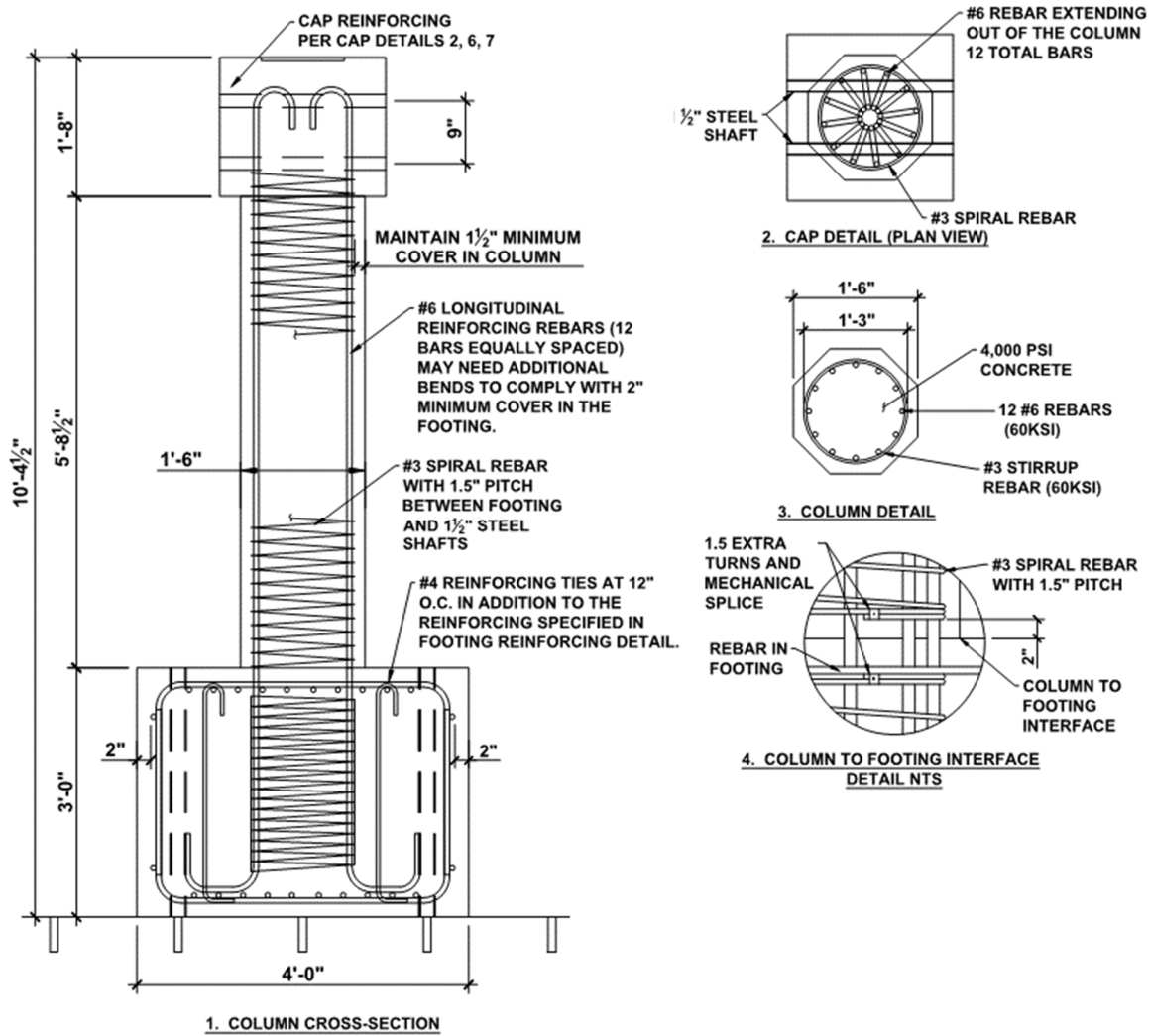


Figure A.2: Cast-in-place column Details.

## A.2 Precast Column Drawings

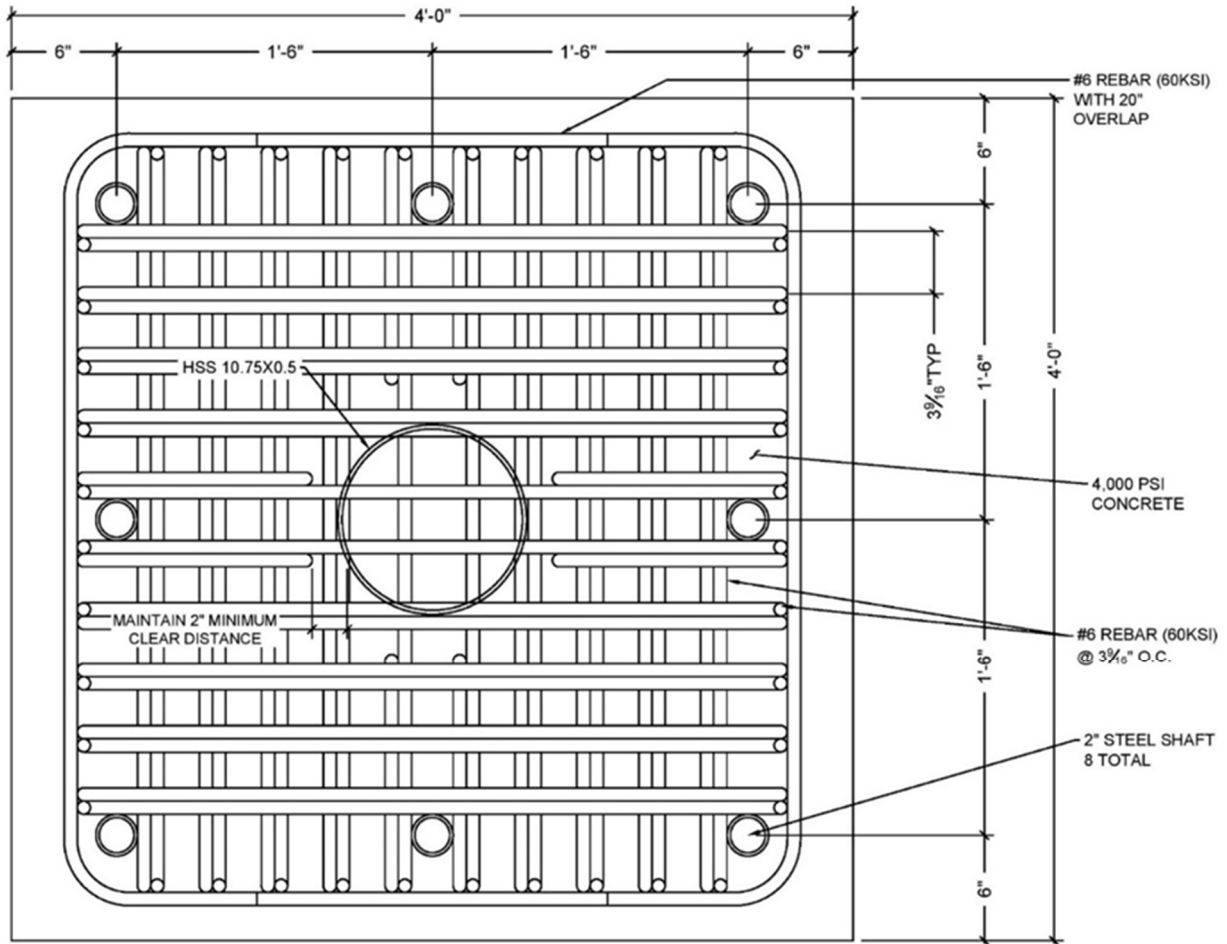


Figure A.3: Precast footing details.

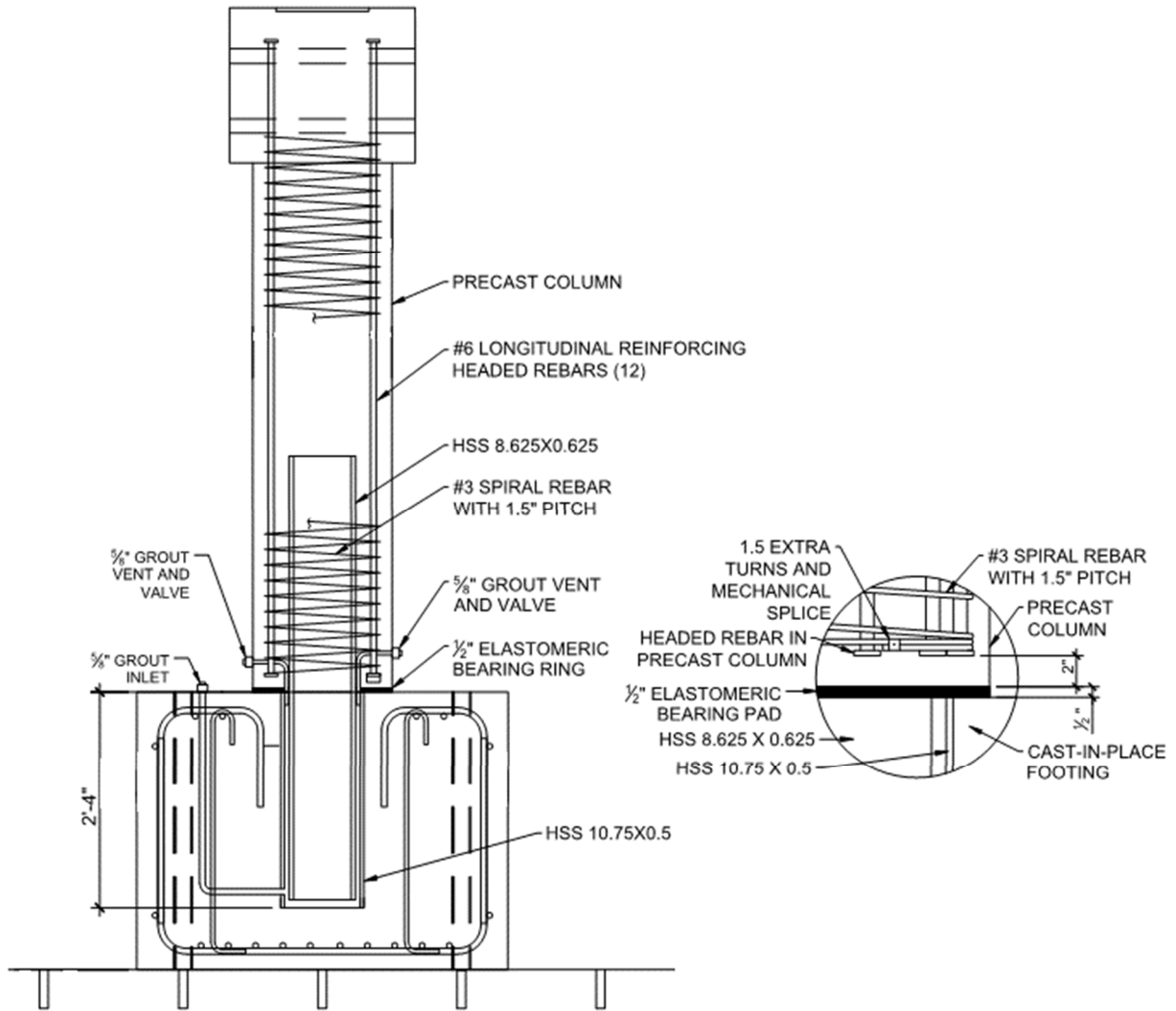


Figure A.4: Precast column details.

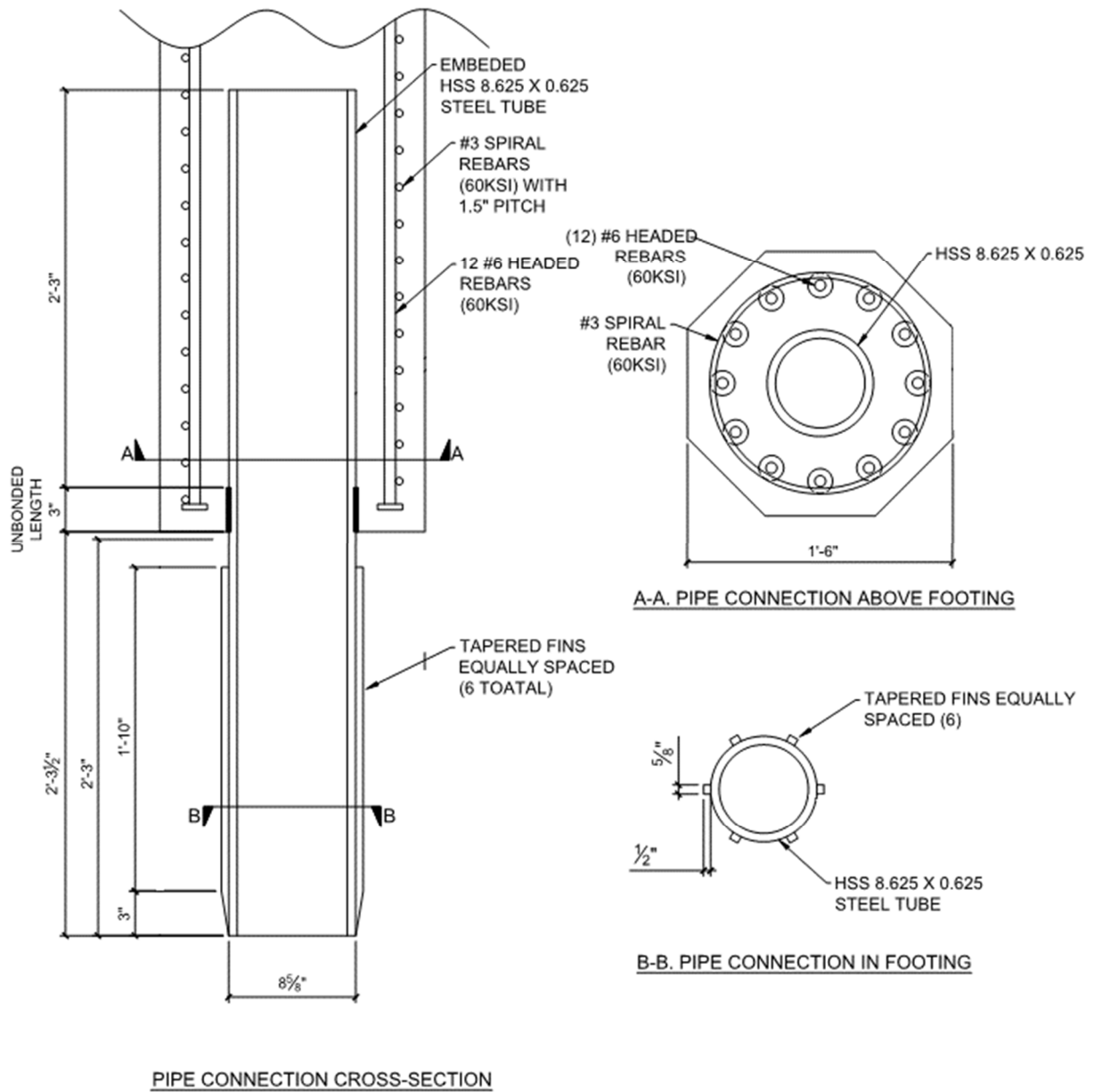


Figure A.5: Connection details for the precast column.

## Appendix B: Design Calculations of the Specimens

### B.1 Cast-In-Place Column Calculations

<p>Circular Column Dimensions</p> <p>Column Diameter = 18 in</p> <p>Cover = 1.5 in</p> <p>Sturup Spacing = 3</p> <p>Long. Bar # = 6</p> <p>Total bars = 12</p> <p><math>D_{core}</math> = 13.5 in</p>	<p>Compression strain = -0.003</p> <p>Tensile strain = 0.002</p> <p><math>f_y</math> = 60 ksi</p> <p><math>f_c</math> = 4 ksi</p> <p><math>E_s</math> = 29000 ksi</p> <p><math>\beta_1</math> = 0.85 (see pg 68)</p> <p><math>\phi</math> = 0.75 (Figure 3.5 pg. 72)</p>	<p>Key Values</p> <p>Input Values</p>
---	--	---------------------------------------

For equivalent rectangular Column (Figure 10.9)

$$B = A_g / (.8D) = 17.67$$

$$H = .8 * D = 14.40$$

$$H_s = D_s * 2/3 = 9.00$$

$$A'_s = 2.65$$

$$Cover = 2.70$$

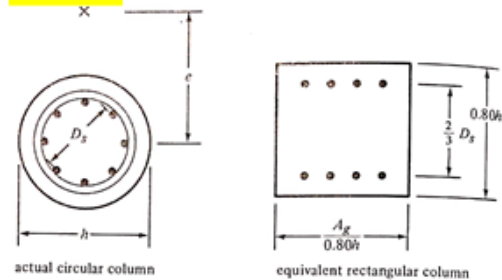


FIGURE 10.9 Replacing a circular column with an equivalent rectangular one.

Determine values of  $y$  and of the steel strains

$y$  = distance from extreme compression fiber to neutral axis

$\epsilon'_s$  = strain in compression reinforcement

$\epsilon_s$  = strain in tension reinforcement

$$y = 0.003 / (0.003 + 0.002) * 14.4 = 8.64 \text{ in.}$$

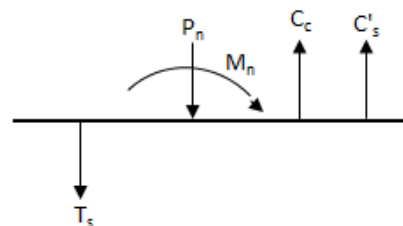
$$\epsilon'_s = ((8.64 - 2.7) / 8.64) * 0.003 = 0.00206 > 0.002 \text{ Yields}$$

$$\epsilon_s = ((14.4 - 8.64 - 2.7) / (14.4 - 8.64)) * 0.002 = 0.00106 < 0.002 \text{ Does Not Yield}$$

$a = \beta_1 * y = 0.85 * 8.64 = 7.34 \text{ in.}$	$a$ = depth of equivalent stress block
$C_c = \beta_1 * a * B * f_c = -441.25 \text{ kips}$	$C_c$ = total compression in the concrete
$C'_s = f_y * A'_s - \beta_1 * A'_s * f_c = -150.03 \text{ kips}$	$C'_s$ = total compression in the compression steel
$T_s = \epsilon_s * E * A_s = 81.68 \text{ kips}$	$T_s$ = total tension in the tensile steel

$$P_n = 509.60 \text{ kips}$$

$$F_e * P_n = 382.20 \text{ kips}$$



$$M_n = 2599.40 \text{ kip-in.} = 216.62 \text{ kip-ft.}$$

$$\phi * M_n = 1949.55 \text{ kip-in.} = 162.46 \text{ kip-ft.}$$

$$\text{Column height} = 78.00 \text{ in.}$$

$$V_u = 24.99 \text{ kip}$$

## B.2 Precast Column Calculations

### Key Values

### Input Values

HSS8.625X0.625

Pipe Connection		$f_y =$	42 ksi	AISC Table 2-4 pg 2-48
Pipe Diameter =	8.625 in.	$f_u =$	58 ksi	AISC Table 2-4 pg 2-48
Pipe Thickness =	0.581 in.	$f_c =$	4 ksi	
Concrete Diameter =	7.463 in.	$E_s =$	29000 ksi	

$$D/t = 14.85 < \text{Good} \quad 103.57$$

$$A_s = 14.68 \text{ in}^2$$

$$A_c = 43.74 \text{ in}^2$$

$$y = 0 \text{ in.} \quad \text{Distance to the neutral axis}$$

WSDOT CH7

Compressive resistance of a member without consideration of flexure

$$P_o = 782.9 \text{ kips} = 0.95f_cA_c + F_{y,st}A_{st} \quad 7.10.2-5$$

Radius to the center of the steel tube

$$r_m = 4.02 \text{ in.} = r - t/2 \quad 7.10.2-9$$

Angle used to define c

$$\theta = 0.00 \text{ degrees} = \sin^{-1}(y/r_m) \quad 7.10.2-8$$

One half the chord length of the tube in compression

$$c = 3.73 \text{ in.} = r_i \cos \theta \quad 7.10.2-7$$

Nominal moment resistance as a function of the parameter y

$$M_n(y) = 1710.58 \text{ kip-in.} = (c(r_i^2 - y^2) - c^3/3) * 0.95f_c + 4ct(r_m^2/r_i)F_y \quad 7.10.2-6$$

$$= 142.5 \text{ kip-ft.}$$

$$\text{Column height} = 78.00 \text{ in.}$$

$$V_u = 21.93 \text{ kip}$$

## Appendix C: Interaction Diagrams and Tables for the Precast Column

### C.1 HSS Pipe Connection $f'_c = 4$ ksi

#### C.1.1 HSS thickness = 0.174 in.

Key Values		Input Values											
$f_y =$	42 ksi	AISC Table 2-4 pg 2-48											
$f_u =$	58 ksi	AISC Table 2-4 pg 2-48											
$f'_c =$	4 ksi												
$E_s =$	29000 ksi												
Pipe Thickness =	0.174 in.												
Pipe D (in.)	Concrete D (in.)	D/t		$A_s$ (in <sup>2</sup> )	$A_c$ (in <sup>2</sup> )	$P_o$ (kips)	$r_m$ (in.)	$\theta$ (deg.)	c (in.)	Mn(y) (kip-ft)			
20	19.65	114.94	> BAD										
18	17.65	103.45	< Good	103.57	9.74	244.72	1339.2	8.91	0.00	8.83	338.7		
15	14.65	86.21	< Good	103.57	8.10	168.61	981.1	7.41	0.00	7.33	216.9		
10	9.65	57.47	< Good	103.57	5.37	73.17	503.6	4.91	0.00	4.83	82.5		

#### C.1.2 HSS thickness = 0.233 in.

Key Values		Input Values											
$f_y =$	42 ksi	AISC Table 2-4 pg 2-48											
$f_u =$	58 ksi	AISC Table 2-4 pg 2-48											
$f'_c =$	4 ksi												
$E_s =$	29000 ksi												
Pipe Thickness =	0.233 in.												
Pipe D (in.)	Concrete D (in.)	D/t		$A_s$ (in <sup>2</sup> )	$A_c$ (in <sup>2</sup> )	$P_o$ (kips)	$r_m$ (in.)	$\theta$ (deg.)	c (in.)	Mn(y) (kip-ft)			
30	29.53	128.76	> BAD										
24	23.53	103.00	< Good	103.57	17.40	434.99	2383.7	11.88	0.00	11.77	804.6		
20	19.53	85.84	< Good	103.57	14.47	299.69	1746.5	9.88	0.00	9.77	515.3		
15	14.53	64.38	< Good	103.57	10.81	165.91	1084.4	7.38	0.00	7.27	258.8		
10	9.53	42.92	< Good	103.57	7.15	71.39	571.6	4.88	0.00	4.77	100.7		

### C.1.3 HSS thickness = 0.291 in.

Key Values
Input Values

$f_y = 42$  ksi      AISC Table 2-4 pg 2-48  
 $f_u = 58$  ksi      AISC Table 2-4 pg 2-48  
 $f_c = 4$  ksi  
 $E_s = 29000$  ksi  
 Pipe Thickness = 0.291 in.

Pipe D (in.)	Concrete D (in.)	D/t		$A_s$ (in <sup>2</sup> )	$A_c$ (in <sup>2</sup> )	$P_o$ (kips)	$r_m$ (in.)	$\theta$ (deg.)	c (in.)	Mn(y) (kip-ft)	
40	39.42	137.46	> BAD								
30	29.42	103.09	< Good	103.57	27.16	679.70	3723.6	14.85	0.00	14.71	1570.8
20	19.42	68.73	< Good	103.57	18.02	296.14	1882.1	9.85	0.00	9.71	588.8
15	14.42	51.55	< Good	103.57	13.45	163.27	1185.2	7.35	0.00	7.21	299.4
10	9.42	34.36	< Good	103.57	8.88	69.66	637.5	4.85	0.00	4.71	118.1

### C.1.4 HSS thickness = 0.349 in.

Key Values
Input Values

$f_y = 42$  ksi      AISC Table 2-4 pg 2-48  
 $f_u = 58$  ksi      AISC Table 2-4 pg 2-48  
 $f_c = 4$  ksi  
 $E_s = 29000$  ksi  
 Pipe Thickness = 0.349 in.

Pipe D (in.)	Concrete D (in.)	D/t		$A_s$ (in <sup>2</sup> )	$A_c$ (in <sup>2</sup> )	$P_o$ (kips)	$r_m$ (in.)	$\theta$ (deg.)	c (in.)	Mn(y) (kip-ft)	
40	39.30	114.61	> BAD								
36	35.30	103.15	< Good	103.57	39.09	978.79	5361.1	17.83	0.00	17.65	2713.5
30	29.30	85.96	< Good	103.57	32.51	674.35	3927.9	14.83	0.00	14.65	1737.8
20	19.30	57.31	< Good	103.57	21.55	292.61	2016.8	9.83	0.00	9.65	661.5
15	14.30	42.98	< Good	103.57	16.06	160.65	1285.1	7.33	0.00	7.15	339.4
10	9.30	28.65	< Good	103.57	10.58	67.96	702.7	4.83	0.00	4.65	135.0

### C.1.5 HSS thickness = 0.465 in.

Key Values
Input Values

$f_y =$	42 ksi	AISC Table 2-4 pg 2-48
$f_u =$	58 ksi	AISC Table 2-4 pg 2-48
$f_c =$	4 ksi	
$E_s =$	29000 ksi	
Pipe Thickness =	0.465 in.	

Pipe D (in.)	Concrete D (in.)	D/t		$A_s$ (in <sup>2</sup> )	$A_c$ (in <sup>2</sup> )	$P_o$ (kips)	$r_m$ (in.)	$\theta$ (deg.)	c (in.)	Mn(y) (kip-ft)	
50	49.07	107.53	> BAD								
48	47.07	103.23	< Good	103.57	69.44	1740.12	9529.0	23.77	0.00	23.54	6429.5
40	39.07	86.02	< Good	103.57	57.75	1198.88	6981.4	19.77	0.00	19.54	4117.6
30	29.07	64.52	< Good	103.57	43.15	663.71	4334.2	14.77	0.00	14.54	2068.0
20	19.07	43.01	< Good	103.57	28.54	285.62	2283.9	9.77	0.00	9.54	804.1
15	14.07	32.26	< Good	103.57	21.23	155.48	1482.6	7.27	0.00	7.04	417.3
10	9.07	21.51	< Good	103.57	13.93	64.61	830.5	4.77	0.00	4.54	167.7

### C.1.6 HSS thickness = 0.581 in.

Key Values
Input Values

$f_y =$	42 ksi	AISC Table 2-4 pg 2-48
$f_u =$	58 ksi	AISC Table 2-4 pg 2-48
$f_c =$	4 ksi	
$E_s =$	29000 ksi	
Pipe Thickness =	0.581 in.	

Pipe D (in.)	Concrete D (in.)	D/t		$A_s$ (in <sup>2</sup> )	$A_c$ (in <sup>2</sup> )	$P_o$ (kips)	$r_m$ (in.)	$\theta$ (deg.)	c (in.)	Mn(y) (kip-ft)	
70	68.84	120.48	> BAD								
60	58.84	103.27	< Good	103.57	108.46	2718.98	14887.2	29.71	0.00	29.42	12554.7
50	48.84	86.06	< Good	103.57	90.20	1873.29	10907.0	24.71	0.00	24.42	8040.2
40	38.84	68.85	< Good	103.57	71.95	1184.69	7523.7	19.71	0.00	19.42	4705.7
30	28.84	51.64	< Good	103.57	53.70	653.16	4737.3	14.71	0.00	14.42	2392.8
15	13.84	25.82	< Good	103.57	26.32	150.40	1676.9	7.21	0.00	6.92	492.7
10	8.84	17.21	< Good	103.57	17.19	61.35	955.2	4.71	0.00	4.42	198.6

## C.2 HSS Pipe Connection $f'_c = 8$ ksi

### C.2.1 HSS thickness = 0.174 in.

Key Values
Input Values

$f_y =$	42 ksi	AISC Table 2-4 pg 2-48
$f_v =$	58 ksi	AISC Table 2-4 pg 2-48
$f_c =$	8 ksi	
$E_s =$	29000 ksi	
Pipe Thickness =	0.174 in.	

Pipe D (in.)	Concrete D (in.)	D/t		$A_s$ (in <sup>2</sup> )	$A_c$ (in <sup>2</sup> )	$P_o$ (kips)	$r_m$ (in.)	$\theta$ (deg.)	c (in.)	Mn(y) (kip-ft)	
20	19.65	114.94	> BAD								
18	17.65	103.45	< Good	103.57	9.74	244.72	2269.2	8.91	0.00	8.83	483.8
15	14.65	86.21	< Good	103.57	8.10	168.61	1621.8	7.41	0.00	7.33	299.9
10	9.65	57.47	< Good	103.57	5.37	73.17	781.7	4.91	0.00	4.83	106.3

### C.2.2 HSS thickness = 0.233 in.

Key Values
Input Values

$f_y =$	42 ksi	AISC Table 2-4 pg 2-48
$f_v =$	58 ksi	AISC Table 2-4 pg 2-48
$f_c =$	8 ksi	
$E_s =$	29000 ksi	
Pipe Thickness =	0.233 in.	

Pipe D (in.)	Concrete D (in.)	D/t		$A_s$ (in <sup>2</sup> )	$A_c$ (in <sup>2</sup> )	$P_o$ (kips)	$r_m$ (in.)	$\theta$ (deg.)	c (in.)	Mn(y) (kip-ft)	
30	29.53	128.76	> BAD								
24	23.53	103.00	< Good	103.57	17.40	434.99	4036.6	11.88	0.00	11.77	1148.6
20	19.53	85.84	< Good	103.57	14.47	299.69	2885.4	9.88	0.00	9.77	712.0
15	14.53	64.38	< Good	103.57	10.81	165.91	1714.9	7.38	0.00	7.27	339.9
10	9.53	42.92	< Good	103.57	7.15	71.39	842.8	4.88	0.00	4.77	123.5

### C.2.3 HSS thickness = 0.291 in.

Key Values
Input Values

$f_y = 42$  ksi      AISC Table 2-4 pg 2-48  
 $f_u = 58$  ksi      AISC Table 2-4 pg 2-48  
 $f_c = 8$  ksi  
 $E_s = 29000$  ksi  
 Pipe Thickness = 0.291 in.

Pipe D (in.)	Concrete D (in.)	D/t		$A_s$ (in <sup>2</sup> )	$A_c$ (in <sup>2</sup> )	$P_o$ (kips)	$r_m$ (in.)	$\theta$ (deg.)	c (in.)	Mn(y) (kip-ft)	
40	39.42	137.46	> BAD								
30	29.42	103.09	< Good	103.57	27.16	679.70	6306.4	14.85	0.00	14.71	2242.6
20	19.42	68.73	< Good	103.57	18.02	296.14	3007.4	9.85	0.00	9.71	782.1
15	14.42	51.55	< Good	103.57	13.45	163.27	1805.6	7.35	0.00	7.21	378.5
10	9.42	34.36	< Good	103.57	8.88	69.66	902.2	4.85	0.00	4.71	140.1

### C.2.4 HSS thickness = 0.349 in.

Key Values
Input Values

$f_y = 42$  ksi      AISC Table 2-4 pg 2-48  
 $f_u = 58$  ksi      AISC Table 2-4 pg 2-48  
 $f_c = 8$  ksi  
 $E_s = 29000$  ksi  
 Pipe Thickness = 0.349 in.

Pipe D (in.)	Concrete D (in.)	D/t		$A_s$ (in <sup>2</sup> )	$A_c$ (in <sup>2</sup> )	$P_o$ (kips)	$r_m$ (in.)	$\theta$ (deg.)	c (in.)	Mn(y) (kip-ft)	
40	39.30	114.61	> BAD								
36	35.30	103.15	< Good	103.57	39.09	978.79	9080.5	17.83	0.00	17.65	3874.4
30	29.30	85.96	< Good	103.57	32.51	674.35	6490.5	14.83	0.00	14.65	2401.8
20	19.30	57.31	< Good	103.57	21.55	292.61	3128.8	9.83	0.00	9.65	851.2
15	14.30	42.98	< Good	103.57	16.06	160.65	1895.6	7.33	0.00	7.15	416.6
10	9.30	28.65	< Good	103.57	10.58	67.96	960.9	4.83	0.00	4.65	156.3

### C.2.5 HSS thickness = 0.465 in.

Key Values
Input Values

$f_y = 42$  ksi      AISC Table 2-4 pg 2-48  
 $f_u = 58$  ksi      AISC Table 2-4 pg 2-48  
 $f_c = 8$  ksi  
 $E_s = 29000$  ksi  
 Pipe Thickness = 0.465 in.

Pipe D (in.)	Concrete D (in.)	D/t		$A_s$ (in <sup>2</sup> )	$A_c$ (in <sup>2</sup> )	$P_o$ (kips)	$r_m$ (in.)	$\theta$ (deg.)	c (in.)	Mn(y) (kip-ft)	
50	49.07	107.53	> BAD								
48	47.07	103.23	< Good	103.57	69.44	1740.12	16141.4	23.77	0.00	23.54	9181.5
40	39.07	86.02	< Good	103.57	57.75	1198.88	11537.2	19.77	0.00	19.54	5691.4
30	29.07	64.52	< Good	103.57	43.15	663.71	6856.3	14.77	0.00	14.54	2716.2
20	19.07	43.01	< Good	103.57	28.54	285.62	3369.3	9.77	0.00	9.54	987.1
15	14.07	32.26	< Good	103.57	21.23	155.48	2073.5	7.27	0.00	7.04	490.8
10	9.07	21.51	< Good	103.57	13.93	64.61	1076.1	4.77	0.00	4.54	187.3

### C.2.6 HSS thickness = 0.581 in.

Key Values
Input Values

$f_y = 42$  ksi      AISC Table 2-4 pg 2-48  
 $f_u = 58$  ksi      AISC Table 2-4 pg 2-48  
 $f_c = 8$  ksi  
 $E_s = 29000$  ksi  
 Pipe Thickness = 0.581 in.

Pipe D (in.)	Concrete D (in.)	D/t		$A_s$ (in <sup>2</sup> )	$A_c$ (in <sup>2</sup> )	$P_o$ (kips)	$r_m$ (in.)	$\theta$ (deg.)	c (in.)	Mn(y) (kip-ft)	
70	68.84	120.48	> BAD								
60	58.84	103.27	< Good	103.57	108.46	2718.98	25219.4	29.71	0.00	29.42	17929.9
50	48.84	86.06	< Good	103.57	90.20	1873.29	18025.5	24.71	0.00	24.42	11114.2
40	38.84	68.85	< Good	103.57	71.95	1184.69	12025.5	19.71	0.00	19.42	6251.6
30	28.84	51.64	< Good	103.57	53.70	653.16	7219.3	14.71	0.00	14.42	3025.7
15	13.84	25.82	< Good	103.57	26.32	150.40	2248.4	7.21	0.00	6.92	562.6
10	8.84	17.21	< Good	103.57	17.19	61.35	1188.3	4.71	0.00	4.42	216.8

## C.4 Cast-in-place Moment Capacities with $f'_c = 4$ ksi

Key values  
Input values

Circular Column Dimensions  
 Cover = 1.5 in.  
 Sturup Spacing = 3 in.  
 Long. Bar # = 6  
 $\emptyset = 0.75$  (Figure 3.5 pg. 72)

Compression strain = -0.003  
 Tensile strain = 0.002  
 $f_y = 60$  ksi  
 $f'_c = 4$  ksi  
 $E_s = 29000$  ksi  
 $\beta_1 = 0.85$  (see pg 68)

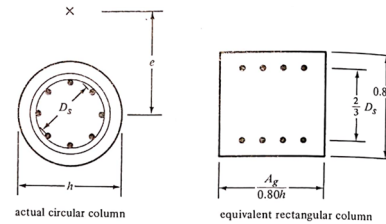


FIGURE 10.9 Replacing a circular column with an equivalent rectangular one.

Appx. Pipe size	D (in.)	$D_{core}$ (in.)	# of bars	$\rho$	B	H	$H_s$	$A'_s$	Cover	y	$\epsilon'_s$	$\epsilon_s$	a (in.)	$C_c$ (kips)	$C'_s$ (kips)	$T_s$ (kips)	$P_n$ (kips)	$\emptyset M_n$ (kip-ft.)
9	18	13.5	12	2.1%	17.67	14.40	9.00	2.65	2.70	8.64	0.00206	0.00106	7.34	-441.25	-150.03	81.68	509.60	162.46
15	24	19.5	22	2.1%	23.56	19.20	13.00	4.86	3.10	11.52	0.00219	0.00119	9.79	-784.44	-275.06	168.09	891.41	410.65
21	30	25.5	33	2.1%	29.45	24.00	17.00	7.29	3.50	14.4	0.00227	0.00127	12.24	-1225.69	-412.58	268.65	1369.63	812.35
27	36	31.5	48	2.1%	35.34	28.80	21.00	10.60	3.90	17.28	0.00232	0.00132	14.69	-1765.00	-600.12	406.77	1958.34	1439.14
33	42	37.5	65	2.1%	41.23	33.60	25.00	14.36	4.30	20.16	0.00236	0.00136	17.14	-2402.36	-812.67	566.33	2648.69	2313.35
39	48	43.5	86	2.1%	47.12	38.40	29.00	19.00	4.70	23.04	0.00239	0.00139	19.58	-3137.77	-1075.22	764.67	3448.32	3512.41
45	54	49.5	110	2.1%	53.01	43.20	33.00	24.30	5.10	25.92	0.00241	0.00141	22.03	-3971.24	-1375.28	993.36	4353.16	5069.64
51	60	55.5	135	2.1%	58.90	48.00	37.00	29.82	5.50	28.8	0.00243	0.00143	24.48	-4902.77	-1687.85	1234.14	5356.48	6982.08
57	66	61.5	160	2.1%	64.80	52.80	41.00	35.34	5.90	31.68	0.00244	0.00144	26.93	-5932.35	-2000.41	1477.24	6455.52	9252.04
63	72	67.5	190	2.1%	70.69	57.60	45.00	41.97	6.30	34.56	0.00245	0.00145	29.38	-7059.99	-2375.49	1768.63	7666.84	12054.57

## Appendix D: Grout Product Data Sheet



# PRODUCT DATA SHEET

## SikaGrout®-328

HIGH PERFORMANCE, PRECISION, GROUT WITH EXTENDED WORKING TIME

### PRODUCT DESCRIPTION

SikaGrout®-328 is a non-shrink, non-metallic, cementitious precision grout powered by ViscoCrete technology. This grout provides extended working time and exceptional physical performance at fluid consistency. A structural, precision grout, SikaGrout®-328 can be placed from fluid to dry pack.

### USES

- Where exceptional one day and ultimate compressive strengths are required.
- Applications requiring a pumpable grout.
- Non-shrink grouting of machinery and equipment, base plates sole plates, precast panels, beams, columns and curtain walls.
- Applications where a non-shrink grout is needed for maximum effective bearing area to transfer optimum load.

- For underwater application in conjunction with Sikament® 100 SC. Consult Technical Service for dosage information. Independent test data is available however on site testing is recommended to confirm performance under actual field conditions.
- For grouting rebar, bolts, dowels and pins, etc.

### CHARACTERISTICS / ADVANTAGES

- Multiple fluidity with one material
- Reaches 10,000 psi in dry pack consistency
- Outstanding performance in fluid state
- Extended working time
- Excellent fluidity - sufficient time for placement
- Contains premium quality quartz aggregate
- Hardens free of segregation
- Non-metallic, will not stain or rust
- Shows positive expansion

### APPROVALS / STANDARDS

- Meets ASTM-C 1107 (Grade B & C)
- SikaGrout®-328 is USDA certifiable

### PRODUCT INFORMATION

<b>Packaging</b>	50 lb (22.7 kg) bag
<b>Appearance / Color</b>	Gray powder
<b>Shelf Life</b>	9 months from date of production if stored properly in original, unopened and undamaged sealed packaging
<b>Storage Conditions</b>	Store dry at 40–95 °F (4–35 °C) Protect from moisture. If damp, discard material

## TECHNICAL INFORMATION

<b>Compressive Strength</b>	(ASTM C-109) 73 °F (23 °C) 50 % R.H.	<b>Dry Pack</b>	<b>Plastic</b>	<b>Flowable</b>	<b>Fluid</b>
	1 day	5,000 psi (34.4 MPa)	4,500 psi (31 MPa)	4,000 psi (27.6 MPa)	3,500 psi (24.1 MPa)
	3 day	8,000 psi (55.2 MPa)	6,500 psi (44.8 MPa)	6,000 psi (41.4 MPa)	5,500 psi (37.9 MPa)
	14 day	9,200 psi (63.4 MPa)	7,000 psi (48.3 MPa)	6,700 psi (46.2 MPa)	6,500 psi (44.8 MPa)
	28 day	10,000 psi (69 MPa)	8,200 psi (56.5 MPa)	8,000 psi (55.2 MPa)	7,500 psi (51.7 MPa)
<b>Flexural Strength</b>		<b>Fluid</b>			(ASTM C-293)
	3 day	1,100 psi (7.6 MPa)			73 °F (23 °C)
	7 day	1,200 psi (8.6 MPa)			50 % R.H.
	28 day	1,300 psi (9 MPa)			
<b>Splitting Tensile Strength</b>		<b>Fluid</b>			(ASTM C-496)
	3 day	350 psi (2.4 MPa)			73 °F (23 °C)
	7 day	400 psi (2.8 MPa)			50 % R.H.
	28 day	650 psi (4.5 MPa)			
<b>Shear Strength</b>		<b>Fluid</b>			(ASTM C-882 modified*)
	3 day	950 psi (6.6 MPa)			
	7 day	1,750 psi (12.1 MPa)			
	28 day	2,000 psi (13.8 MPa)			
*Mortar scrubbed into substrate at 73 °F (23 °C) and 50 % R.H.					
<b>Freeze-Thaw Stability</b>	300 Cycles	99 %			(ASTM C-666)

## APPLICATION INFORMATION

<b>Mixing Ratio</b>	<b>Dry Pack</b>	<b>Plastic</b>	<b>Flowable</b>	<b>Fluid</b>	
	5.5–6.0 pts (2.6–2.8 L)	6.5–7.0 pts (3.1–3.3 L)	7.0–7.5 pts (3.3–3.5 L)	8.0–8.5 pts (3.8–4 L)	
<b>Coverage</b>	0.44 ft <sup>3</sup> (0.01 m <sup>3</sup> ) per bag at hfluid consistency (Coverage figures do not include allowance for surface profile and porosity or material waste)				
<b>Layer Thickness</b>	<b>Min.</b>		<b>Max.</b>		
	1/2" (12.7 mm)		6" (152.4 mm)		
For application thicknesses of 6" or greater, consult Sika's Technical Service Department.					
<b>Flowability</b>	<b>Dry Pack</b>	<b>Plastic<sup>1</sup></b>	<b>Flowable<sup>1</sup></b>	<b>Fluid<sup>2</sup></b>	
	10–25 %	100–125 %	124–145 %	20–60 sec	
<sup>1</sup> ASTM C-1437 <sup>2</sup> ASTM C-939					
<b>Product Temperature</b>	65–75 °F (18–24 °C)				
<b>Ambient Air Temperature</b>	> 45 °F (7 °C)				
<b>Substrate Temperature</b>	> 45 °F (7 °C)				
<b>Set Time</b>		<b>Dry Pack</b>	<b>Plastic</b>	<b>Flowable</b>	<b>Fluid</b>
	Initial	<15 min	>2 hr	>3 hr	>4 hr
	Final	<2 hr	<6 hr	<7 hr	<8 hr

Product Data Sheet  
SikaGrout®-328  
July 2018, Version 01.01  
020201010010000081

BUILDING TRUST



## SURFACE PREPARATION

- Surface must be clean and sound. Remove all deteriorated concrete, dirt, oil, grease, and other bond-inhibiting materials from the area to be repaired.
- Anchor bolts to be grouted must be de-greased with suitable solvent.
- Concrete must be sound and roughened to promote mechanical adhesion.
- To ensure optimum repair results, the effectiveness of decontamination and preparation should be assessed by a pull-off test.
- Substrate should be Saturated Surface Dry (SSD) with clean water prior to application. No standing water should remain during application.

## FORMING

- For pourable grout, construct forms to retain grout without leakage.
- Forms should be lined or coated with bond-breaker for easy removal.
- Forms should be sufficiently high to accommodate head of grout.
- Where grout-tight form is difficult to achieve, use SikaGrout®-328 in dry pack consistency.

## MIXING

- Pour the water in the recommended proportion into a suitable mixing container.
- **DO NOT OVER WATER!**
- Ambient and material temperature should be as close as possible to 70 °F. If higher, use cold water; if colder, use warm water.
- While mixing slowly, add the powder to the water.
- Mix thoroughly for at least 5 minutes with low speed (400-600 rpm) using a Sika mixing paddle or a jiffy paddle to avoid entraining too much air and until homogenous with no lumps.

## EXTENSION WITH AGGREGATES

- For deeper applications (plastic and flowable consistency only), 25 lbs. of 3/8" (9.5 mm) coarse aggregate can be added.
- The aggregate must be non-reactive (reference ASTM C-1260, C-227 and C-289), clean, well graded, saturated surface dry, have low absorption and high density, and comply with ASTM C-33 size number 8 per Table 2.
- Variances in aggregate may result in different strengths.
- Add pea gravel after the water and SikaGrout®-328.

## APPLICATION

- Within 60 minutes after mixing, place grout into forms in normal manner to avoid air entrapment.
- Vibrate, pump, or ram grout as necessary to achieve flow or compaction.

- SikaGrout®-328 must be confined leaving minimum exposed surface.
- After grout has achieved final set, remove forms, trim or shape exposed grout shoulders to designed profile.
- SikaGrout®-328 is an excellent grout for pumping, even at high flow. For pump recommendations, contact Technical Service.

## CURING TREATMENT

- Wet cure for a minimum of 3 days or apply a curing compound which complies with ASTM C-309 on exposed surfaces.

## LIMITATIONS

- Do not use as a patching or overlay mortar or in unconfined areas.
- As with all cement based materials, avoid contact with aluminum to prevent adverse chemical reaction and possible product failure. Insulate potential areas of contact by coating aluminum bars, rails, posts etc. with an appropriate epoxy such as Sikadur 32 Hi-Mod.

## BASIS OF PRODUCT DATA

Results may differ based upon statistical variations depending upon mixing methods and equipment, temperature, application methods, test methods, actual site conditions and curing conditions.

## OTHER RESTRICTIONS

See Legal Disclaimer.

## ENVIRONMENTAL, HEALTH AND SAFETY

For further information and advice regarding transportation, handling, storage and disposal of chemical products, user should refer to the actual Safety Data Sheets containing physical, environmental, toxicological and other safety related data. User must read the current actual Safety Data Sheets before using any products. In case of an emergency, call CHEMTREC at 1-800-424-9300, International 703-527-3887.

**DIRECTIVE 2004/42/CE - LIMITATION OF EMISSIONS OF VOC**

0 g/l

(EPA method 24)

**LEGAL DISCLAIMER**

- **KEEP CONTAINER TIGHTLY CLOSED**
- **KEEP OUT OF REACH OF CHILDREN**
- **NOT FOR INTERNAL CONSUMPTION**
- **FOR INDUSTRIAL USE ONLY**
- **FOR PROFESSIONAL USE ONLY**

Prior to each use of any product of Sika Corporation, its subsidiaries or affiliates ("SIKA"), the user must always read and follow the warnings and instructions on the product's most current product label, Product Data Sheet and Safety Data Sheet which are available at [usa.sika.com](http://usa.sika.com) or by calling SIKA's Technical Service Department at 1-800-933-7452. Nothing contained in any SIKA literature or materials relieves the user of the obligation to read and follow the warnings and instructions for each SIKA product as set forth in the current product label, Product Data Sheet and Safety Data Sheet prior to use of the SIKA product.

SIKA warrants this product for one year from date of installation to be free from manufacturing defects and to meet the technical properties on the current Product Data Sheet if used as directed within the product's shelf life. User determines suitability of product for intended use and assumes all risks. User's and/or buyer's sole remedy shall be limited to the purchase price or replacement of this product exclusive of any labor costs. **NO OTHER WARRANTIES EXPRESS OR IMPLIED SHALL APPLY INCLUDING ANY WARRANTY OF MERCHANTABILITY OR FITNESS FOR A PARTICULAR PURPOSE. SIKA SHALL NOT BE LIABLE UNDER ANY LEGAL THEORY FOR SPECIAL OR CONSEQUENTIAL DAMAGES. SIKA SHALL NOT BE RESPONSIBLE FOR THE USE OF THIS PRODUCT IN A MANNER TO INFRINGE ON ANY PATENT OR ANY OTHER INTELLECTUAL PROPERTY RIGHTS HELD BY OTHERS.**

Sale of SIKA products are subject to the Terms and Conditions of Sale which are available at <https://usa.sika.com/en/group/SikaCorp/termsandconditions.html> or by calling 1-800-933-7452.

**Sika Corporation**  
201 Polito Avenue  
Lyndhurst, NJ 07071  
Phone: +1-800-933-7452  
Fax: +1-201-933-6225  
[usa.sika.com](http://usa.sika.com)

**Sika Mexicana S.A. de C.V.**  
Carretera Libre Celaya Km. 8.5  
Fracc. Industrial Balvanera  
Corregidora, Queretaro  
C.P. 76920  
Phone: 52 442 2385800  
Fax: 52 442 2250537



Product Data Sheet  
SikaGrout®-328  
July 2018, Version 01.01  
020201010010000081

SikaGrout-328-en-US-(07-2018)-1-1.pdf

**BUILDING TRUST**

